

MAGNETIC RESONANCE STUDIES
OF
ORGANOMETALLIC CATIONS AND CLUSTERS

By

LIJUAN LI, B.Sc.

A Thesis

Submitted to the School of Graduate Studies

in Partial Fulfilment of the Requirements

for the Degree

Doctor of Philosophy

McMaster University

February, 1992

(c) Copyright by Lijuan Li, 1992

MAGNETIC RESONANCE STUDIES OF ORGANOMETALLIC COMPLEXES

DOCTOR OF PHILOSOPHY (1992)
(Chemistry)

McMASTER UNIVERSITY
Hamilton, Ontario

TITLE: Magnetic Resonance Studies of Organometallic Cations and Clusters

AUTHOR: Lijuan Li, B.Sc. (Jilin University, P.R.China)

SUPERVISORS: Professor M. J. McGlinchey
Professor D. R. Eaton

NUMBER OF PAGES: xviii, 183

To my parents and Kai

Abstract

This thesis describes the application of magnetic resonance methods to some problems in organometallic chemistry. The reactions of nitroso compounds with the (cyclohexadienyl)Fe(CO)₃ cation have been investigated by using ESR spectroscopy and yield nitroxides of the type (OC)₃Fe(C₆H₇)(Ar)N-O•, and also the corresponding C₆H₅(Ar)N-O• radical. With bulky nitrosoarenes, such as C₆Me₅NO, isomers are observed in which the aryl ring rotation is slow on the ESR time-scale. The analogous reactions with the cyclohexadienyl cation derived from the B ring of (ergosteryl acetate)Fe(CO)₃ lead to attack at the central carbon, i.e., at C-7. Subsequent hydrogen migration leads to the (5,7-diene)Fe(CO)₃ complex bearing the aryl nitroxide at the 7-position. In contrast, the reaction of [(η⁵-cyclohexadienyl)Fe(CO)₃]⁺BF₄⁻ with 2-methyl-2-nitrosopropane yields the bis(*t*-butyl)nitroxide radical and the most interesting observation is that the intensity of the ESR signal varies in an oscillatory manner with time. This is the first oscillating reaction that can be followed by ESR spectroscopy. The experimental results and a mechanistic rationale are described.

In the second part of the thesis, a 1- and 2-dimensional ¹³C NMR study on the carbonyl migration processes in trimetal clusters is discussed. The variable-temperature ¹³C NMR spectra of the clusters (C₅H_nMe_{5-n})MCo₂(CO)₈CCO₂-*i*-Pr,

where $n = 5, 4,$ and 0 and $M = \text{Mo}$ and W , reveal the existence of two interconverting rotamers whereby the $\text{CpM}(\text{CO})_2$ vertex is oriented either *proximal* or *distal* to the capping carbonyl group. Simulation of the carbonyl exchange process reveals that the migration of CO ligands between Co and Mo has the same activation energy barrier as the interconversion of *proximal* and *distal* cyclopentadienyl rings; it is proposed that these fluxional processes are correlated. Use of a capping fragment derived from a natural product such as menthol or podocarpic acid renders the cluster chiral and allows the detection of slowed carbonyl exchange between the diastereotopic cobalt centers.

The 125.7 MHz ^{13}C NMR spectrum of $\text{CH}_3\text{CCo}_3(\text{CO})_8\text{P}(\text{cyclo-C}_6\text{H}_{11})_3$ at -90°C exhibits a 1:2:1:2:2 carbonyl pattern consistent with the triply-bridged structure found in the solid state, showing that carbonyl exchange can be slowed on the NMR time scale. The coalescence behavior of the ^{13}CO resonances can be simulated by invoking a mechanism in which a completely bridge-opened structure is required; local rotation of each $\text{Co}(\text{CO})_3$ vertex is shown to be rapid. 2D-EXCHANGE spectroscopy is used as an independent probe for the fluxional processes and shows that, in accord with the bridge-opened model, all carbonyl sites do not exchange at the same rate. It is also demonstrated that rotation about the cobalt—phosphorus and $\text{P}-\text{C}_{\text{ipso}}$ bonds is slowed on the NMR time-scale.

ACKNOWLEDGEMENTS

I would like to express my sincere gratitude to my supervisors, Dr. M. J. McGlinchey and Dr. D. R. Eaton for the valuable guidance and continuous help they generously provided throughout the course of this work. Dr. McGlinchey has always been a great source of encouragement and support. No matter how busy he was, he always had time to listen to my concerns, help me with any problem, chemistry or others. Dr. Eaton and Dr. McGlinchey's expertise in chemistry made me recognize the novel oscillating reaction, otherwise it would have been thrown in the recycling can. I appreciate Dr. Eaton's offering me the opportunity to work for him in Canada, and I am proud of being his last graduate student.

I would like to thank Dr. A. D. Bain for serving on my supervisory committee and also for the assistance and helpful suggestions he has offered during this period. I could probably never have figured out the 2D NMR experiment without his help.

I am greatly indebted to Dr. R. E. Perrier, Dr. K. A. Sutin and Dr. M. F. D'Agostino for helping me with some synthetic work. I am grateful to Ian Thompson for his assistance with the ESR spectrometer and Brian Sayer for helping me to obtain beautiful NMR spectra of my compounds. I would also like to thank Dr. Don Hughes and George Timmins from the NMR and IR facilities, and Dr. R. Smith and F. Ramelan from the Mass Spectrometry Lab.

Special thanks go to Barbara, for her patience in losing her valuable time which was grasped by Dr. McGlinchey to spend helping me with my research, and for her great help with my little boy, Christopher.

To everyone who has worked in Dr. Eaton's lab during my stay: Tony, Traci, Mike and Bruce, and to everyone in Dr. McGlinchey's group: Richard, Karen, Debbie, Bavani, Mike D., Kris, Patty, Andreas D., Lisa, Peter, Tim, Mike H., Anne, Anja, Andreas F., Matthias and Jörg. Thank you for your friendship and help in chemistry. You made me feel that school is a fun place to go. I am specially grateful to Traci and Kirt for being good friends to me and being patient with my broken English when I first came to Canada. Special thanks go to Kris for her friendship and help; also to Jan and Ian for taking the time to answer my questions.

I would also like to thank the staff in the Departmental office for their help provided in one way or another. I am grateful to Carol Dada for being a friend and teaching me Canadian culture.

The funding from the Department of Chemistry and McMaster University, which provided the Teaching Assistantships and Scholarships, and the Ontario Government, which provided Ontario Graduate Scholarships, are gratefully acknowledged.

Finally, to my parents, brothers and sisters, I am eternally grateful for their love and support in the past. Especially, thanks go to my husband Kai for always being willing to discuss my research and other interests. He means everything to me.

TABLE OF CONTENTS

	PAGE
CHAPTER ONE: INTRODUCTION	
1.1 Basic Theory of Electron Paramagnetic Resonance Spectroscopy	2
1.1.1 Introduction	2
1.1.2 The Zeeman Hamiltonian	3
1.1.3 Hyperfine Coupling	6
1.1.4 Line Shapes and Intensities	10
1.2 Spin Trapping Techniques and the Reactions of Nitroso Compounds with Diamagnetic Species.	12
1.2.1 Introduction	12
1.2.2 Nitroxide Radical Structure	14
1.2.3 Spin trapping techniques	14
1.2.3 Alternative Spin Traps	17
1.2.4 Reactions of Nitroso Compounds with Diamagnetic Materials.	18
1.3 Oscillating Reactions	19
1.3.1 Introduction	19

	PAGE
1.3.2 Descriptive Aspects of Oscillatory Kinetics	22
1.4 Fluxionality of Organometallic Compounds	26
1.4.1 Synthesis of Cobalt Clusters	26
1.4.2 Introduction to Fluxionality	29
1.4.3 NMR Techniques to Study Fluxionality	30
1.4.3.1 Line Shape Analysis	31
1.4.3.2 Spin-Saturation Transfer Spectroscopy	33
1.4.4 Applications of 2D EXSY Techniques	49

**CHAPTER TWO: THE REACTIONS OF NITROSOARENES WITH CATIONIC
CYCLOHEXADIENYL COMPLEXES OF IRON TRICARBONYL: AN ESR STUDY**

2.1 Introduction	64
2.2 Results	66
2.2.1 Reaction of Cation 40 with C_6H_5NO	66
2.2.2 Reaction of Cation 40 with C_6HMe_4NO	69
2.2.3 Reaction of Cation 40 with C_6Me_5NO	71
2.2.4 Reaction of Steroidal Cation 42 with C_6H_5NO	74
2.2.5 Reaction of Steroidal Cation 42 with C_6Me_5NO	76
2.2.6 Reaction of Steroidal Cation 42 with C_6HMe_4NO	76

	PAGE
2.3 Discussion	76
2.3.1 Assignments of the ESR Spectra	80
2.3.2 Mechanistic Considerations	85
2.3.3 Reactions of ArNO with the Steroidal Cation, 42	90
2.4 Future Work	95

CHAPTER THREE:

THE REACTION OF $[(\eta^5\text{-cyclohexadienyl})\text{Fe}(\text{CO})_3]^+ \text{BF}_4^-$ WITH 2-METHYL-2-NITROSOPROPANE: AN UNEXPECTED OSCILLATING REACTION

3.1 Introduction	96
3.2 Results and Discussion	97
3.3 Future Work	112

CHAPTER FOUR: HIGH-FIELD NMR STUDY OF VERTEX ROTATION IN

$(\text{C}_5\text{H}_n\text{Me}_{5-n})\text{MCo}_2(\text{CO})_8\text{CR}$ CLUSTERS (M = Mo, W)

4.1 Introduction	113
4.2 Results and Discussion	117
4.2.1 ^{13}C NMR and Infrared Spectroscopy	117

	PAGE
4.2.2 MoCp Vertex Rotation and CO Exchange	124
4.2.3 Chiral Clusters	130
CHAPTER FIVE:	
VARIABLE-TEMPERATURE 1- AND 2-DIMENSIONAL ^{13}C NMR STUDIES ON	
$\text{CH}_3\text{CCo}_3(\text{CO})_8\text{P}(\text{cyclo-C}_6\text{H}_{11})_3$: THE MECHANISM OF CARBONYL MIGRATION	
5.1 Introduction	135
5.2 Results and Discussion	137
5.3 Future Work	152
CHAPTER SIX: EXPERIMENTAL	155
REFERENCES	164

LIST OF FIGURES

	PAGE
1.1. Zeeman levels of α and β states.	4
1.2. ESR spectrum of biphenylene anion.	8
1.3. Line Shapes	11
(a) Lorentzian line;	
(b) Gaussian line;	
(c) derivative of the Lorentzian line.	
1.4. Sketches of typical types of kinetics.	24
(a). Monctonic;	
(b). Overshoot-undershoot;	
(c). Damped oscillatory;	
(d). Sustained oscillations (limit cycle).	
1.5. Energy level diagram for exchanging spins.	36
1.6. (a). A partial spectrum of 13 in $\text{CD}_2\text{Cl}_2\text{-CHFCI}_2$, at -118°C .	43
(b). $1\ \mu\text{s}$ after applying a 180° pulse at 55.5ppm .	
(c). A difference spectrum obtained by subtracting (b) from that obtained at $10\ \text{ms}$.	

	PAGE
1.7. 2D EXSY diagrams for N,N-dimethylacetamide, showing the exchange of the two methyl groups for five different temperatures.	50
1.8. 2-D ³¹ P contour map for Cr(CO) ₂ (CS)[(MeO) ₃ P] ₃ in deuteriotoluene at 61°C on a Varian XL-300 spectrometer. All three isomers exhibit an AB ₂ coupling pattern.	53
1.9. 2D ¹³ C NMR spectrum of [Ir ₄ (CO) ₁₁ Br] ¹⁻ at 175K.	57
2.1. ESR spectra from the reaction of 40 with C ₆ H ₅ NO.	68
(a) in CH ₃ CN.	
(b) simulation of (a) using the data in Table 2.1.	
(c) in CH ₂ Cl ₂ after 6 days.	
(d) simulation of (C ₆ H ₅) ₂ N-O•.	
2.2. ESR spectra from the reaction of 40 with C ₆ Me ₄ HNO in 1:1 CH ₃ CN/CHCl ₃	72
(a) after 30 minutes.	
(b) after 20 hours.	
(c) after 4 days.	
2.3. ESR spectra from the reaction of 40 with C ₆ Me ₄ HNO in 1:1 benzene / dimethylsulfoxide	73
(a) after 30 minutes.	

	PAGE
(b) simulation of (a) using the data in Table 2.2.	
(c) after 18 hours.	
(d) after 5 days.	
2.4. ESR spectra from the reaction of 42 with C ₆ H ₅ NO in CH ₃ CN	75
(a) after 3 hours.	
(b) after 27 hours.	
(c) simulation of (b) using the data in Table 2.1.	
2.5. ESR spectra from the reaction of 42 with C ₆ Me ₅ NO in CH ₃ CN	77
(a) after 3 hours.	
(b) after 6 hours.	
(c) after 9 hours.	
(d) after 21 hours.	
2.6. (a) Space-filling model of 48 in which attachment of the ArNO fragment at C-5 causes unfavorable interaction with the methyl group at C-10.	94
(b) Space-filling model of 50 in which attachment of the ArNO fragment at C-7 causes no problematic steric interactions with the methyl groups.	
(c) Space-filling model of 49 in which attachment of the ArNO fragment at C-9 causes unfavorable interactions with the methyl groups at C-10 and at C-13.	

	PAGE
3.1. The time-dependent ESR spectra observed when 3×10^{-2} mmol of 40 reacts with a 24-fold excess of t-BuNO.	103
3.2. ESR spectra for the reaction of 1.6×10^{-2} mmol of 40 with a 15-fold excess of t-BuNO.	105
3.3. ESR spectra arising from the reaction of 2×10^{-2} mmol of 40 and a 3.5-fold excess of t-BuNO.	106
4.1. Low temperature 125 MHz ^{13}C NMR spectra in the metal carbonyl region for (a) 66 and 69 (b) 67 and 70 (c) 68 and 71 .	120
4.2. Sections of the infrared spectra of the clusters 64 , 70 and 68 in solution in methylene chloride, and in the solid state as KBr pellets.	122
4.3. View of $(\text{C}_5\text{Me}_5)\text{MoCo}_2(\text{CO})_8\text{C-CO}_2\text{-}i\text{-Pr}$, 68 , showing the atom numbering scheme.	126
4.4. Experimental and simulated 62.86-MHz ^{13}C variable-temperature NMR spectra of 67 in the metal carbonyl region.	129
4.5. Variable-temperature 125 MHz ^{13}C NMR spectra in the metal carbonyl region for 78 .	132
4.6. CHEMX model of the cluster 78 in which the C_5H_5 ligand is <i>proximal</i> to the capping group and the bulky menthol substituent lies over the cobalt-cobalt vector.	134

	PAGE
5.1. ^{13}C NMR spectra of $\text{CH}_3\text{CCo}_3(\text{CO})_8\text{P}(\text{cyclo-C}_6\text{H}_{11})_3$, 63 , at 183K and 263K.	139
5.2. Experimental and simulated variable-temperature ^{13}C NMR spectra of $\text{CH}_3\text{CCo}_3(\text{CO})_8\text{P}(\text{cyclo-C}_6\text{H}_{11})_3$, 63 , in the metal carbonyl region.	140
5.3. Contour plot representations of NOESY experiments at -90°C ; the mixing time (τ_m) is 7 ms in (a) and 10 ms in (b).	146
5.4. Experimental and simulated variable-temperature ^{13}C NMR spectra of $\text{CH}_3\text{CCo}_3(\text{CO})_8\text{P}(\text{cyclo-C}_6\text{H}_{11})_3$, 63 , in the cyclohexyl ring region.	148
5.5. Peak coalescence pattern for the cyclohexyl carbons of 63 .	149
5.6. Views of the X-ray crystal structure of 63 ; (a) shows the chair conformations of the cyclohexyl rings. (b) is a view along the phosphorus—cobalt bond showing the relative orientations of the rings.	151

List of Schemes

	PAGE
1.1. The reaction of phenyl <i>tert</i> -butyl nitron with a radical.	16
1.2. The reactions of nitrosoarenes with olefins.	19
1.3. The trichloroalkane reaction in cluster preparation.	27
1.4. The mechanism of interconversion of different isomers in 13 .	42
1.5. Three possible isomers of 25 .	51
1.6. Possible mechanisms for the interconversion of the mer-I and mer-II isomers.	54
1.7. Mechanism of CO exchange in 30 .	58
1.8. The lowest energy exchange process of 36 .	61
1.9. Two intramolecular fluxional processes occurring in 37 and 38 in solid state.	63
2.1. Synthetic route to the steroidal cation 42 .	81
(I) Mercuric acetate / acetic acid.	
(II) (Benzylideneacetone)Fe(CO) ₃ .	
(III) [(C ₆ H ₅) ₃ C] ⁺ BF ₄ ⁻	
(IV) HPF ₆	

	PAGE
2.2. Possible sites of reaction of nitrosoarenes with the steroidal cation 42 .	92
3.1. The reaction of 40 with nitrosoarenes.	98
3.2. The rearrangement of a steroidal nitroxide.	99
3.3. The ESR spectra of the products arising from the reaction of 40 with t-BuNO.	101
3.4. A speculative mechanism for the reaction of 40 with t-BuNO.	110
4.1. Synthetic Routes to Mixed Metal Clusters.	115
4.2. Rotation of a CpMo(CO) ₂ Vertex relative to a Triangular Face.	117
4.3. Synthetic Routes to the Chiral Clusters 78 and 79 .	131
5.1. Proposed scrambling mechanism for the CO ligands of 63 ; rapid local rotation can occur at the bridge-opened stage.	143

List of Tables

	PAGE
1.1. Groups incorporated into the $\text{Co}_3(\text{CO})_9\text{C-R}$ cluster using the R-CCl_3 reaction.	28
2.1. ESR parameters for phenyl nitroxide radicals.	70
2.2. ESR parameters for durene- and pentamethylbenzene nitroxide radicals.	78

CHAPTER ONE

INTRODUCTION

This thesis deals with the structures and molecular dynamics of several different types of organometallic molecules. Initially, we shall discuss the synthesis and characterization of a series of nitroxide radicals whose behavior is best studied by electron spin resonance spectroscopy. Therefore, we provide an introduction to E.S.R. spectroscopy as a necessary guide to understanding these systems. Recent work by Baird¹ and his colleagues has emphasized the importance of organometallic radicals and rôle of ESR spectroscopy in characterizing them.

Subsequently, the fluxional behavior of some diamagnetic organo-transition metal clusters was investigated. These systems are most conveniently studied by nuclear magnetic resonance spectroscopy, and a summary of the important features of this technique is presented. NMR is a very versatile method which can be applied to molecular rearrangements having low (1 - 5 kcal/mol), medium (5 - 20 kcal/mol) or high (>20 kcal/mol) activation energy. The most widely used method for intermediate activation energies involves the measurement of the spectrum over a wide temperature range and subsequently simulating the line-broadened spectra so as to obtain rate constants. We have used this approach

to monitor the rate of vertex rotations in mixed metal clusters.

A NMR recently developed method takes advantage of 2-dimensional NMR techniques, and these have been used to elucidate the mechanisms of carbonyl exchange in cobalt clusters. Some recent examples, in which the fluxional behavior of organometallic clusters has been examined, are described in this introductory section.

1.1 *Basic Theory of Electron Paramagnetic Resonance Spectroscopy*

1.1.1 Introduction

The first topic covered in this thesis describes the chemistry of some nitroxide radicals and the spectroscopic technique relied upon most heavily for the characterization of such species is electron paramagnetic resonance (EPR) spectroscopy. It is commonly referred to as Electron Spin Resonance (ESR) when organic radicals are studied. The theory of this technique will be developed only to the extent required to interpret the experiments completed in these projects.²⁻⁴

There is some confusion in the literature about the units which should be used when discussing ESR spectroscopy. Magnetic fields are commonly referred to in Gauss (G), rather than Tesla (T) or mT of SI units. The conversion is $1\text{G} = 10^{-4}\text{T} = 0.1\text{mT}$.

In this thesis, H represents external magnetic field and \hat{H} represents the Hamiltonian.

1.1.2 The Zeeman Hamiltonian

Electron Spin Resonance Spectroscopy is a magnetic resonance technique which involves the interaction of the magnetic moment of an unpaired electron, μ_e , with a magnetic field, H . The energy (E) of this interaction can be represented by,

$$E = \mu_e H \quad \dots (1.1)$$

The magnetic moment μ_e of the electron is given by

$$\mu_e = -g\beta S \quad \dots (1.2)$$

Here S is the spin angular momentum vector of the electron. g is a dimensionless constant called the g factor or g value and β is the electron Bohr magneton, equal to $e\hbar/2mc$, where $-e$ and m are the charge and mass of the electron.

The interaction between the electron magnetic moment and an applied field H is represented by the Hamiltonian

$$\hat{H} = -\mu_e H \quad \dots (1.3)$$

If the magnetic field is defined to be in the z direction this simplifies to

$$\hat{H} = g\beta HS_z \quad \dots (1.4)$$

The energies of the two spin states, α ($m_s = + 1/2$) and β ($m_s = - 1/2$) are $+1/2g\beta H$ and $-1/2g\beta H$ respectively. Application of an oscillating field of a suitable frequency (ν), perpendicular to H induces transitions between these Zeeman levels. (Fig. 1.1)

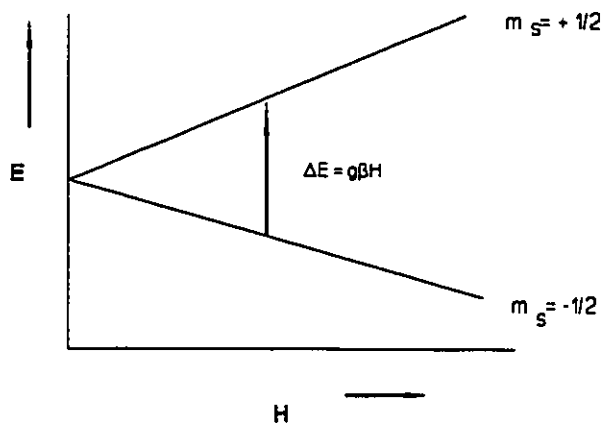


Figure 1.1 Zeeman levels of α and β states.

$$\Delta E = h\nu = g\beta H \Delta m_s = g\beta H \quad \dots (1.5)$$

It is important to note that the nuclei of a paramagnetic molecule also interact with the magnetic field. This perturbs the Zeeman energy levels slightly and the Hamiltonian must be modified to

$$\hat{H} = g\beta HS_z - g_N \beta_N H I_z + A S_z I_z \quad \dots (1.6)$$

where I_z is the allowed component of nuclear spin in the z direction, g_N is the g factor for the nucleus and β_N is the nuclear magneton. Since the magnitude of $g\beta$ is much larger than the $g_N\beta_N$ term, the nuclear term is a very small perturbation. The selection rules for the transition are $\Delta m_s = \pm 1$ and $\Delta m_l = 0$.

Although any appropriate combination of frequency and field can be used to achieve resonance, an ESR spectrometer operates at a fixed microwave frequency. The spectrum is scanned by varying the magnetic field. An X-band spectrometer operates at a frequency of approximately 9500 MHz, while a Q-band spectrometer operating at about 35,000 MHz requires a stronger magnet. As with NMR, the higher frequency increases sensitivity and resolution, but the higher field technique is not commonly employed for ESR since the problem with dielectric loss is much greater. In addition, a Q-band spectrometer has a very small cavity which has some practical experimental difficulties and is commonly employed for studies at very low temperature.

For the free electron $g = 2.002322$ and most organic radicals have g factors very close to this value. The g value in ESR spectroscopy is analogous to the chemical shift in NMR, but the transitions in NMR spectroscopy are of much lower energy than those in ESR. This is a direct result of the much lower value of $g_N\beta_N$ ($g_N\beta_N = \gamma_N\hbar$) compared to $g\beta$. NMR uses radio frequency rather than microwave radiation, and NMR requires much stronger magnetic fields. In ESR

the g value in $\Delta E = g\beta H$ is changed to indicate transitions of different energies, but in NMR spectroscopy the g_N value remains constant and a shielding constant (σ) is introduced to modify the field to an "effective" field.

$$\Delta E = -g_N\beta_N(1-\sigma)H\Delta m_l \quad \dots (1.7)$$

1.1.3 Hyperfine Coupling

The magnetic moment of an electron and nuclei are coupled *via* the so-called contact interaction which was first introduced by Fermi. Therefore, in addition to the g value, another useful spectral parameter in ESR spectroscopy is the hyperfine coupling constant (A), analogous to the spin-spin coupling constant (J) in NMR. The spin Hamiltonian must include a new term

$$\hat{H} = AS \cdot I \quad \dots(1.8)$$

If the magnetic field is applied along the z direction, this term simplifies, for the first order perturbation, to

$$\hat{H} = AS_z I_z \quad \dots(1.9)$$

When the energy of the resonance is large compared to the hyperfine interaction, the high field approximation is satisfactory, and the expression

$$\Delta E = g\beta H + g\beta m_i A \quad \dots (1.9)$$

is valid. Therefore, the resonance for the free electron is split by the nuclei.

Most free radicals contain several magnetic nuclei; in some molecules these may be grouped into magnetically equivalent sets. Sometimes the nuclei may be equivalent by virtue of the symmetry of the molecule; in other cases the equivalence may be accidental. For n equivalent nuclei in a paramagnetic molecule, there will be $2nI+1$ lines in the ESR spectrum, where I is the nuclear spin. For example, when there is only one nucleus with spin of one, then the number of lines will be three, all with equal intensity; if there are three equivalent nuclei each with spin one half, the total number of lines will be four. For $I = 1/2$, the relative intensities are proportional to the coefficients of the binomial expansion of $(1+x)^n$. For non-equivalent nuclei, the number of lines in the ESR spectrum will be

$$\prod_i (2n_i I_i + 1) \quad \dots (1.10)$$

Where, \prod_i indicates a product over all value of i .

For example, the biphenylene anion, **1**, has two sets of four equivalent protons. Interaction of the electron with the four protons give rise to a quintet (1:4:6:4:1). However, each of these lines is split further into a smaller quintet to give a spectrum with 25 lines. (Figure 1.2)

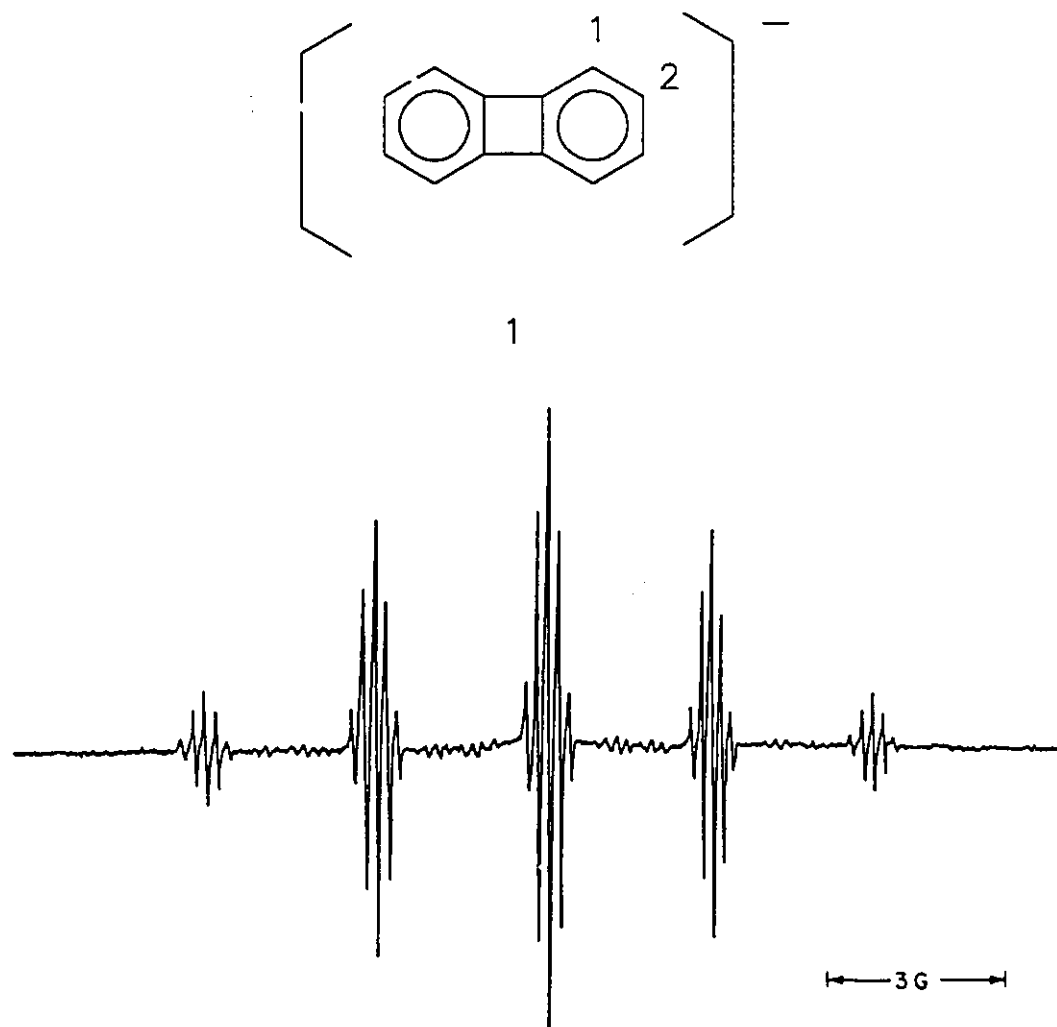


Figure 1.2 ESR spectrum of biphenylene anion.

Analysis of a hyperfine splitting pattern is often not this straightforward. Some of these lines may overlap and low intensity lines may be hidden in the baseline. More often a successful analysis requires some experience. The positions of lines in a spectrum are expected to be symmetric about a centre point.

Asymmetry may be caused by superposition of two spectra, attributable to differences in their g values. Analysis of the outer wings of the splitting pattern is the usual starting point when faced with a complicated ESR spectrum. The separation of the two outermost lines is always the smallest hyperfine splitting. The sum of the hyperfine splitting constants (absolute value) for all nuclei can be calculated by the separation in Gauss between the outermost lines, which may be very weak and may therefore be missed. For $I = 1/2$, the sum of the hyperfine splitting constants is equal to the separation, while for $I = 1$, there is a factor of two. In cases where resolution is poor or lines are too numerous, it may be advantageous to carry out a computer simulation of the spectrum based on assumed hyperfine splitting and linewidth. When several hyperfine splittings are present or more than one radical is present, it is imperative to carry out a computer simulation as a test of the analysis.

In addition to the splitting pattern, the magnitude of the coupling constant provides information about the paramagnetic molecule. The magnitude of the hyperfine coupling constant is related to the unpaired electron density at the nucleus of an atom, $\rho(r_N)$. $\rho(r_N)$ is simply the difference of the probability of finding the average number of electrons at the nucleus with α spin or with β spin.

$$A = (4\pi/3)g\beta\gamma_N\hbar\rho(r_N) \quad \dots (1.11)$$

If the nucleus is in an environment where an excess of electrons has β spin, $\rho(r_N)$

is negative. This results in a negative spin density. Hyperfine coupling results from the direct occupation of atomic s-orbital of the coupled nucleus ($A_H = 508$ G for the H atom). If the unpaired electron is located in a p- or d-orbital, it might be expected that the coupling constant would be zero. However, occupation of p- and d-orbitals or occupation of orbitals on adjacent atoms can induce a spin-density at the nucleus by spin polarization. Therefore, in a radical such as NH_3^+ , where the unpaired electron is in a p orbital, the magnitude of the coupling constant resulting from polarization can be calculated from

$$A_N = \rho_N Q_N \quad \dots (1.12)$$

where ρ_N is occupation of the p orbital on nitrogen, and Q_N is a constant representing the total effect of polarization from spin on nitrogen. Q values are specific to any nucleus.

1.1.4 Line Shapes and Intensities

Lorentzian shapes are usually observed for ESR lines of systems in solution if the concentration of paramagnetic centres is low. The resonance has a sharp peak and the width between the points where the absorption has half its maximum height is $2/T_2$, where T_2 is spin-spin relaxation time, as shown in Figure 1.3(a). Lines will approach the Gaussian shape if the peak is a superposition of many

components and this situation often occurs with NMR in crystalline solids [Figure 1.3(b)]. The main difference between the two types of line shape is that a Lorentzian drops off very much more slowly in the outer wings of the line.

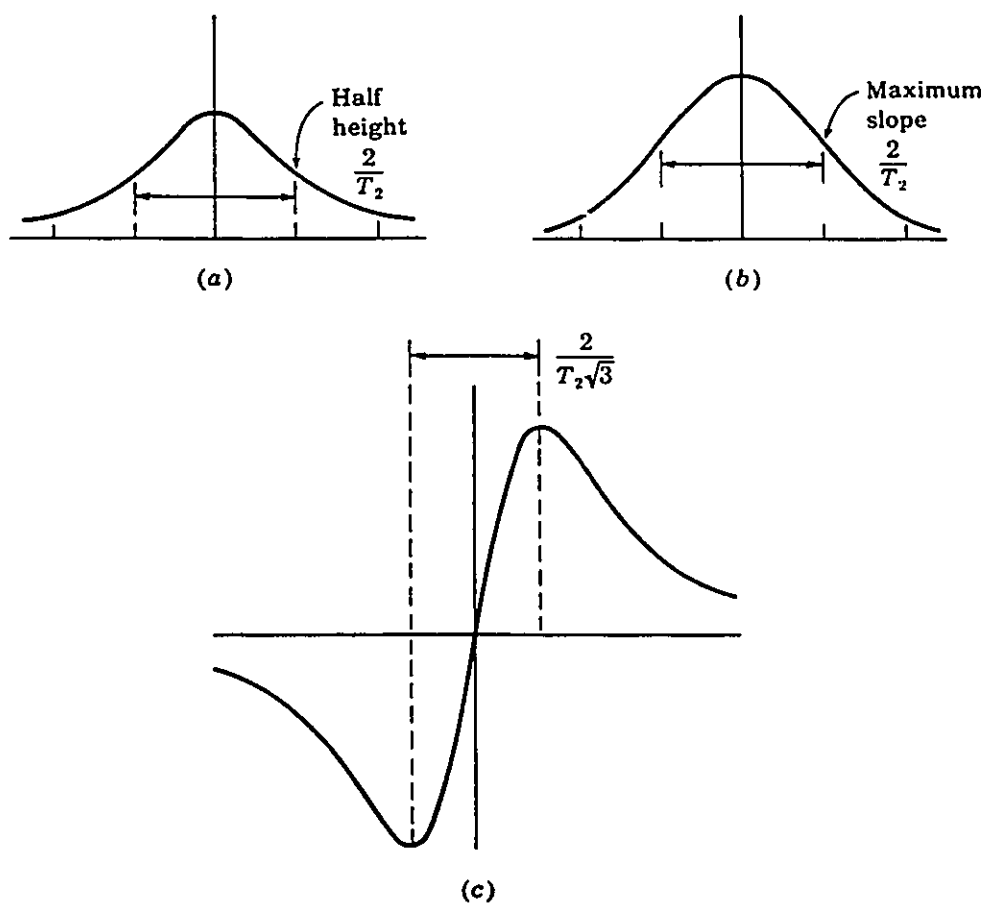


Figure 1.3 Line Shapes (a) Lorentzian line; (b) Gaussian line;
 (c) derivative of the Lorentzian line.

An NMR spectrometer usually records the absorption directly, but in ESR the instrument is designed to record the first derivative of the absorption line shape. The ESR spectrum of a radical in solution with a Lorentzian line then has the characteristic form shown in Figure 1.3(c). The two peaks of the derivative curve correspond to points of maximum slope in the absorption, and the separation between them is $2/T_2\sqrt{3}$, or $2/T_2$ for a Gaussian line. The derivative of the absorption signal may be increasing or decreasing on the left hand side, depending on the phase adjustment of the phase detector or the polarity of the recorder connection. The phase of the recorded signal is totally irrelevant to its interpretation. One is the mirror image of the other. Recorded spectra of either phase are found in the literature.

1.2 *Spin Trapping Techniques and the Reactions of Nitroso Compounds with Diamagnetic Species.*

1.2.1 Introduction

The direct detection and identification of short-lived free radicals by ESR is possible only if the radicals are produced in relatively high concentrations in the ESR spectroscopy cavity by intense *in situ* irradiation or by rapid-mixing flow systems. Sometimes ESR equipment has been substantially modified to increase

sensitivity and resolution.

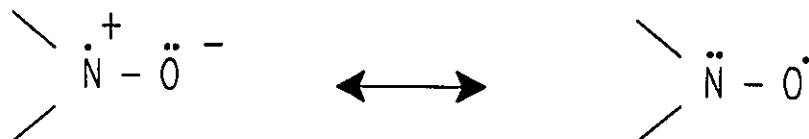
Two indirect techniques for the detection and identification of low concentrations of free radicals in reacting systems have been developed: CIDNP⁵ and spin trapping. The former depends on the strong polarization of certain nuclear spins by the unpaired electron during the molecule's existence as a free radical. The latter involves trapping of a reactive free radical by an addition reaction to produce a more stable radical.

There are several confusing concepts which are spin trapping, spin labelling and spin probes since some similarities exist among them. Janzen and Blackburn⁶ named the technique of detecting and identifying short-lived free radicals by addition to an unsaturated function to produce an ESR detectable radical "spin trapping". In contrast, when a nitroxide bearing molecule⁷ is covalently attached to another molecule or macromolecule of interest, then the molecule or macromolecule is considered to be spin labelled. The intent, of course, is that the presence of the nitroxide grouping will not significantly perturb the behavior of the spin labelled molecule in the system under study. The term spin probe, then, refers to a nitroxide-containing molecule, or other stable radical, which is not covalently attached to molecules of the system under study. The distinction between the latter two terms is not always clear-cut, since spin-labelled molecules themselves often become spin probes when used to study complex systems.⁸

1.2.2 Nitroxide Radical Structure

The real name for nitroxides should be nitroxyl radicals, since nitroxides does not reflect the radical nature of these species and is at variance with the official nomenclature rules for organic compounds. The name nitroxides have been used in the literature and this project.

Nitroxide radicals are compounds containing the $RR'N-O\bullet$ group, which has one unpaired electron. The structure of this fragment can be conceived as a superposition of two resonance structures:



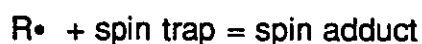
The contribution of the first or second structure to the ground state may be different, depending on the effects of conjugation and on the polarity of the medium. Stable nitroxyl radicals are polar and deeply colored solids or liquids.⁹

1.2.3 Spin trapping techniques

The use of radical addition reactions to detect short-lived radicals was first proposed by Janzen in 1965.¹⁰ Since then this technique has been extensively

developed.⁶ Now it has become a powerful method widely used for the detection of short-lived paramagnetic intermediates in thermally, photochemically, and radiation-induced reactions as described in several review articles.¹¹⁻¹⁶

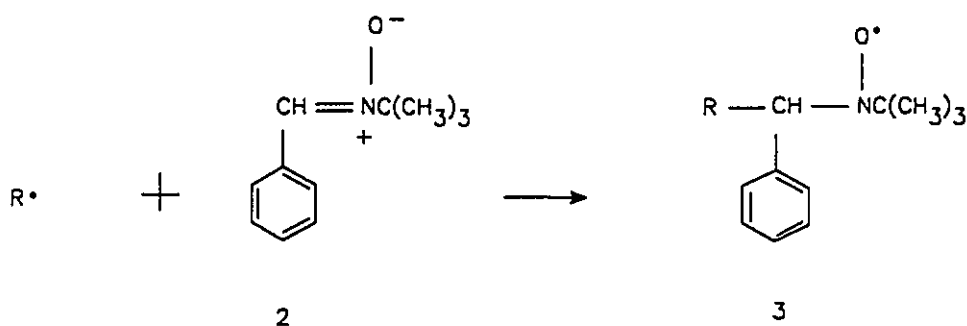
The chemistry involved can be simplified as follows:



Normally, $R\bullet$ is an unstable radical, and the spin adduct is a more stable nitroxide radical. The ESR spectrum of the spin adduct may be examined at leisure and the structure of the short-lived radical $R\bullet$ deduced from the analysis. This technique has been extensively applied to the identification of free radicals generated by the photolysis of organometallic compounds.¹⁷

There are two major groups of complexes which can be used as spin traps. They are nitroso compounds and nitrones.¹⁸ Although both of them react rapidly with reactive free radicals, the latter method suffers from the disadvantage that the hyperfine splittings of the radical are too small to be observed, excepted for a_N , and so important information is lost. For example, phenyl *tert*-butyl nitrone, **2**, has been employed in a number of reactions by Janzen *et al.*^{5,19-21} (Scheme 1.1)

The nitrone **2** seems to have a greater thermal and photochemical stability than 2-nitroso-2-methylpropane (*t*-BuNO), but it has the very considerable disadvantage that the spectrum of the derived nitroxide **3** normally exhibits only a nitrogen triplet and a proton doublet. The identity of the trapped radical may be



Scheme 1.1 The reaction of phenyl *tert*-butyl nitronium ion with a radical.

inferred only from precise measurements of a_N and a_H . Furthermore, the changes in these splitting constants as a function of $R\cdot$ are comparable in magnitude with variations brought about by changes in solvent.

However, the nitronium ion scavenger has been used in the solid state for trapping gas phase radicals produced in a stream of an unreactive carrier gas. These elegant experiments apparently are impossible to perform with the use of *tert*-nitrosoalkanes, since these scavengers are present as ESR inactive dimers in the solid state.²¹

The reactions of nitroso compounds with radicals can be described in a general form:



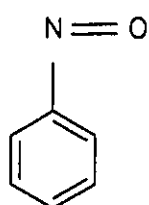
Along with the main triplet splitting caused by the ^{14}N nucleus of the nitroxide group, the ESR spectra of nitroxides will show secondary splittings which originated from magnetic nuclei in the part of the nitroxide radical derived from the trapped radical $\text{R}\cdot$. From these splittings it was in many cases possible to determine the structure of the trapped radicals. The magnitude of the main ^{14}N splittings was also of value for the identification of the trapped radical. Thus the a_{N} value of the unsymmetrical nitroxide formed by trapping of alkyl radicals was in the range between 11 and 16 G, whereas trapped alkoxy radicals, $\text{RO}\cdot$ gave rise to nitroxides with a_{N} between 27 and 29G. Trapping of acyl radicals, $\text{RC}\cdot=\text{O}$, gave nitroxides with a_{N} values between 6 and 8 G.^{14,22,23}

1.2.3 Alternative Spin Traps

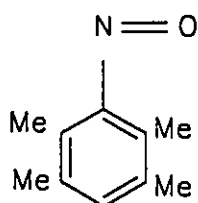
Although nitrosobenzene, **4**, is a useful spin trap whose spin adducts show characteristic finger-print spectra, the assignment of ESR spectra of the spin adducts is very tedious because of their complexity.

Among alternative spin traps, nitrosodurene, **5**, and nitroso-pentamethylbenzene, **6**, have proved to be particularly interesting compounds because of the following advantages.²⁴

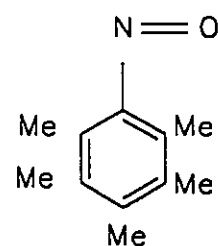
(1) The nitroxides formed have simple ESR spectra: In general, no resolvable splitting due to the aromatic ring of the spin adducts of nitrosodurene



4



5



6

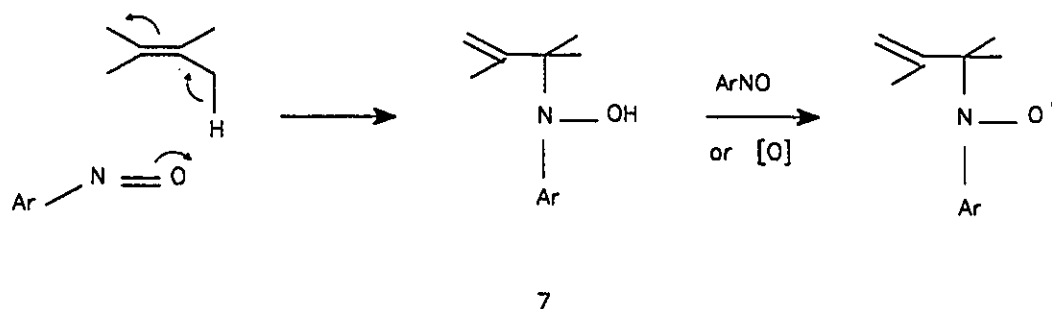
and nitrosopentamethylbenzene is observed.

(2) Nitrosodurene does not undergo photolysis to produce detectable paramagnetic species. A benzene solution of nitrosodurene irradiated with light from a 1 kW high-pressure mercury lamp did not show any ESR signal.²⁵ Accordingly, nitrosodurene can be used as a spin trap in photochemistry.

1.2.4 Reactions of Nitroso Compounds with Diamagnetic Materials.

Using a nitroso compound as a spin trap to react with an unstable radical is not the only way to form a nitroxide radical. Sullivan reported the observation of a series of extremely stable alkenylarylnitroxides in 1966.²⁶ These radicals were prepared by a novel condensation reaction between phenylnitroso compound and

an olefin. The initial stage appears to be an "ene" addition with rearrangement of the double bond to give a hydroxylamine 7. Then, the hydroxylamine formed is oxidised by the nitroso compound to give the nitroxide observed²⁷⁻²⁹ (Scheme 1.2).



Scheme 1.2 The reactions of nitrosoarenes with olefins.

1.3 Oscillating Reactions

1.3.1 Introduction

Oscillations are familiar phenomena in mechanical systems and in electrical circuits. Direction of motion of an object or an electric current may repeatedly reverse itself with or without damping of the amplitude of oscillation, and repetitive standing or travelling waves may be generated in a continuous medium.

Oscillations in chemical system are not common.³⁰

There are some similarities and differences among the mechanical, electrical and chemical systems.

(1). Mechanical system

In a frictionless (conservative) oscillating mechanical system, the sum of potential and kinetic energies remains constant while they are repeatedly interconverted. Both a coordinate and a momentum have to be used simultaneously to define the instantaneous state. If any friction is present, inertia repeatedly carries the system through the position of minimum potential energy to which it will eventually decay.

(2). Electrical system

In an electrical oscillator the voltage and the current behave very much like potential and kinetic energies, respectively, and both must be stated to define the instantaneous state. The overshoot arises because induction associated with the current behaves very much like mechanical inertia. The oscillations repeatedly carry the voltage through the value to which the system eventually decays, if there is no external source of power.

(3). Chemical system

In a closed chemical system at constant temperature and pressure, the Gibbs free energy is somewhat analogous to a potential energy in a mechanical

system or a voltage in an electrical system. However, the instantaneous state and its rate of change are uniquely defined by specifying the activities of all chemical species and the dynamic laws of the system. There is no dynamic property like a momentum or current that can be specified independently of the free energy of a chemical system and that can be coupled to it conservatively and reversibly. Therefore, chemical change in a closed system leads irreversibly to entropy increase and/or heat evolution.

Thus, many chemists assumed that chemical oscillators are impossible. It was not widely recognized until the 1960's that oscillations are possible for some chemical systems provided they are far enough from equilibrium.³¹ Oscillating reactions have been observed in homogeneous systems^{32,33} and in homogeneous gas reactions³⁴. In far-from-equilibrium chemical systems it is the intermediate or catalyst species that oscillate around pseudo-steady-state values as the free energy of the system monotonically decreases. However, even for these species, the final approach to equilibrium is monotonic.

An acidic bromate solution can oxidize various organic compounds, and the reaction is catalyzed by species like cerous and manganous ions that can generate 1-equivalent oxidants with quite positive reduction potentials. Belousov³⁵ first observed oscillations in such a system, and Zhabotinsky made extensive studies of both temporal³⁶ and spatial³⁷ oscillations.

1.3.2 Descriptive Aspects of Oscillatory Kinetics

When one thinks of oscillation, chemical or otherwise, one usually pictures simple, periodic behaviour in which each cycle is exactly the same as its predecessor. However, periodic oscillation need not be simple, and chemical oscillation is not always periodic.³⁸

In view of the relationship to mechanism, it is important to distinguish and characterize some particular types of oscillatory or non-oscillatory kinetic response and to define carefully various descriptive features. The basic types are listed below.³⁹

Nonperiodic Forms

Pure Monotonic— as illustrated in Figure 1.4(a). The kinetics are described by a rising or decaying curve, and can generally be represented in the form

$$y(t) = C \pm D(t) \quad \dots(1.3.1)$$

where C is a constant, $D(t)$ is a monotonically decaying function such that $D(\infty) = 0$. The kinetics are nonoscillatory.

Overshoot-Undershoot — as illustrated in Figure 1.4(b). In this case the kinetics appear to exhibit an oscillatory response. However, the response is not periodic. Such kinetics can be represented in the form

$$y(t) = C + \sum (\pm) D_i(t) \quad \dots(1.3.2)$$

where $D_i(t)$ is a distinct monotonically decaying function such that $D_i(\infty) = 0$. In general, such curves can exhibit only a finite number (at most $n - 1$) of overshoots and undershoots relative to the final value. In addition they are not periodic — *i.e.*, the time between maxima is not constant.

Periodic Forms

Damped Oscillatory — as illustrated in Figure 1.4(c). In this case the kinetics can usually be represented as

$$y(t) = C + D(t)P(t,\omega) \quad \dots(1.3.3)$$

where $P(t,\omega)$ is some periodic function with fundamental frequency ω and normalized to unit amplitude. It may be noted that the kinetics exhibit an infinite number of maxima and minima, although the amplitude gradually decreases to zero as $t \rightarrow \infty$. In practice, it is often difficult to distinguish this case from the overshoot-undershoot case. Thus, if $D(t)$ becomes very small, further oscillations may not be observable and the kinetics may appear to be of the previous form (Equation 1.3.2).

Sustained Oscillatory — as illustrated in Figure 1.4(d). In this case the kinetics can be represented as

$$y(t) = C + A P(t,\omega) \quad \dots(1.3.4)$$

where A is a constant and the periodic oscillations represented by $P(t,\omega)$ persist as $t \rightarrow \infty$.

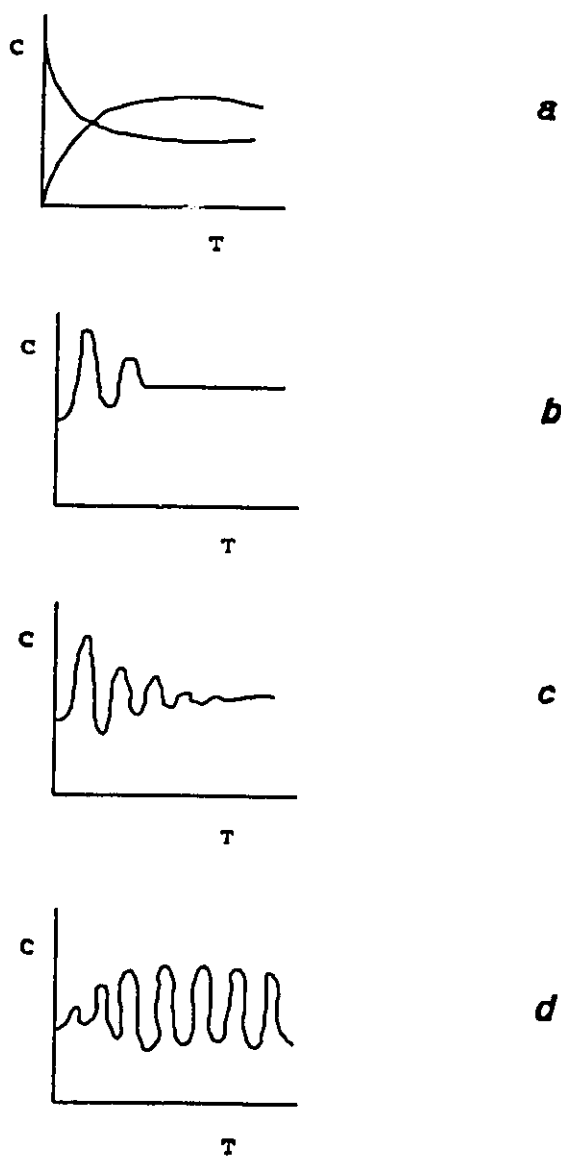


Figure 1.4 Sketches of typical types of kinetics. (a). Monotonic; (b). Overshoot-undershoot; (c). Damped oscillatory; (d). Sustained oscillations (limit cycle). C and T represent concentration and time, respectively.

General Oscillatory — In this general case the kinetics can usually be represented as

$$y(t) = y'(t) + A(t)P(t,\omega) \quad \dots(1.3.5)$$

where $y'(t)$ is the short time average (*i.e.*, the apparent mean value); $A(t)$ is the amplitude modulating function which is slowly varying compared to the periodic component; and $P(t,\omega)$ is the periodic function with normalized amplitude. The function $A(t)$ may be increasing or decreasing, and may approach a constant.

More complicated forms of kinetic response exist and may require a sum of several periodic functions for their description.

Overall, they all possess the following features:

(1) Unlike mechanical and electrical oscillations, chemical systems oscillate around an unstable steady state and they never pass through the point at which all species have equilibrium or steady state values simultaneously.

(2) When oscillations occur it is the concentrations of intermediate or catalyst species which change. In order to describe the trajectory of any homogeneous chemical oscillator, two phase-determining intermediates (at least) are needed.

(3) Oscillations are driven by the overall decrease in free energy as reactants are converted into products in a far-from-equilibrium system.

(4) The minimum kinetic requirement for chemical oscillation is that the

steady state solution to the dynamic equations is unstable to small fluctuations—it evolves to another state which is sometimes oscillatory in nature.

(5) It is necessary to have some feedback interaction to destabilize a steady state. An oscillating system also exhibits a delayed feedback at positions far from the steady state. The necessity for delayed feedback requires there to be at least 3 net dynamic processes each involving at least one of those species.

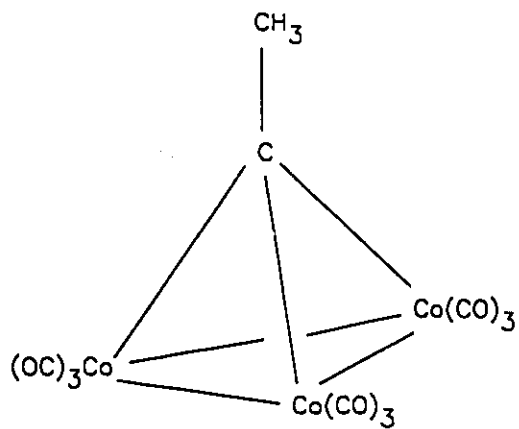
1.4 Fluxionality of Organometallic Compounds

1.4.1 Synthesis of Cobalt Clusters

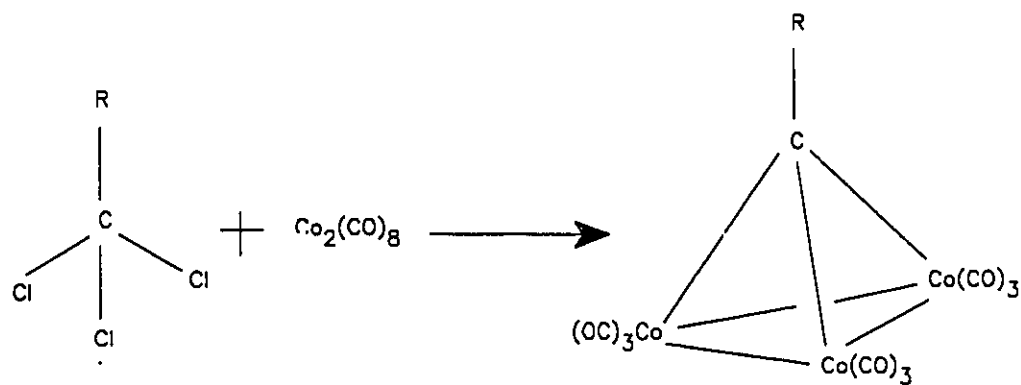
Tetrahedral carbonyl-tricobalt clusters have been known since the late 1950's. The first reported molecule of this kind was discovered when the dicobalt cluster $\text{Co}_2(\text{CO})_6(\text{C}_2\text{H}_2)$ was heated in methanol solution in the presence of aqueous sulfuric acid to give $\text{Co}_3(\text{CO})_9\text{C-CH}_3$, **8**.⁴⁰

It was not long before an improved synthesis of the tricobalt clusters was reported. Reaction of a trichlorinated aliphatic compound with dicobalt octacarbonyl was found to lead to the replacement of the three chlorine atoms by $\text{Co}(\text{CO})_3$ moieties^{41,42,43} as shown in Scheme 1.3.

This technique has been widely utilized since then to synthesize tricobalt clusters with a variety of groups bound to the carbonyl carbon. A selection of these groups is presented in Table 1.1.



8



Scheme 1.3 The trichloroalkane reaction in cluster preparation.

Table 1.1: Groups Incorporated into the $\text{Co}_3(\text{CO})_9\text{C-R}$ Cluster Using the R-CCl_3 Reaction.⁴⁴

Type of Group	R	Yield (%)
Halogen	Cl	46
Aliphatic	CH_3	43
Aromatic	C_6H_5	29
Silyl	$\text{Si}(\text{CH}_3)_3$	41
esters	$\text{C}(=\text{O})\text{OCH}_2\text{CH}_3$	53
alcohols	CH_2OH	0.8
alkenes	$\text{CH}=\text{CH}_2$	45

Though the synthesis of the clusters must be carried out in an anhydrous, oxygen-free environment because of the air-sensitivity of the $\text{Co}_2(\text{CO})_8$ starting material, the finished products are mostly air-stable, with melting points generally above 373K. The complexes are strongly coloured — commonly deep purples, greens, and browns — which aids in the purification process.

1.4.2 Introduction to Fluxionality

Chemists have always been fascinated with molecules that possess more than one thermally accessible structure and which, under certain conditions (especially temperatures) of interest, may pass from one to another of these structures fairly rapidly. This phenomenon is known as fluxionality. It has also been termed stereochemical non-rigidity when the rearrangements can be detected by some chemical or physical means. Molecules whose different configurations are chemically equivalent are considered to be fluxional. These should not be confused with molecules that possess configurations which are chemically non-equivalent. The process by which this class of molecules interconverts configurations is called isomerization or tautomerization, e.g., between keto and enol forms of acetone.

When looking at molecules, one has a tendency to think of static structures, especially in clusters. This is evidenced by the increasing importance of X-ray diffraction as an analytical technique in cluster chemistry. The diffraction methods by which molecular structure is determined are termed instantaneous because the interaction between the molecule and the diffraction wave (10^{-18} to 10^{-20} sec.) is shorter than the time required for molecular motions (10^{-14} sec.) but are still faster than molecular interconversions. A spectrum employing one of these techniques usually is an indication of all molecular configurations present.

1.4.3 NMR Techniques to Study Fluxionality

Although a large number of physical techniques has been used to investigate dynamic processes in organometallic chemistry, the most versatile technique is NMR spectroscopy since the time scale of interaction (10^{-1} to 10^{-9} sec) is comparable with the lifetimes of the configurations present.⁴⁵

The use of variable-temperature NMR allows for some degree of control in the rearrangements occurring in a particular molecule. Ideally one would like to freeze a molecule in a particular conformation and then allow it to undergo fluxional behaviour. In most cases this is impossible. Instead one has to settle for slowing down the rearrangements, observing signals for each configuration at low temperature and making them rapid enough at high temperature so an average signal from all the configurations is observed. The rearrangements between configurations have activation energies associated with them. The temperature range of study for NMR spectrometers ranges from -150°C to $+150^{\circ}\text{C}$ allowing for activation energies between 6 to 25 kcal/mole to be measured.

In addition to determining activation barriers for these rearrangements, NMR is useful in distinguishing whether the process is inter- or intramolecular. In intermolecular processes spin-spin coupling is lost.

1.4.3.1 Line Shape Analysis

For many complexes, line shape analysis has proven to be a reliable and powerful method of obtaining activation energy data.⁴⁶ The method involves obtaining NMR spectra for a number of different temperatures. For a simple two-site uncoupled system, the appearance of the NMR spectrum is fairly simple. At "fast" exchange rates [$k_{\text{rate}} \gg (\nu_A - \nu_B)$], a single peak centred at the population average is observed. At slow exchange rates [$k_{\text{rate}} \ll (\nu_A - \nu_B)$] two sharp signals are observed, separated by $(\nu_A - \nu_B)$. At intermediate rates of exchange, broadened or coalesced spectra are observed. Multisite exchange spectra are more complicated but the changes in appearance to the NMR spectrum are basically the same: sharp peaks broaden and coalesce, with the emergence of sharp peaks centred at population-averaged positions. It is possible to determine the activation parameters from such raw data through either (a) Coalescence Temperature Approximations or (b) Band Shape Curve Fitting. Each of these approaches will be briefly discussed.

(a) Coalescence Temperature Approximations

One can obtain an estimate of the rate constant at the "coalescence temperature", for an exchange process between two equally populated sites which exhibit no spin-spin coupling and have a chemical shift difference of $\Delta\nu$ when no exchange is occurring. The "coalescence" temperature corresponds to the

temperature at which the two lines merge into a single broad line. The rate of interconversion can be calculated from equation (1.4.1.)

$$k_{\text{coal}} = \pi\Delta\nu/1.414 \quad \dots (1.4.1)$$

From this single rate constant, an estimate of the free energy of activation at the coalescence temperature, $\Delta G_c^\#$ may be obtained by use of Eyring equation (Eq.1.4.2)

$$k_c (\text{rate}) = (RT/Nh)\exp(-\Delta G_c^\#/RT) \dots (1.4.2)$$

where $\Delta G_c^\# =$ free energy of activation (kcal/mol)

$R =$ gas constant = 1.987×10^{-3} kcal/deg mol

$N =$ Avogadro constant = 6.022×10^{23} molecules/mol

$h =$ Planck constant = 1.584×10^{-37} kcal s

Combination of Eq.1.4.1 and 1.4.2, and rearrangement, gives:

$$\Delta G_c^\# = RT_c (\ln\sqrt{2R/\pi Nh} + \ln T_c/\delta\nu) \dots (1.4.3)$$

T_c is the coalescence temperature. The first term of the equation is a constant, 22.96. Thus, the chemical shift separation of two peaks and the temperature of coalescence can be used to give a value for the energy barrier between the two isomers represented by the peaks. It must be noted that (1.4.1) is valid only when there are equal populations in the two states at equilibrium. For

this reason, the energy calculation using (1.4.3) can only be performed when there is an equal distribution of the molecules between the possible isomers.

(b) Computer Band Shape Simulations

This method involves visually comparing theoretical computer generated NMR spectra with experimentally obtained variable temperature curves. The rate of interconversion between exchanging sites is altered until a visual match to the experimental lineshape is found. By calculating the rate constants for a number of temperatures, a rate constant versus temperature data table is compiled. This data may be analyzed by constructing an Arrhenius plot where $\ln k$ is plotted against $1/T$ (Eq.1.4.4).

$$\ln k = -E_a/RT + \ln A \quad \dots (1.4.4)$$

The energy of activation is then extracted from the slope.

In this thesis, the computer program EXCHANGE which was generously provided by Professor R. E. D. McClung (University of Alberta) is used for the band shape simulations.

1.4.3.2 Spin-Saturation Transfer Spectroscopy

Since the discovery of the fluxionality of $\text{Fe}(\eta^1\text{-C}_5\text{H}_5)(\eta^5\text{-C}_5\text{H}_5)(\text{CO})_2$ there has been considerable interest in the dynamic behavior of polyenes and polyenyls

attached to metals.⁴⁷ In part, interest was raised from the realization that the mechanism could be determined from the observation of differential line broadening during the onset of fluxionality. By the early seventies it appeared that the dynamic behavior of polyene and polyenyl metal complexes could be interpreted in terms of the least motion model with the metal undergoing [1,2]-shifts coupled with carbonyl scrambling.⁴⁸ Subsequently, a number of observations were made which were very difficult to explain using this approach. Thus, $(\eta^4\text{-C}_8\text{H}_8)\text{-Fe}(\text{CO})_3$, **9**, is highly fluxional with $\Delta G^\ddagger = 6.8$ kcal/mol while $[(\eta^2\text{-C}_8\text{H}_8)\text{M}(\eta^5\text{-C}_5\text{H}_5)\text{-(CO)}_2]^+$, **10**, (M = Fe, Mn), and $[(\eta^6\text{-C}_8\text{H}_8)\text{Fe}(\eta^5\text{-C}_5\text{H}_5)]^+$, **11**, have $\Delta G^\ddagger > 20$ Kcal/mol.⁴⁹⁻⁵² Mingos developed a theoretical model⁵³ for the dynamic behavior of these systems based on the Woodward-Hoffmann rules⁵⁴ of organic chemistry. This theory permitted the explanation of concomitant carbonyl scrambling and metal migration in **9** and the increase in activation energy found in **10** and **11**. A review of the fluxional organometallic system examined the application of these rules.⁵⁵

For many complexes, line-shape analysis has proven to be a reliable and powerful method of obtaining activation energy data. However, there are several difficulties associated with using line shape analyses:

(a). It is frequently restricted to values of the Gibbs activation energy which fall in the range of $\Delta G^\ddagger = 5 - 16$ Kcal/mol, *i.e.*, corresponding to a rate constant, k , of $10^2 - 10^8$ s⁻¹ because of instrumental limitations and thermal stability of the compound.⁵⁶

(b). Line-shape analysis frequently requires a pure compound, but quite often an organometallic compound exists as a mixture of different isomers.^{57,58}

(c). Some of the organometallic compounds are thermally unstable which prohibits heating of the sample so as to probe directly an exchange process by standard NMR line-shape analysis.⁵⁹

(d). There may be more than one fluxional process which occurs on the NMR time scale and line shape analysis cannot differentiate between them.^{60,61}

(e). Overall, line shape analysis simply provides information on the rate at which a nucleus leaves each site. It provides no information on the fate of each type of nucleus. As a consequence, the mechanism must be deduced from incomplete information.⁵⁷

It was impossible to study the fluxionality of some organometallic compounds which have high activation energies until B.E. Mann applied the magnetization transfer method to the complexes. The importance of this is that the rate range that is accessible by this method, down to 10^{-2} s^{-1} , is much slower than that which can be measured by exchange broadening. The magnetization transfer approach to fluxionality is superior to line shape analysis since it permits attachment of the label of non-equilibrium Boltzmann population to each site, and the movement of each nucleus can therefore be monitored. This provides unambiguous information on the fluxional pathway and mechanism.⁵⁶

(A). Magnetization Transfer Measurements

In this experiment, one of the exchange sites is "labelled" with a non-equilibrium Boltzmann population. Chemical exchange transfers this "label" to other exchanging sites in the molecule, where it can be detected in the form of a decrease in the intensity of the signals from these sites.⁵⁶ Consider the energy level diagram, Figure 1.5,⁵⁶

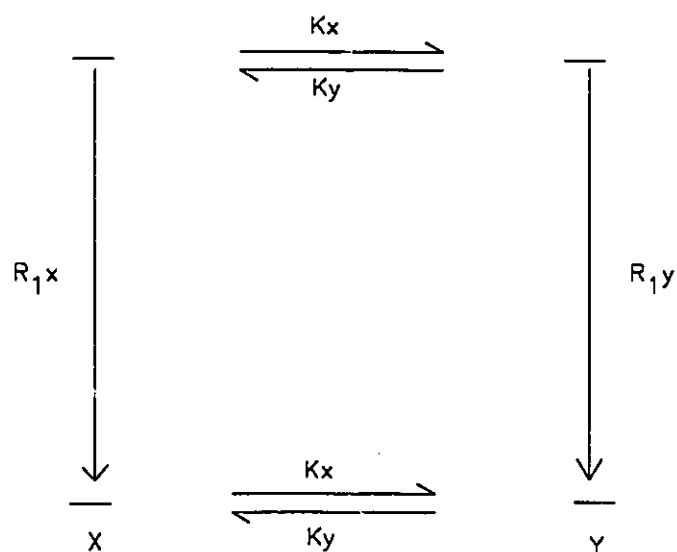


Figure 1.5 Energy level diagram for exchanging spins.

For a representative spin in two species, X and Y, which are slowly interconverting with first order rate constants k_x and k_y . The equilibrium constant is k_x/k_y , and at equilibrium each species will have a Boltzmann distribution in its spin states.

Exchange between X and Y takes place without change of spin state, so the energy level diagram shows separate equilibria for both upper and lower energy levels. Now, selective saturation of the X resonance increases the population of its upper level at the expense of the lower level. Therefore, there is increased transfer of spins to the upper level of Y and decreased transfer to its lower level. The population distribution of Y will approach that of X. However, spin-lattice relaxation of Y, at a rate R_{1Y} , will always tend to return the population distribution of Y to normal.

There is, therefore, a competition between saturation transfer at a rate, k_x , and a relaxation at a rate, R_{1Y} . If relaxation is much more rapid than exchange, then the population distribution at Y will remain unchanged; in contrast, if exchange is much faster than relaxation, Y will be completely saturated. When the rates are comparable, and significant but incomplete population changes are induced at Y, then the rate k_x can be measured. The importance of this method is that processes that occurring with rate constants of roughly 10^{-2} to 10^2 s⁻¹ may be probed.⁵⁶

The power of this method is apparent in multisite exchange processes. For a system consisting of n magnetically non-equivalent sites, when one site is saturated then equation (1.4.5) applies for the i^{th} site:^{62,63}

$$dM_i/dt = - \sum_{j=1(i \neq j)}^n k_{ij} M_j + \sum_{j=1(i \neq j)}^n k_{ji} M_i + \{M_i(\infty) - M_i\}/T_{1i} \quad \dots(1.4.5)$$

where T_{1i} is the spin-lattice relaxation time for site i , k_{ij} is the first order rate constant for exchange from site i to site j , M_i is the magnetization at site i at time t , and $M_i(\infty)$ is its equilibrium magnetization.

The easiest method to use, especially if the exchange is between two sites, is to decouple at one site. Most NMR spectrometers are equipped to decouple ^1H but not other nuclei.⁶⁴ Both the alternative methods are essentially the same. One uses a low-power transmitter to apply a selective π pulse to one side, and in the other this selective pulse is generated using the DANTE pulse sequence.⁶⁵

(1). Magnetization Transfer using Decoupling:

This experiment was first proposed by Forsen and Hoffman.^{66,67} It is easily performed by using the pulse sequence

$$\begin{aligned} &^1\text{H (observed)} \quad (D_1 - D_2 - \pi/2 - \text{acquire})_n \\ &^1\text{H (decouple)} \quad (\text{on} \quad \text{off} \quad \quad \quad)_n \quad \dots(1.4.6) \end{aligned}$$

where D_1 is a relaxation delay, typically $5T_{1i}$, and D_2 is a variable time to give the exchange rate, with values ranging from 0 to $5T_{1i}$.

This method has been applied to $(\eta^6\text{-C}_8\text{H}_8)\text{Cr}(\text{CO})_3$, **12**, to demonstrate that the mechanism of exchange is predominantly [1,3] shifts, with a small contribution

from [1,2] shifts.⁶⁸ Previous work using line shape analysis had failed to distinguish between [1,3] and random shifts.⁶⁹

(2). Magnetization Transfer using Selective Pulses: The DANTE Pulse Sequence.⁷⁰

In this technique the longitudinal magnetization of a resonance is measured as a function of time after the perturbation of another resonance with which it is exchanging. This perturbation may be a 180° pulse, e.g., the selective inversion which may easily be achieved using a DANTE (Delays Alternating with Nutations for Tailored Excitation) pulse sequence with cumulative flip angle 180° on resonance:

$$(\alpha - D)_n \quad \dots(1.4.7)$$

This DANTE pulse sequence consists of a regular train of identical, short, strong radiofrequency pulses, each with flip angle $\alpha \ll \pi$ radian, spaced D seconds apart. Only those resonances that are offset from the transmitter by $\Delta\nu = n/D$ Hz, where n is an integer, are excited to a significant extent. Fourier analysis of the pulse sequence is approximately equivalent to the superposition of a number of continuous radiofrequency signals with frequencies spaced $1/D$ Hz apart, which can be regarded as "sidebands" symmetrically disposed with respect to the

transmitter frequency at ν_0 , $\nu_0 \pm 1/D$, $\nu_0 \pm 2/D$, etc.. For the magnetization close to one of these sideband conditions, the pulse sequence acts just like a weak selective pulse. A suitable choice of transmitter frequency ν_0 and repetition rate $1/D$ will ensure that only one side band (normally the first sideband at $\nu_0 \pm 1/D$ falls with the spectrum of interest).

For magnetization transfer measurements, the DANTE pulse sequence is modified to give the sequence

$$\{ D_1 - (\alpha - D_2)_m - \alpha - D_3 - \pi/2 - \text{acquire} \}_n \quad \dots(1.4.8)$$

In this case a selective π pulse is applied through the $m + 1$ small α pulses. During the period D_3 , chemical exchange transfers the magnetization from the selectively excited signal and the degree of transfer is measured by applying the $\pi/2$ general pulse. D_3 is an experimental variable and normally the experiment is repeated ca. 10 times with value of D_3 varying from $1 \mu\text{s}$ to $5T_1$.⁵⁵

Two major problems can lead to erroneous results from these measurements. These problems are associated with the use of an abundant nucleus, e.g., ^1H , ^{19}F , or ^{31}P . The experiment involves perturbing the Boltzmann population of one nucleus and examining how that perturbation is transferred to the other sites. This perturbation can be transferred by the NOE mechanism.⁵⁶ NOE only occurs significantly intramolecularly in compounds containing more than

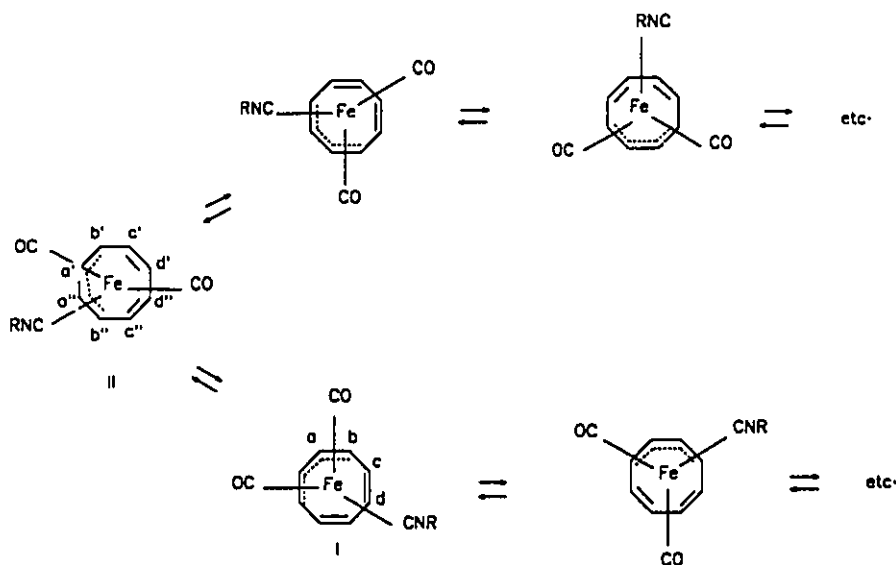
one ^1H environment, and it builds up at a rate determined by T_1 . Hence this problem can be avoided by using low abundance nuclei, e.g., ^{13}C , where ^{13}C - ^{13}C NOEs are negligible, by examining intramolecular exchange, or by setting the conditions, e.g., temperature, so that the exchange is fast compared with R_{1Y} . Decoupling can remove intramolecular coupling, preventing the use of peak heights for the rate measurements and necessitating integration of the spectra. This problem is easily avoided by using the decoupler to perturb the system and then turning it off before observing the effect of the perturbation.

Hails, Mann and Spencer^{71,72} provided the first direct experimental evidence which differentiates between the Woodward-Hoffmann rules and the least motion coupled with carbonyl scrambling. They prepared $[\text{Fe}(\eta^4\text{-C}_8\text{H}_8)(\text{CO})_2\text{L}]$, $\text{L} = \text{MeNC}$, Pr^iNC , Bu^iNC , PhNC , $2,6\text{-Me}_2\text{C}_6\text{H}_3\text{NC}$, $2,4,6\text{-Me}_3\text{C}_6\text{H}_2\text{NC}$, and $\text{P}(\text{OMe})_3$. The detailed mechanistic investigation was performed with $\text{L} = \text{CNPr}^i$, **13**, using ^{13}C magnetization transfer since at low temperature isomers I and II are present in approximately equal concentration. The mechanism using the Woodward-Hoffmann rules makes predictions as to the interconversion of isomers and the movement of specific carbon atoms in the cyclo-octatetraene ring (Scheme 1.4).

The ^{13}C NMR spectrum is shown in Figure 1.6. The specific 180° pulse was applied to the signal b' or b'' at δ 55.5 ppm. At -118°C the subsequent transfer of magnetization was monitored as a function of time. Magnetization transfer occurred first to the signals at δ 86.6, a , and δ 128.2 ppm, c' or c'' , and was a

maximum after ca. 10ms, see Figure 1.6(c) where it is displayed as the difference between this spectrum and that after 1 μ s to emphasize the changes.

This observation is completely consistent with Scheme 1.4 where the inverted magnetization at carbon b' is first transferred to sites c' and a. The mechanism involving least motion would transfer magnetization to a' and c' first while carbonyl scrambling would transfer it to b and b". This is inconsistent with experimental observations and both the least motion and carbonyl scrambling mechanisms can be rejected as being the predominant mechanism for this compound. This example clearly showed that the magnetization transfer measurements can provide a powerful check of mechanism and prove the validity of the Woodward-Hoffmann mechanism.



Scheme 1.4 The mechanism of interconversion of different isomers in **13**.

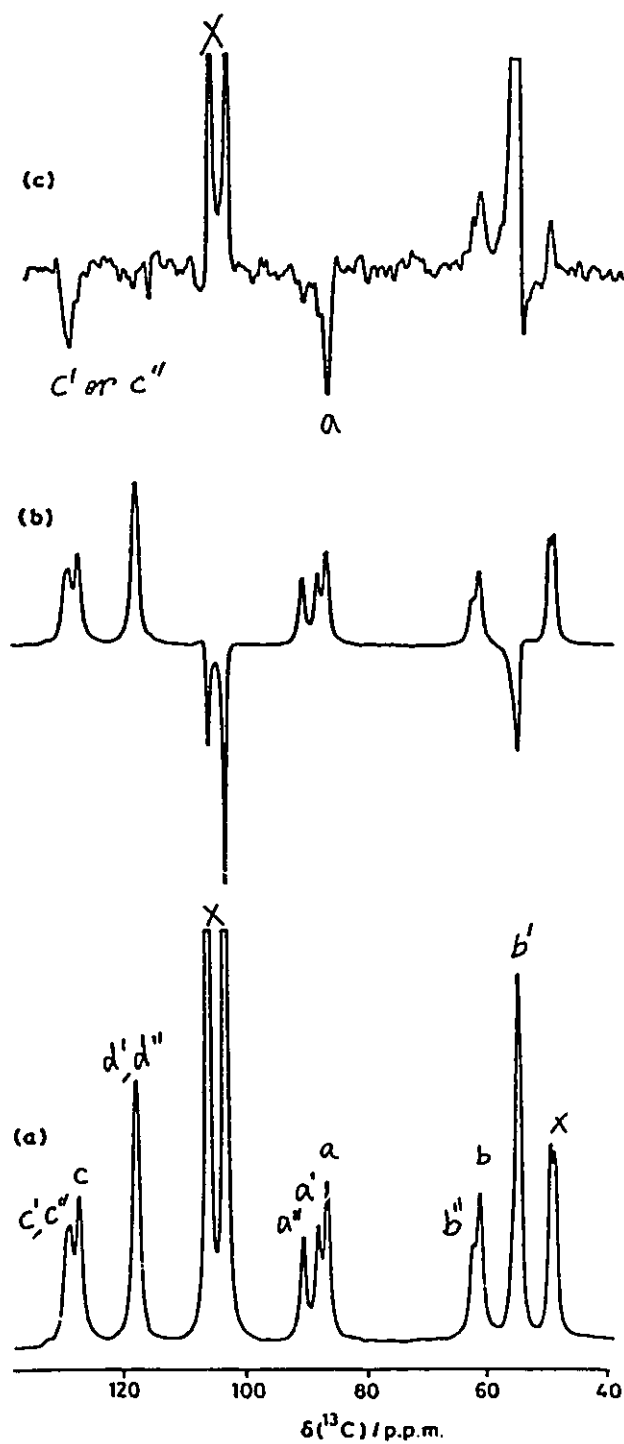


Figure 1.6(a). A partial spectrum of **13** in CD_2Cl_2 - CH_2Cl_2 , at -118°C .

(b). 1 μs after applying a 180° pulse at 55.5 ppm.

(c). A difference spectrum obtained by subtracting (b) from that obtained at 10 ms.

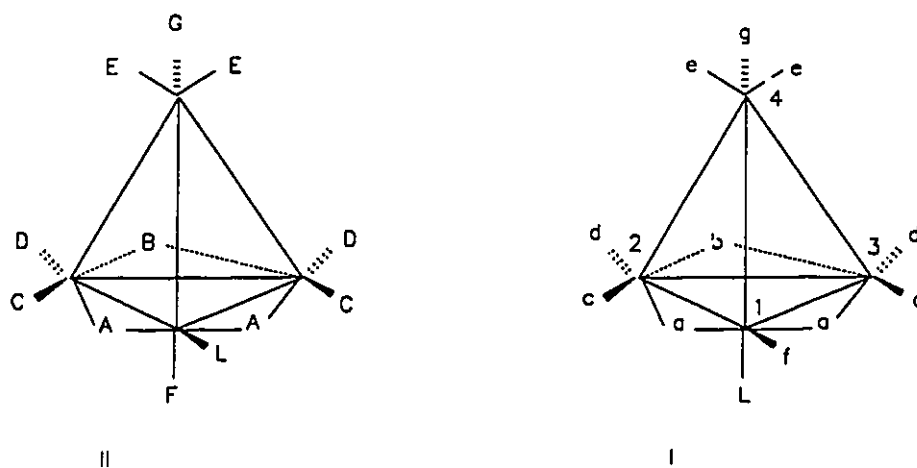
This method has also been used to study the mechanism of fluxionality of $[\text{Ru}(\eta^6\text{-C}_8\text{H}_8)(\eta^4\text{-C}_7\text{H}_9)]$, **14**, and $[\text{Ru}(\eta^4\text{-C}_8\text{H}_8)(\eta^4\text{-C}_7\text{H}_8)\text{L}]$ [$\text{L} = \text{PEt}_3$ or $\text{P}(\text{OMe})_3$], **15**. ($\text{C}_7\text{H}_8 = \text{bicyclo}[2.2.1]\text{hepta-2,5-diene}$).⁷³ The previous line shape analysis of **14** has shown that all the signals broaden by the same amount at the onset of fluxionality, and coalesce to give a singlet at high temperatures, which allows one to deduce that the mechanism is either a [1,3]-shift or a random shift.⁷⁴ However, the magnetization transfer measurements indicate that the dominant mechanism of **14** and **15** is not a random shift, or a [1,3]-shift, but a [1,5]-shift, with the [1,3]-shift occurring at a slower rate. Takats and McClung studied $(\eta^3\text{-C}_7\text{H}_7)\text{-Os}(\text{CO})_3(\text{SnPh}_3)$ which exists as a mixture of two noninterconverting geometrical isomers. Both isomers exchange by [1,5]-shifts.⁷⁵ In addition, this method has been quantitatively applied to the osmium complex, $[\text{Os}(\eta^6\text{-C}_8\text{H}_8)(\eta^4\text{-C}_8\text{H}_{12})]$, ($\text{C}_8\text{H}_{12} = \text{cyclo-octa-1,5-diene}$). The results showed four separate fluxional processes at different temperatures and 16-electron intermediates are involved.⁷⁶

The fluxional behavior of a large number of compounds with a σ -polyenyl ligand can be expected to follow the same rules as found for organic migration reactions involving polyenyl groups. However, Heinekey and Graham⁷⁷ reported that σ -cycloheptatriene derivative of rhenium, $(\text{CO})_5\text{Re}(\eta^7\text{-C}_7\text{H}_7)$, **16**, was fluxional by a [1,7]-shift while only the [1,5] pathway was observed for $(\eta^7\text{-C}_7\text{H}_7)\text{SnPh}_3$, **17**.^{78,79} A further investigation by Graham indicated that the ruthenium derivative $(\eta^5\text{-C}_5\text{H}_5)\text{Ru}(\text{CO})_2(\eta^7\text{-C}_7\text{H}_7)$, **18**, displayed two concurrent fluxional pathways, a [1,5] and a [1,7] shift.⁸⁰

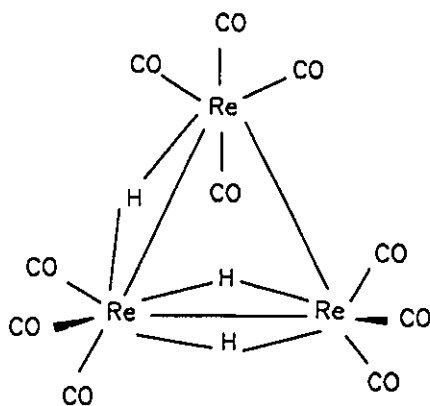
Another major application of the magnetization transfer method is to study the mechanism of carbonyl fluxionality in clusters. An important mechanism of carbonyl scrambling on clusters was proposed by Cotton in 1966,⁸¹ it is called the merry-go-round. It involves concerted bridge opening and closing of the carbonyl ligands to move them around the cluster. Most studies of carbonyl scrambling on clusters have relied on line shape analysis. This method yields little information on the mechanism. The Forsen-Hoffmann method permits the labelling of one carbonyl with a non-equilibrium magnetization, and this magnetization can be followed as it moves through the molecule. Unfortunately, only a few experiments have been reported. One of the examples of the application of this technique was to $\text{Ir}_4(\text{CO})_{11}\text{PEt}_3$, **19**. There are two isomers I and II which exist in the solution. The ratio is 6:1.

There are seven different carbonyl sites for each isomer.^{82,83} Selective π DANTE pulses were applied to five carbonyls, separately. The results indicate that the fully bridge-opened species is not involved in the process. R. Ros obtained similar results in the study of $\text{Ir}_4(\text{CO})_9(\mu_2\text{-CO})_2(\mu_2\text{-SO}_2)$, **20**.⁸⁴ Recently, the quantitative analysis has been completed and a computer program to fit the data is now available.^{85-87,62,63} This procedure has been used to study the fluxional process in $[\text{Re}_3(\text{CO})_{10}\text{H}_3]^{2-}$, **21**. Four separate rate processes were obtained.⁸⁸ The lowest energy process being the local scrambling of the carbonyls of the doubly hydride bridged $\text{H}_2\text{Re}(\text{CO})_3$ unit; the next process can be viewed as "olefin"

$\text{ReH}(\text{CO})_4$, rotation about the "acetylene" $[(\text{OC})_3\text{Re}(\mu\text{-H})_2\text{Re}(\text{CO})_3]^2-$, followed by the signal hydride moving to the unbridged edge and finally local carbonyl scrambling on the $\text{ReH}(\text{CO})_4$.



19



21

These results clearly demonstrate the inherent dangers in using line shape analysis to determine the mechanism of multisite exchange problems.

Magnetization transfer studies, however, can be quite demanding and time-consuming as each line has to be perturbed in turn while observing the response of all other lines. For closely spaced resonances a sufficiently selective perturbation of a single line may even be impossible.⁸⁹

(B). Two Dimensional Techniques — 2-D Exchange Spectroscopy (NOESY, EXSY)

2D chemical exchange spectroscopy (EXSY or NOESY) developed by Ernst,^{89,90} is an almost ideal alternative to magnetization transfer studies in the sense that all exchange pathways can be elucidated simultaneously by a simple and uncritical technique. The pulse sequence is:

$$D_p - \pi/2 - D_1 - \pi/2 - D_{c,i} - \pi/2 - D_2 \quad \dots(1.4.8)$$

There are three 90° pulses and four independent time period: preparation, evolution, mixing and detection. In each time period a different type of information on the spin system is acquired. During the preparation interval, transverse magnetization vectors are created (*i.e.*, signals are generated). The first 90° pulse

generates transverse magnetization in a non-selective fashion so that, during the evolution period D_1 , all the various magnetizations evolve according to their specific chemical shift anisotropies—"frequency labelled". A second 90° pulse returns the modulated magnetization back to the Z-axis. These two pulses create an effect similar to the one created by the selective 180° pulse in the spin saturation transfer experiment. In the next time interval, mixing or exchange occurs and thus magnetization is transferred to the other exchange sites. At the end of the mixing period, the final 90° pulse converts the Z-components back into the observable transverse magnetization which is sampled as a function D_2 , the acquisition time. This experiment is repeated, during which the evolution time, D_1 , is incrementally increased. This yields a data matrix $S(D_1, D_2)$ which, after two-dimensional Fourier transformation yields a two dimensional spectrum $S(f_1, f_2)$. The f_1 frequency axis represents the normal 1D-NMR spectrum, as it precesses during the evolution time before the exchange take place. The f_2 frequency axis represents the 1D-NMR spectrum after the exchange period has taken place. In the absence of any exchange, peaks are observed only along the diagonal in the 2D-exchange spectrum. The presence of off-diagonal signals (cross-peaks) indicates that an exchange process has occurred during the mixing time involving the spins with chemical shifts connected by the cross peaks. The intensity of the cross peak is proportional to the mixing time and the rate of interconversion. In a qualitative 2D EXSY experiment, the absence of the length of the mixing period

is very important. If it is too short, the probability that the transfer occurs is too small. If it is too long, other transfers other than one-step pathways proceed. Certainly, NOE and J-coupling will also contribute to the cross-peaks.⁹¹ From the literature overview of the dynamic stereochemical systems studied up to now by the 2D EXSY experiment, it seems to provide most useful information in *uncoupled* spin systems or in those that somehow can be treated as such. Thus scalar couplings complicate the interpretation of 2D EXSY spectra much more than they do in 1D NMR and make it almost impossible in strongly coupled systems.

An example of the 2D method applied to N,N- dimethylacetamide, **22**, is shown in Figure 1.7. From an examination of Figure 1.7 it is clear that "off-diagonal" peaks are created and observed in the "slow exchange" region of the dynamic process. If the rate is too slow, then only diagonal elements will be observed. While if the rate is too fast, a coalesced or fast exchange spectrum will be observed which will contain little useful information.

1.4.4 Applications of 2D EXSY Techniques

2D EXSY spectroscopy provides a very valuable method for determining the exchange pathways of nuclei. The first application of this technique to study a chemical exchange process in an organometallic complex was reported in 1982 by Benn.⁹² Since then, only a few 2D NMR studies have been reported for

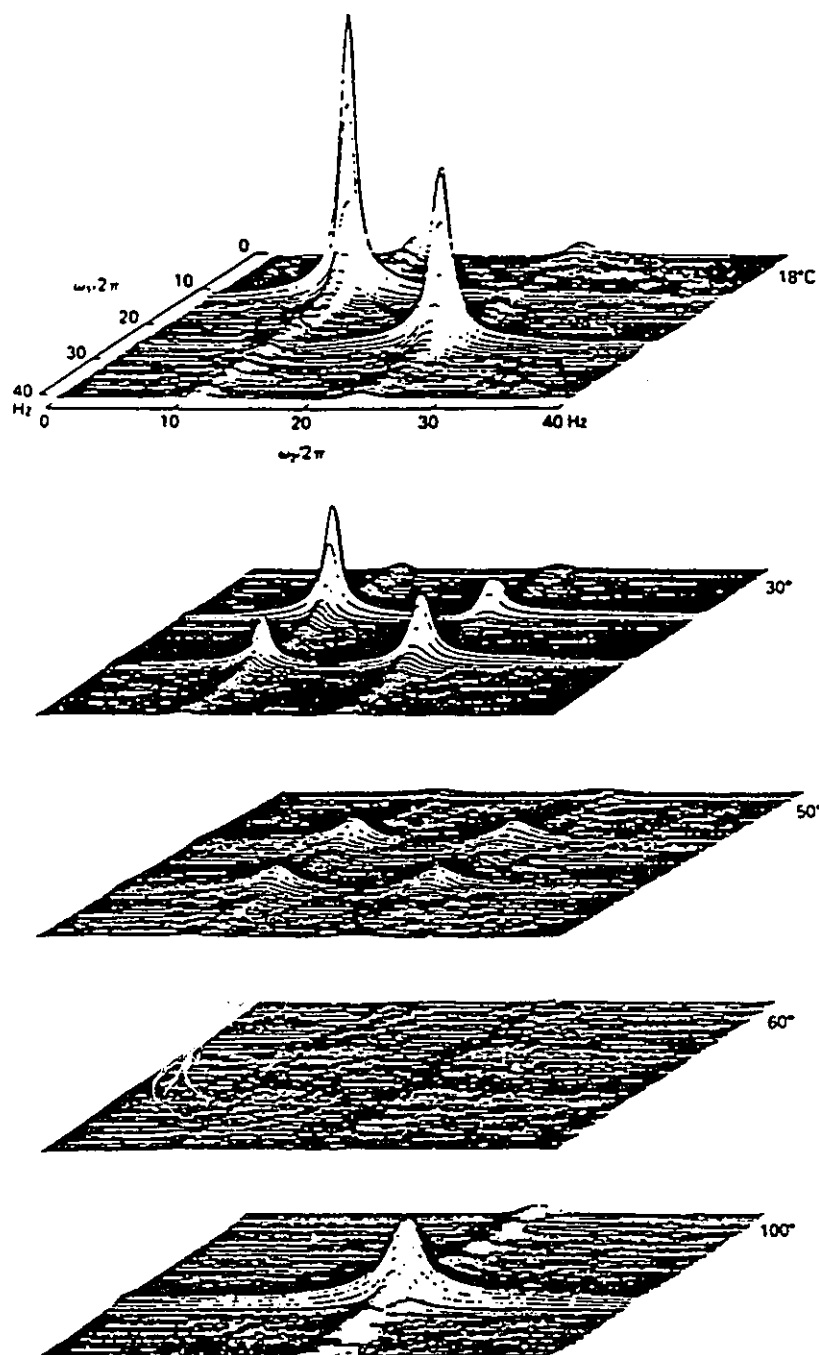
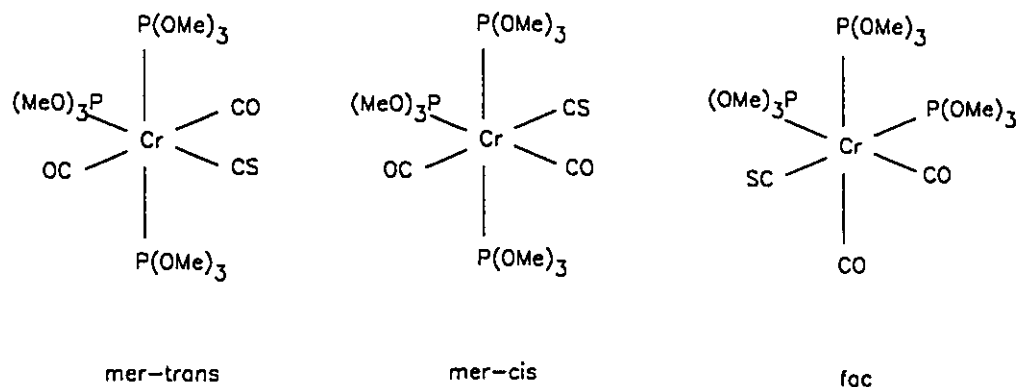


Figure 1.7 2D EXSY diagrams for N,N-dimethylacetamide, showing the exchange of the two methyl groups for five different temperatures.

transition organometallic complexes. They can be divided into two groups. One is using this technique to study the intramolecular exchange of different isomers.

Butler has used this experiment to map out the exchange pathway in $\text{Cr}(\text{CO})_2(\text{CS})\{\text{P}(\text{OMe})_3\}_3$, **25**.^{93,94} All the three possible isomers are present in solution, **fac**, **mer-trans** and **mer-cis**. (see Scheme 1.5).



Scheme 1.5 Three Possible isomers of **25**.

The NOESY experiment in Figure 1.8 clearly demonstrates exchange between isomers. Thus the two equivalent ^{31}P nuclei at δ 191.4 from the **mer-cis** isomer clearly exchange with both types of phosphorus in the **mer-trans** isomer, at δ 188.6 and δ 181.2. The exchange of the **mer-trans** and **mer-cis** isomer provides convincing proof of a dynamic rearrangement *via* a trigonal twist mechanism rather than a bicapped tetrahedron (See Scheme 1.6). The bicapped

tetrahedron mechanism would preserve the coupling pattern for each phosphorus nucleus in the two isomers while, for the trigonal prismatic twist, the triplet would become a doublet and the doublet of the trans phosphorus atom would be transformed into a triplet. No exchange was definitively detected involving the **fac** isomer.

The second major application is to study fluxional molecules. Benn's group first published the 2D EXSY ^{13}C data for the fluxional cycloheptatriene complex, $(\eta^4\text{-C}_7\text{H}_8)\text{CoCp}$, **27**.⁹⁵ From the 2D contour map, there is clear evidence of chemical exchange of C-1 with C-6, C-2 with C-5, and C-3 with C-4. One possible mechanism for these exchanges (not involving C-7 of the methylene group) involves a series of two consecutive 1,2-shifts. It should be remembered, however, that 1,3-shifts or a dissociative mechanism could not be ruled out on the basis of the available evidence.

The first 2D EXSY experiment applied in organometallic clusters was published in 1985 by Hawkes and coworkers.⁹⁶ They determined both the relaxation ($R_1 = 0.21 \text{ s}^{-1}$) and the rate of intramolecular CO exchange ($k = 1.21 \text{ s}^{-1}$) between the equatorial and axial CO groups in the basal plane of the molecule on the terminal osmium atoms of $\text{Os}_3\text{H}_2(\text{CO})_{10}$, **28**; this was done on a heavily ^{13}C enriched sample, that, in an interesting combined COSY-EXSY experiment, also allowed the determination of ^{13}C - ^{13}C coupling constants. It was concluded that for this relatively simple system the one-dimensional method (selective inversion of

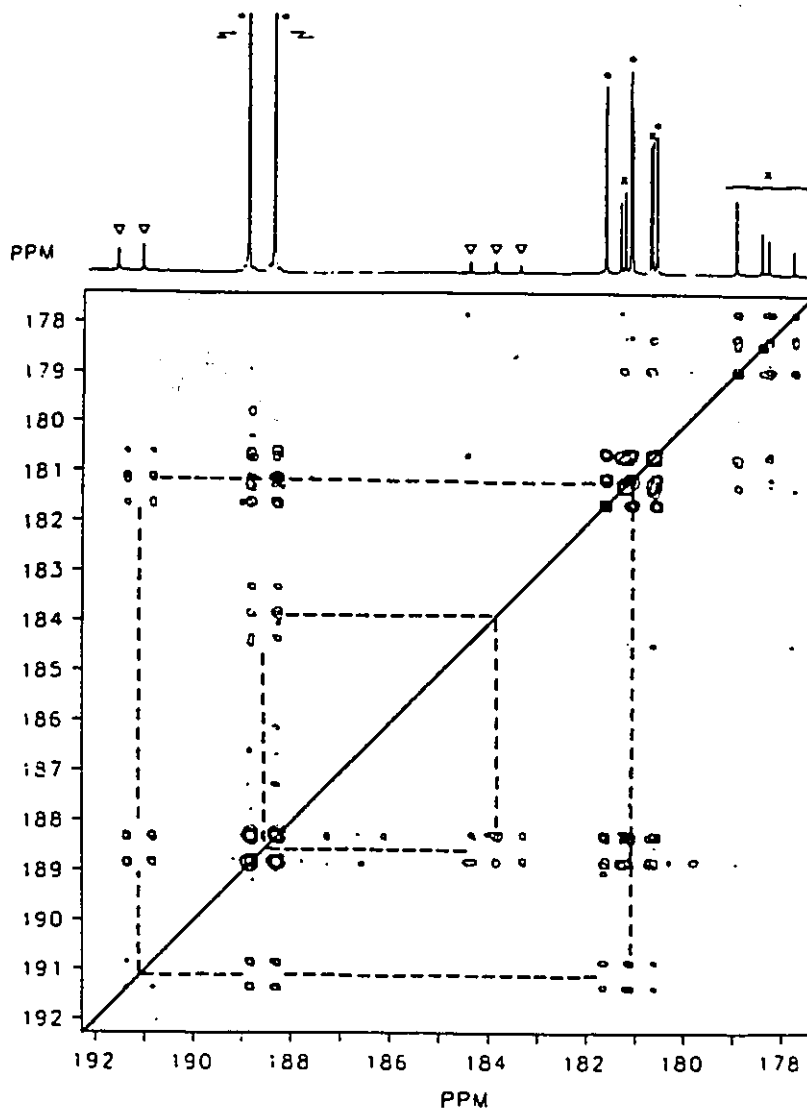
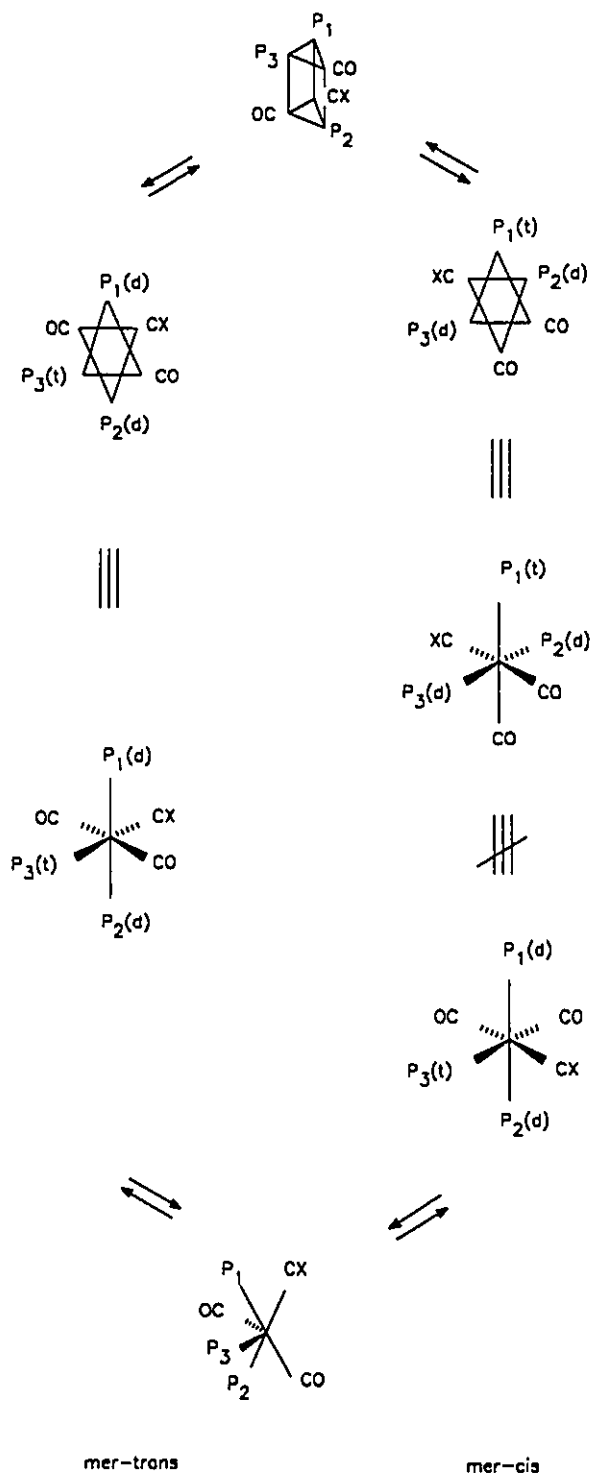


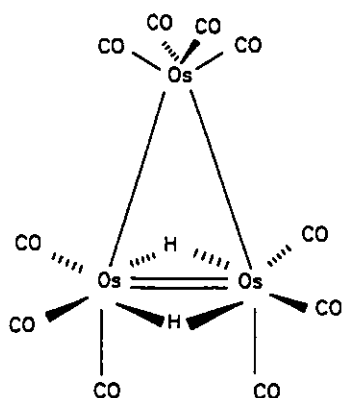
Figure 1.8 2-D ^{31}P contour map for $\text{Cr}(\text{CO})_2(\text{CS})[(\text{MeO})_3\text{P}]_3$ in deuteriotoluene at 61°C on a Varian XL-300 spectrometer. All three isomers exhibit an AB_2 coupling pattern.

∇ , mer-cis; $*$, mer-trans; X, fac.

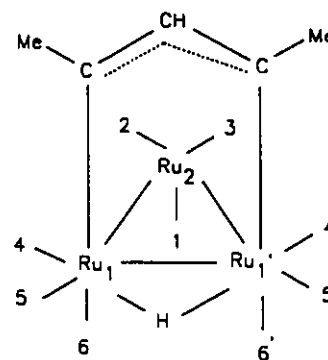


Scheme 1.6 Possible mechanisms for the interconversion of the **mer-I** and **mer-II** isomers.

one of the exchanging resonances) was more economical in spectrometer time than the 2D EXSY experiment. However, it was anticipated that in the application of these methods to more complex multisite exchange problems, the two dimensional approach may prove more valuable. A subsequent similar study was performed on $\text{Ru}_3(\mu\text{-H})(\text{CO})_9(\text{CH}_3\text{C}=\text{CH}-\text{CCH}_3)$, **29**.⁹⁷ The results indicated that there was no exchange between the CO's on Ru^2 and the CO's on Ru^1 and Ru^1' . The rates of these local rotations were determined the same value of 3.83 s^{-1} .



28



29

In 1988, Strawczynski *et al.* reported a successful qualitative application of the 2D EXSY spectroscopy and variable-temperature ^{13}C -NMR to study the CO-site exchange in $[\text{Ir}_4(\text{CO})_{11}\text{Br}]^{1-}$, **30**.⁹⁸ The structure of **30** is shown in Scheme 1.7. The three bridging CO's define the basal plane containing three Ir-atoms of the tetrahedral metal core. Terminal CO's are either apical if located on the fourth Ir-atom, radial when located more or less in the basal plane, or axial if approximately

perpendicular to this basal plane. The Br-atom is located on a basal Ir-atom and is axial according to the X-ray crystal structure. From the line-shape analysis, they were able to decide that the lowest energy process was the a-b-d-f site exchange which consistent with the merry-go-round process of the basal CO's. The 2D ^{13}C NMR spectra is shown in Figure 1.9. The a-b-d-f site exchange is clearly visible. The second fluxional process is also apparent, when a mixing time of 50 ms is used. This process corresponds to a site exchange d-c-e, while a, b, and f do not exchange with c or e. Since two apical CO's (e) now participate in the exchange, this second exchange process must involve CO ligands bridging to alternative faces of the Ir_4 tetrahedron.

Scheme 1.7 shows the possible mechanism, starts with synchronous edge-bridging of 2 CO's on one of the two triangular faces of configuration I which share the $\text{Ir}_1\text{-Ir}_4$ edge. This leads to the radial isomer II from which a second synchronous bridging of 2 CO's brings about the observed d-c-e exchange (configuration III) and leaves the unique apical CO (g) in its pseudo-*trans*-position relative to the Br ligand. This rules out the possibility of an unbridged intermediate (configuration IV) which has been proposed for the axial isomer of $\text{Ir}_4(\text{CO})_{11}(\text{PEt}_3)$, since if configuration IV is considered, a site exchange of a and f (configuration V) becomes inevitable, and is not consistent with the experimental results.

They also investigated two complexes $[\text{Ir}_4(\text{CO})_{10}(\text{diarsine})]$, **31**, and $\text{Ir}_4(\text{CO})_7(\mu\text{-CO})_3(1,5\text{-cyclooctadiene})$, **32**, bear a bidentate ligand chelating one

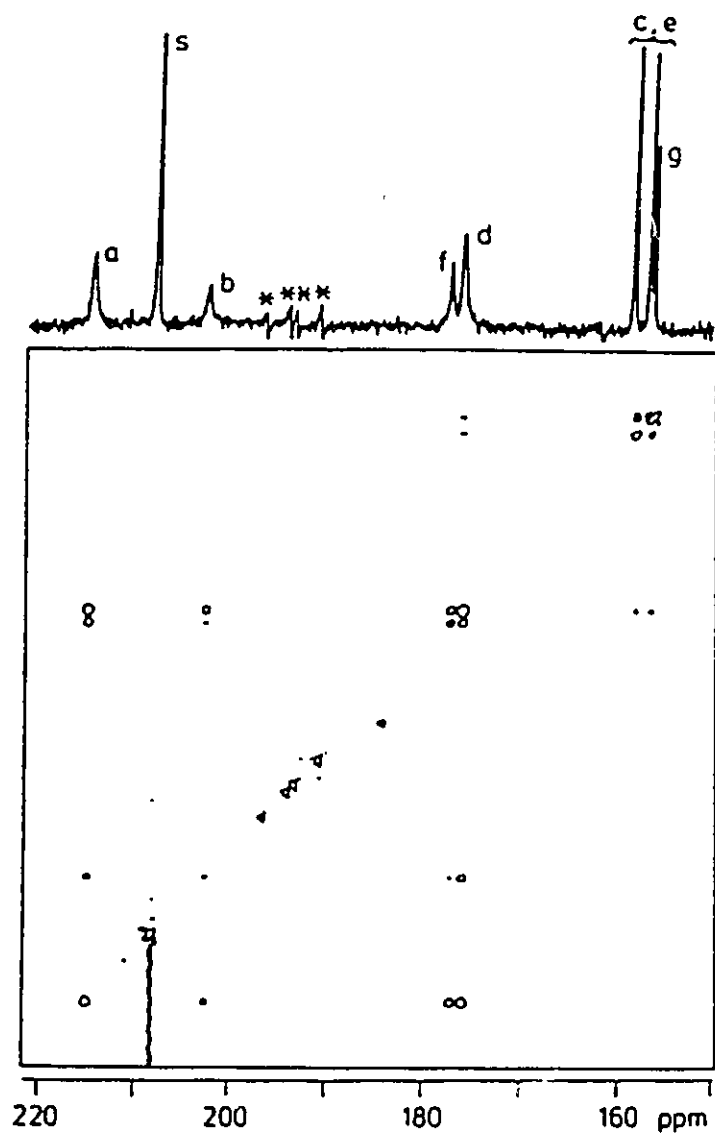
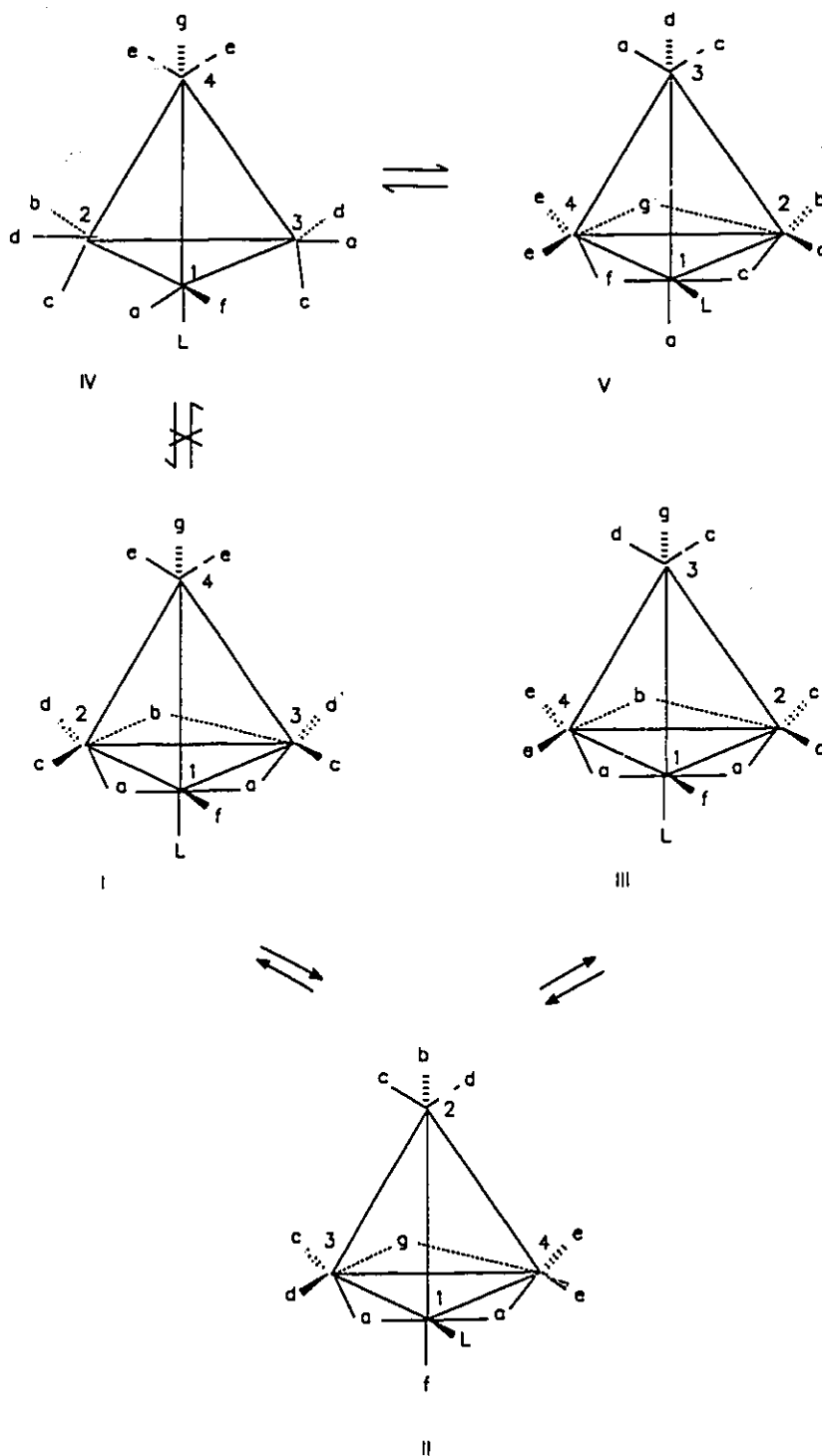
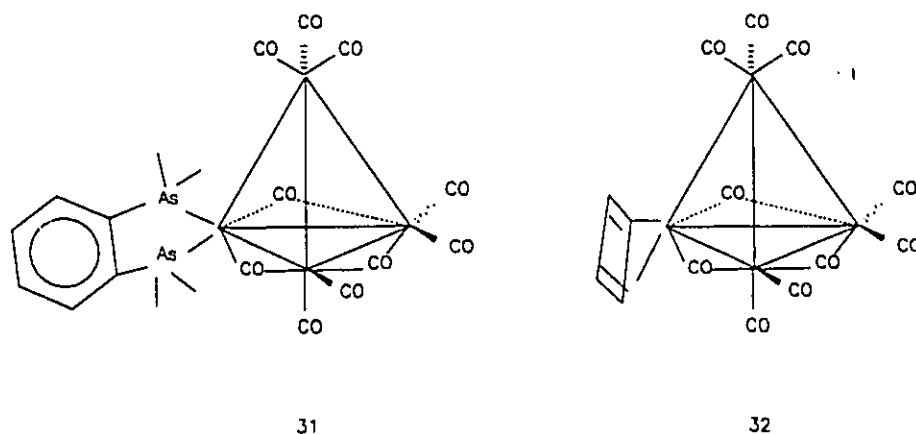


Figure 1.9 2D ^{13}C NMR spectrum of $[\text{Ir}_4(\text{CO})_{11}\text{Br}]^{1-}$ at 175K (mixing time: 50 ms; s = solvent; * = reflected signals).

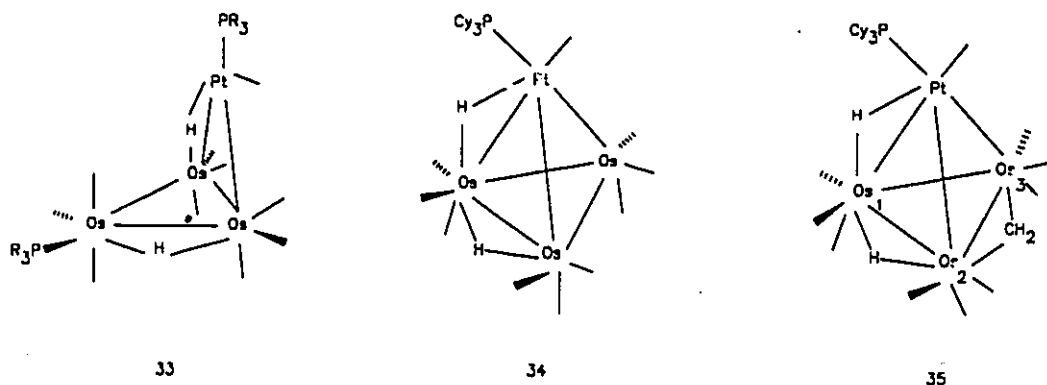


metal atom of the basal face of the Ir_4 tetrahedron.⁹⁹ The CO-site exchange with lowest activation energy proceeds *via* a concerted edge-bridging of CO's to an alternative face of the metal core in **31**, where as that in **32** occurs *via* an unbridged intermediate.



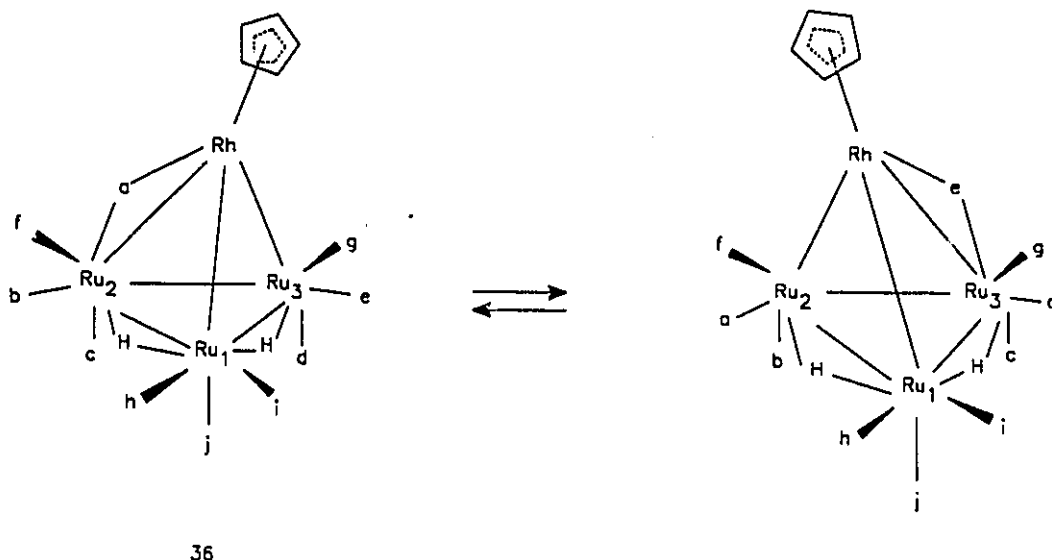
In 1988, Ewing *et al.* studied the fluxional behavior of the tetrahedro-triosmium-platinum clusters.¹⁰⁰ ^{13}C EXSY NMR studies on $[\text{Os}_3\text{Pt}(\mu\text{-H})_2(\text{CO})_{10}(\text{PCy}_3)_2]$, **33**, ($\text{Cy} = \text{c-C}_6\text{H}_{11}$), show high-energy CO exchange between Pt and Os and suggest a novel "flipping" of the butterfly framework through a planar transition state. In 1989, Farrugia reported similar complexes of $\text{Os}_3\text{Pt}(\mu\text{-H})_2(\text{CO})_9(\text{PCy}_3)(\text{CNCy})$, **34**, and $\text{Os}_3\text{Pt}(\mu\text{-H})_2(\mu\text{-CH}_2)(\text{CO})_9(\text{PCy}_3)(\text{CNCy})$, **35**.¹⁰¹ 1D and 2D EXSY ^{13}C NMR spectra reveal two CO exchange processes, a lower energy tripodal rotation in the two equivalent $\text{Os}(\text{CO})_3$ groups ($\Delta G^\ddagger_{200} = 12.4 \text{ Kcal/mol}$) and

a higher energy process, commensurate with the hydride mobility, which completely scrambles all CO ligands ($\Delta G^\ddagger_{225} = 14.4$ Kcal/mol). The 2D EXSY experiment of **35** shows three CO exchange processes; separate tripodal rotations of two of the $\text{Os}(\text{CO})_3$ groups ($\Delta G^\ddagger_{318} = 19.2$ and 21.1 Kcal/mol) and the racemization of the cluster by hydride migration ($\Delta G^\ddagger_{318} = 20.2$ Kcal/mol).



Lindsell and his co-workers also reported the 2D EXSY NMR studies on $[\text{RhRu}_3(\mu\text{-H})_2(\mu\text{-CO})(\text{CO})_9(\eta\text{-C}_5\text{H}_5)]$, **36**.¹⁰² It involves a pairwise exchange of eight CO groups resulting from a "rocking motion" of CO ligands around a single Rh-Ru(2)-Ru(3) triangular face. (We note that it is actually a "merry-go-round" of the CO's around the triangular face. See Scheme 1.8).

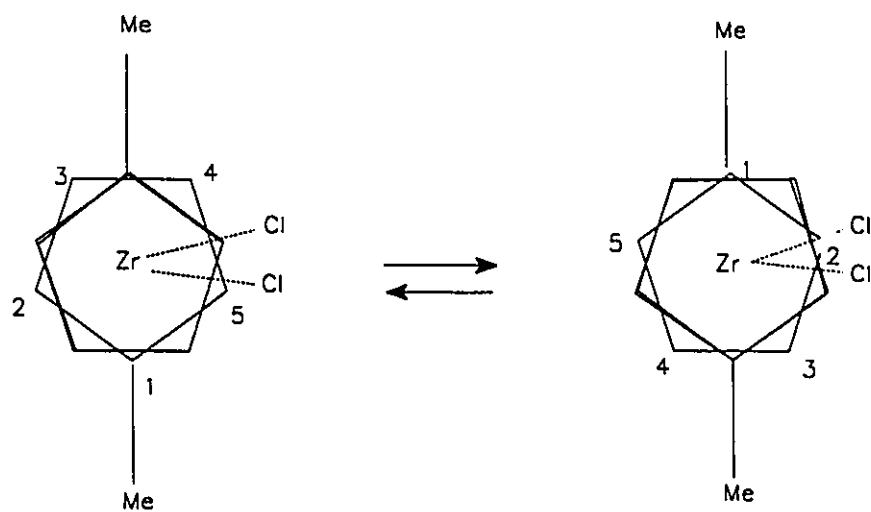
Benn in 1988 reported the first solid-state 2D Exchange ^{13}C CP/MAS NMR spectra of organometallic compounds.¹⁰³ ^{13}C CP/MAS spectra of various



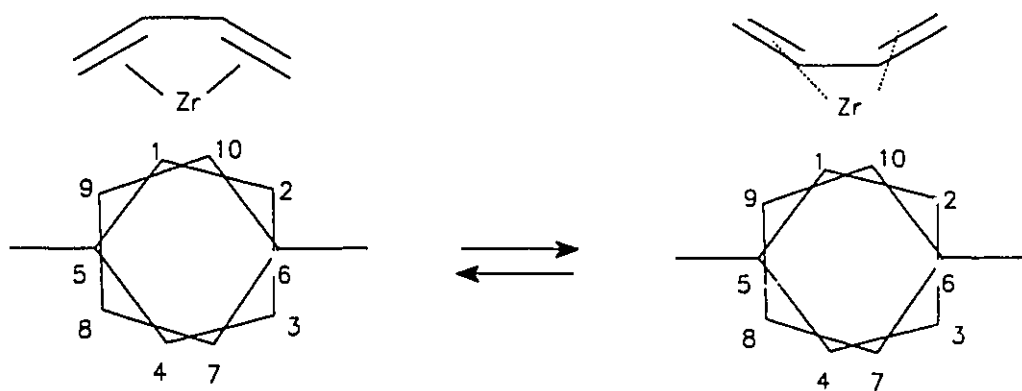
Scheme 1.8 The lowest energy exchange process of **36**.

microcrystalline bent metallocenes of the type $(\eta^5\text{-}^R\text{Cp})_2\text{ML}_2$ have been obtained ($\text{M} = \text{Zr}, \text{Hf}$; $\text{R} = \text{alkyl}$; $\text{L} = \text{Cl}$; **37**, $\text{L}_2 = \text{alkyl-substituted } \eta^4\text{-C}_4\text{H}_6$, **38**). ^{13}C 2D exchange spectrum of **37** in 333 K reveals that in the solid state there is slow rotation of the ^RCp rings around the central metal coordination axis. This process leads to pairwise coalescence of the methine carbons. Line-shape analysis yields $\Delta\text{G} = 16.9 \text{ Kcal/mol}$ as barrier for the $^{\text{Me}}\text{Cp}$ rotation. The barrier increases significantly when more bulky substitutes ($\text{R} = \text{Et}, t\text{-Bu}$) are introduced. In contrast, in the solution spectra of **37** between 180 and 300 K there are only two signals for the methine carbons,¹⁰⁴ indicating that under these conditions the barrier for ^RCp

rotation is less than 5 Kcal/mol. 2D CP/MAS exchange spectra of **38** can be explained by diene topomerization (See Scheme 1.9). The results indicate that many fluxional processes known to occur in solution can occur in the solid state. Furthermore, these processes can be easily monitored by 2D CP/MAS particularly if variable-temperature facilities are available.



37



38

Scheme 1.9 Two intramolecular fluxional processes occurring in **37** and **38** in solid state.

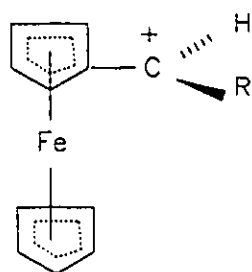
CHAPTER TWO

THE REACTIONS OF NITROSOARENES WITH CATIONIC CYCLOHEXADIENYL COMPLEXES OF IRON TRICARBONYL: AN ESR STUDY

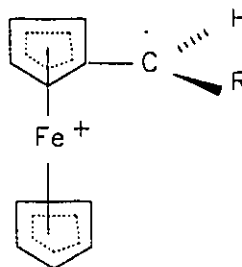
2.1 *Introduction*

There are several reports in which the reaction of nitroso compounds with diamagnetic organometallic complexes yields nitroxide radicals. Cais *et al.*^{105,106} studied the reactions of nitrosobenzene with cationic iron complexes with substituted cyclopentadienyl, cycloheptadienyl and other dienyl ligands. In the first type of compound the ferrocene **39a** had a CHR^+ substituent and it was suggested that reaction might occur *via* a structure **39b** containing Fe^{3+} and CHR moieties. Spin trapping of the latter fragment seemed a very reasonable experiment to try. Nitroxide radicals corresponding to addition at the $\text{CHR}\cdot$ group were indeed detected but the observation that the precursor CH_2OH compounds gave the same products with equal ease cast doubts on the radical mechanism. An alternative mechanism involving nucleophilic attack by the nitrosobenzene was suggested. Subsequent X-ray crystallographic studies of both iron and osmium analogues of

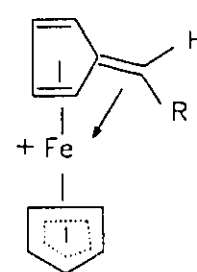
39 reveal that the exocyclic methylene is bent towards the metal by 20° and so the best representation of the ferrocenylmethyl cation may well be that shown in **39c**.^{107,108} Returning to the reactions of nitroso compounds with organometallic molecules, we note that Belousov and Kolosova have recently reported the reactions of 2-methyl-2-nitroso-propane with a number of iron carbonyls. A variety of radicals, including some nitroxides, were observed by ESR and the mechanisms of the reactions were discussed in some detail.¹⁰⁹



39 a



39 b



39 c

In the present project, we describe initially the reactions of several nitroso compounds with the $[(\eta^5\text{-cyclohexadienyl})\text{tricarbonyliron(II)}]^+$ cation, **40**. This complex, which is particularly notable for the stabilization of the organic cation brought about by complexation, should provide a site for facile nucleophilic attack by the nitroso compound. This complex is also a model for cationic derivatives of

steroids, and spin labelling of the steroidal system¹¹⁰ has considerable potential for structural and stereochemical studies. Thus, having established the reactivity pattern for the model system **40**, we then describe the behavior of several nitroso-arenes with the novel cation **42** in which the metal-stabilized cyclohexadienyl system is located in the steroidal B ring.¹¹¹

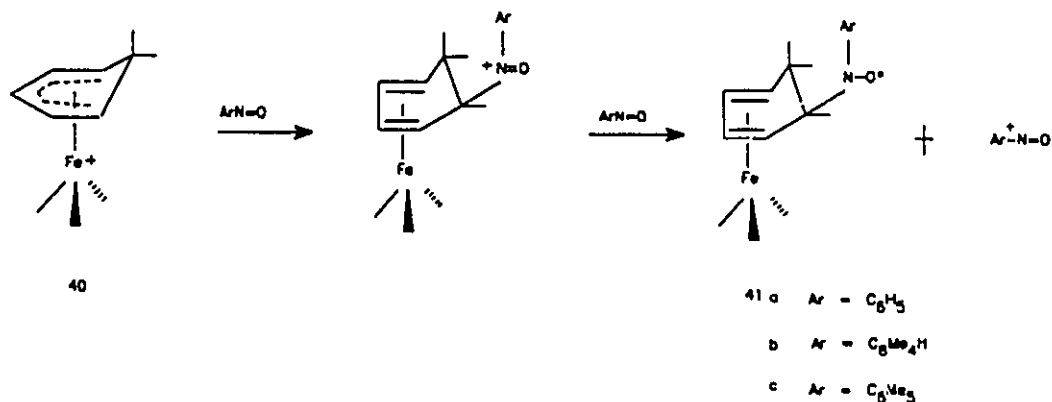
2.2 Results

[[η^5 -Cyclohexadienyl]tricarbonyliron(I)]⁺tetrafluoroborate, **40**, was allowed to react with nitrosobenzene, nitroso-2,3,5,6-tetramethylbenzene (nitrosodurene) and also with nitroso-pentamethylbenzene. In each case nitroxide radicals were detected by ESR spectroscopy and we describe each separately since their reactions are not identical.

2.2.1 Reaction of Cation 40 with C₆H₅NO

Upon mixing a well-degassed solution of **40** in acetonitrile with nitrosobenzene at ambient temperature, an ESR spectrum appears within about 20-30 minutes. This spectrum (see Figure 2.1a) comprises a triplet of quintets. The triplet structure is ascribed to ¹⁴N hyperfine splitting ($a_N = 11.2\text{G}$) and the pseudo-quintet to ¹H coupling where four protons exhibit almost equivalent

hyperfine coupling ($a_H = 3.0G$). The radical has a g value of 2.0067 and the spectrum remains unchanged after several days in a sealed ESR tube. The spectrum disappears if the tube is irradiated with a high pressure mercury lamp and in this case no other ESR signal is observed. The spectrum illustrated in Figure 2.1a is attributed to the nitroxide radical **41a** formed by addition of C_6H_5NO to the cationic carbon atom of the iron complex **40**.



If the above reaction is carried out in dichloromethane rather than in acetonitrile, the same ESR spectrum is initially observed. However, this radical is not stable in CH_2Cl_2 and, after one day, a complex spectrum develops which eventually simplifies to that shown in Figure 2.1c. This latter radical is very stable and has been identified as diphenylnitroxide. A simulated spectrum, using literature hyperfine coupling constants¹¹² is presented as Figure 2.1d.

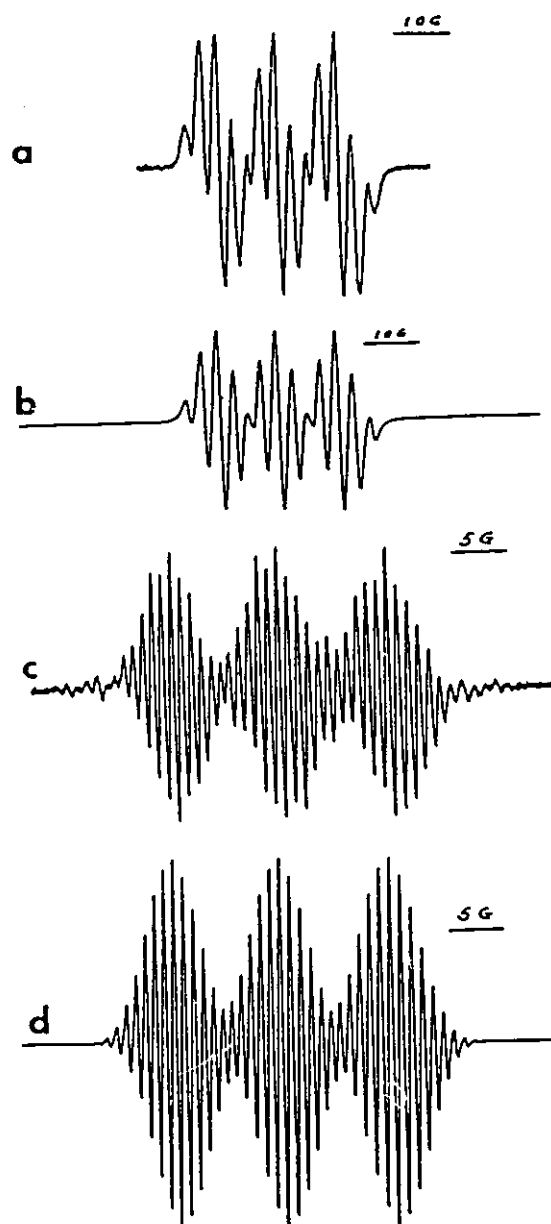




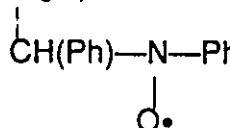



Figure 2.1 ESR spectra from the reaction of **2** with C_6H_5NO . (a) in CH_3CN ; (b) simulation of (a) using the data in Table 2.1; (c) in CH_2Cl_2 after 6 days; (d) simulation of $(C_6H_5)_2N-O\cdot$ using data from ref. 116.

Although $(C_6H_5)_2NO\cdot$ is clearly the major product of the reaction, there are also some additional lines from a second radical. During this reaction the colour of the solution changes from yellowish-green to dark yellow and the formation of some brown precipitate is observed. The ESR parameters obtained from the above spectra are collected in Table 2.1.

2.2.2 Reaction of Cation 40 with C_6HMe_4NO

Nitrosodurene has some advantage over nitrosobenzene as a spin trap in that the resulting ESR spectra are generally simpler and hence easier to analyse. In the solid, and also in solution, nitrosodurene exists as a colourless dimer.¹¹² When such a solution is warmed a light green colour appears and this has been attributed to dissociation of the dimer to reactive monomer. It was found that, even at room temperature when the concentration of monomer is very small, nitrosodurene reacts with **40** and the product gives an ESR spectrum. The mixture of the cationic iron complex, **40**, and C_6HMe_4NO is not soluble in either pure acetonitrile or pure chloroform; there is, however, sufficient solubility in a 1:1 mixture of these solvents to obtain ESR spectra. The initial spectrum (Figure 2.2a) is a triplet of doublets ($a_N = 13.75G$, $a_H = 3.6G$, $g = 2.0069$) as anticipated. However, over a period of several days, new and more complex spectra appear as shown in Figure 2.2b.

Table 2.1 ESR parameters for phenylnitroxide radicals.

Substances	Solvent	Temp	g	a value(G)	Ref.
$(\text{CO})_3\text{FeC}_6\text{H}_7\text{N}-\text{Ph}$ 	CH_2Cl_2	293K	2.006 ₇	N: 11.2 H(<i>o,p</i>): 3.0 H(CH): 3.0	This work
	CH_3CN	293K	2.006 ₇	N: 11.2 H(CH): 3.0 H(<i>o,p</i>): 3.0	This work
$(\text{CO})_3\text{FeC}_7\text{H}_9\text{N}-\text{Ph}$ 	CH_2Cl_2	293K		N: 11.1 H(CH): 2.95 H(<i>o,p</i>): 3.0	106
$\text{C}_5\text{H}_5\text{FeC}_5\text{H}_4$ 	CH_2Cl_2	R.T.	2.006 ₇	N: 10.9 H(CH): 2.95 H(<i>o</i>): 2.73;2.95 H(<i>p</i>): 2.95 H(<i>m</i>): 1.0	105
$\text{S}-\text{N}-\text{Ph}^a$ 	CH_3CN	293K	2.006 ₈	N: 11.0 H(β -H): 2.95 H(γ -H): 0.98 H(<i>o,p</i>): 2.75 H(<i>m</i>): 0.98	This work
$\text{C}_6\text{H}_{11}-\text{N}-\text{Ph}$ 	C_6H_{12}	300K		N: 10.5 H(<i>o,p</i>): 3.0 H(CH): 3.0	132
$\text{Ph}-\text{N}-\text{Ph}$ 	CH_2Cl_2 DMSO	298K		N: 10.1 H(<i>o,p</i>): 1.9 H(<i>m</i>): 0.9	116

^a S = steroidal group, see text.

The final spectrum (Figure 2.2c) corresponds to a very stable radical and no subsequent changes were observed over a further period of four days. Very similar spectra were obtained in $\text{CH}_3\text{CN}/\text{CH}_2\text{Cl}_2$ (1:1) mixtures. However, if the reaction is run in a 1:1 mixture of dimethylsulfoxide and benzene there is evidence for a second less abundant radical and the spectrum (Figure 2.3a) can be simulated (Figure 2.3b) as a superposition of two six-line spectra with an intensity ratio of 4:1. The parameters extracted from this analysis were $a_{\text{N}} = 13.4\text{G}$, $a_{\text{H}} = 3.3\text{G}$, and $g = 2.0068$ for the more intense species and $a_{\text{N}} = 13.95\text{G}$, $a_{\text{H}} = 12.3\text{G}$, $g = 2.0060$ for the minor component. It may be noted that the parameters for the more intense species are very similar to those obtained in $\text{CH}_3\text{CN}/\text{CHCl}_3$ mixtures. These spectra also changed with time to give initially a complex spectrum (Figure 2.3c) but finally reverted to a six-line spectrum (Figure 2.3d) very similar to the initial more intense spectrum. Further spectra were obtained in other mixed solvent systems containing chloroform or methylene chloride in addition to benzene and DMSO. The radicals obtained were essentially the same as those of Figure 2.3 suggesting that acetonitrile is necessary to obtain the spectrum shown in Figure 2.2c. Hyperfine coupling constants and g values obtained from the nitrosodurene spectra are collected in Table 2.2.

2.2.3 Reaction of Cation 40 with $\text{C}_6\text{Me}_5\text{NO}$

The reaction was examined in mixtures of DMSO and benzene (1:1) and in benzene alone. The results in the two solvent systems were very similar.

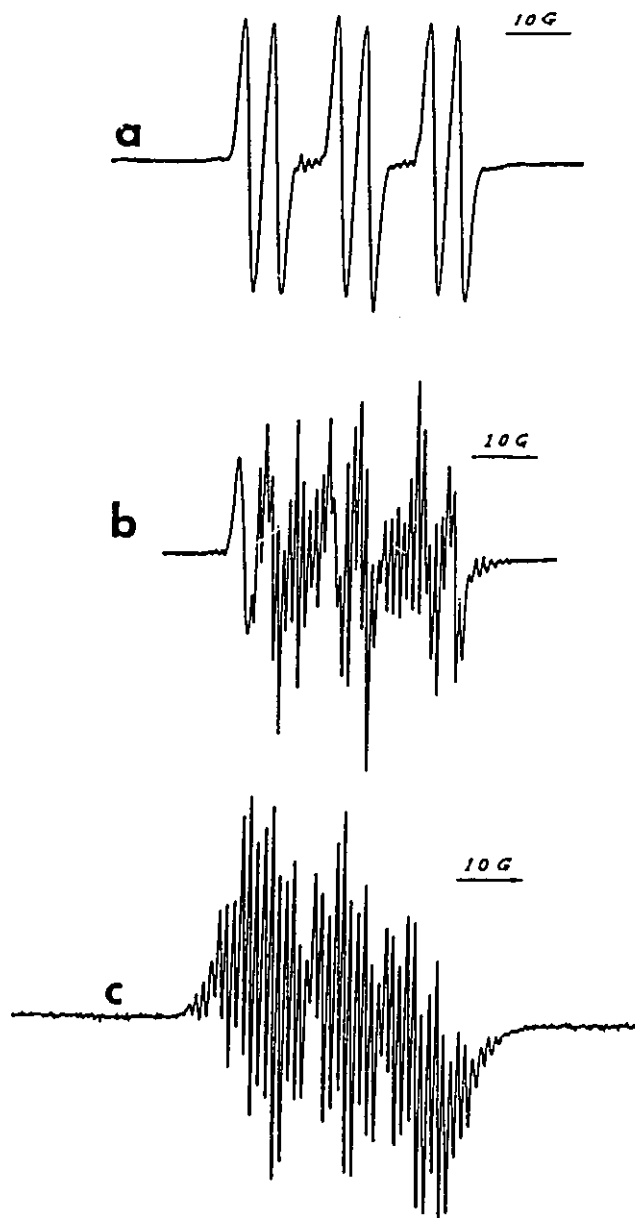


Figure 2.2 ESR spectra from the reaction of **2** with C_6Me_4HNO in 1:1 $CH_3CN/CHCl_3$ (a) after 30 min; (b) after 20 h; (c) after 4 days.

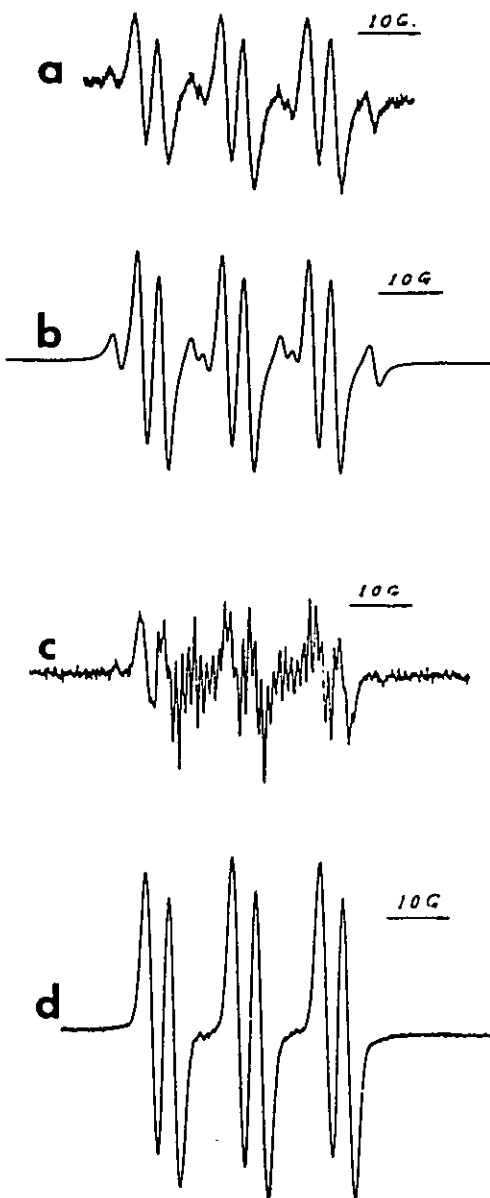


Figure 2.3 ESR spectra from the reaction of **2** with C_6Me_4HNO in 1:1 benzene/dimethylsulfoxide. (a) after 30 min; (b) simulation of (a) using the data in Table 2.2; (c) after 18 h; (d) after 5 days.

In both cases, the initial spectra consisted principally of two six-line patterns which in this case were of roughly equal intensity. There are two additional lines in the wings of the spectrum which we are unable to assign. The hyperfine parameters obtained from the two six-line spectra are very similar to those obtained from the corresponding nitrosodurene reaction. On standing, more complex, but not analysable, spectra appear. Eventually most of the additional lines disappear and a six-line spectrum corresponding to one of the original spectra is left as was the case for nitrosodurene in the DMSO/benzene solvent mixture. The data for this set of spectra are given in Table 2.2.

2.2.4 Reaction of 42 with C₆H₅NO

The steroidal cation **42** reacts with nitrosobenzene in acetonitrile solution almost immediately and causes a colour change from yellowish-green to yellow and, after a day, it becomes red. The spectrum shown in Figure 2.4a is that observed after 3 hours and exhibits the expected triplet pattern for the nitrogen coupling as well as the hyperfine interactions with the phenyl protons. However, there is an extra and unanticipated relatively large doublet splitting (2.95G) which, over the course of 24 hours, gradually disappears. The final spectrum (Figure 2.4b) still exhibits hyperfine coupling to the C₆H₅N moiety but the 2.95G doublet splitting has disappeared. The data are collected in Table 2.1.

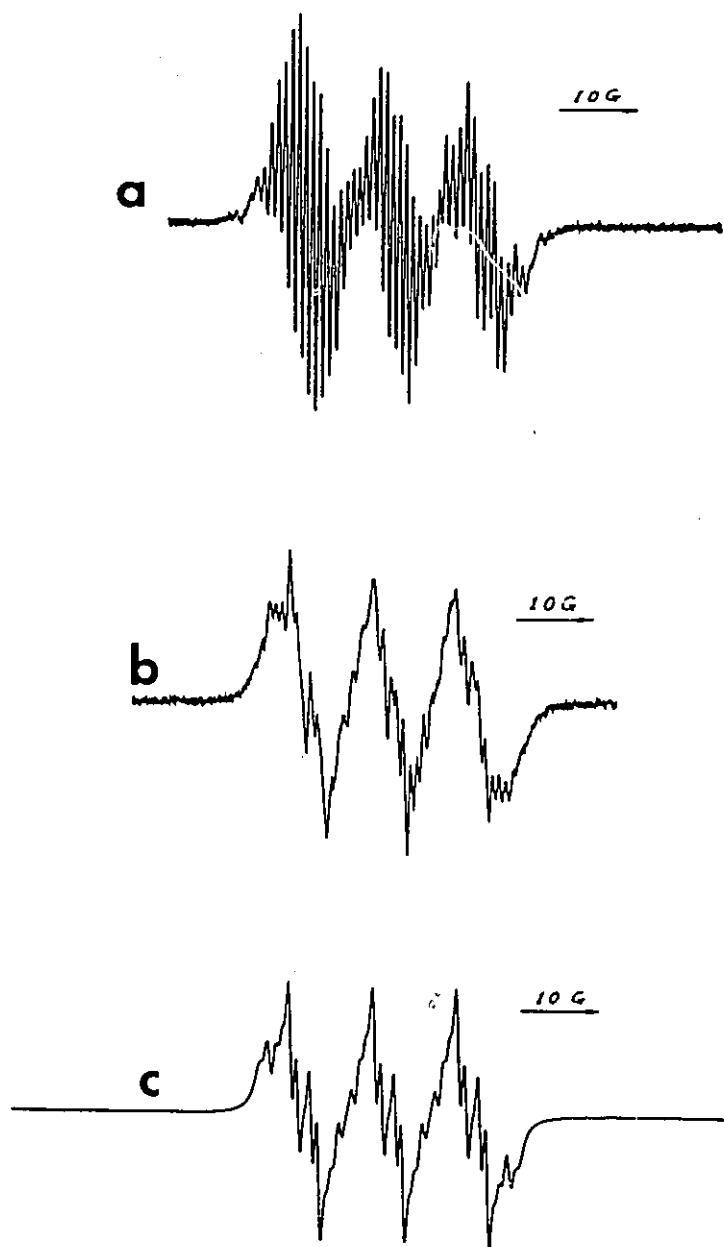


Figure 2.4 ESR spectra from the reaction of **42** with $\text{C}_6\text{H}_5\text{NO}$ in CH_3CN . (a) after 3 h; (b) after 27 h; (c) simulation of (b) using the data in Table 2.1.

2.2.5 Reaction of 42 with C₆Me₅NO

The ESR spectrum initially produced when **42** reacts with nitrosopentamethylbenzene reveals a triplet of doublets overlapping a simple triplet (Figure 2.5a); over a period of 10 hours the latter feature (i.e. the triplet gradually increases at the expense of the former. The final spectrum (after 21 hours) is shown as Figure 2.5d and exhibits a hyperfine interaction only with nitrogen.

2.2.6 Reaction of 42 with C₆HMe₄NO

Nitrosodurene and **42** give ESR spectra almost identical to those produced in the analogous nitrosopentamethylbenzene reaction.

2.3 *Discussion*

[(Cyclohexadienyl)Fe(CO)₃]⁺ systems such as **40** are thermally- and air-stable cations which react readily with nucleophiles¹¹⁴ and so are valuable synthetic intermediates. Steroidal analogues of **40** are also known in which the delocalized system is sited in the A ring. It is only very recently that B ring cationic systems have become available. Attempts to remove the 9 hydrogen from the iron tricarbonyl complex of ergosteryl acetate are thwarted by the bulk of the

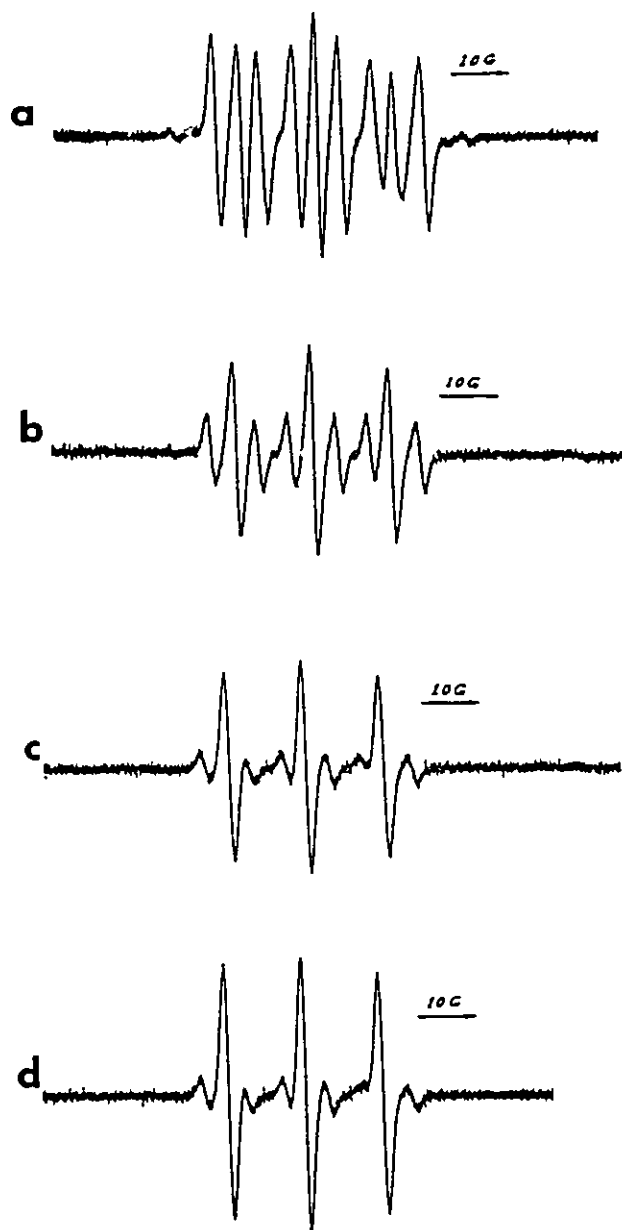


Figure 2.5 ESR spectra from the reaction of **42** with C_6Me_5NO in CH_3CN . (a) after 3 h; (b) after 6 h; (c) after 9 h; (d) after 21 h.

Table 2.2 ESR parameters for durene- and pentamethylbenzene nitroxide radicals.

Substances	solvent	Temp.	g value	a value(G)	Ref.
$\text{C}_6\text{H}_{11}-\text{N}-\text{Ar}^{\text{a}}$ $\quad \quad \quad $ $\quad \quad \quad \text{O}\cdot$	C_6H_6	300K	2.006 ₀	N: 13.57 H: 6.93	134
$\text{Ph}-\text{CHMe}-\text{N}-\text{Ar}$ $\quad \quad \quad $ $\quad \quad \quad \text{O}\cdot$	C_6H_6	300K	2.006 ₀	N: 13.8 H: 3.77	134
$(\text{CO})_3\text{FeC}_6\text{H}_7-\text{N}-\text{Ar}$ $\quad \quad \quad $ $\quad \quad \quad \text{O}\cdot$	CH_2Cl_2 CH_3CN	293K	2.006 ₉	N: 13.7 H: 4.2	This work
	CH_3Cl CH_3CN	293K	2.006 ₉	N: 13.75 H: 3.6	This work
	DMSO C_6H_6	293K	g(1)= 2.006 ₈ g(2)= 2.006 ₀	N(1): 13.4 H(1): 3.3 N(2): 13.95 H(2): 12.3	This work
	DMSO/ C_6H_6 CH_2Cl_2 CH_3Cl (CCl_4)	293K	g(1)= 2.006 ₆ g(2)= 2.006 ₁	N(1): 13.6 H(1): 3.4 N(2): 14.1 H(2): 12.5	This work
$\text{Me}_3\text{C}(\text{C}_6\text{H}_8)-\text{N}-\text{Ar}$ $\quad \quad \quad $ $\quad \quad \quad \text{O}\cdot$	CD_3CN CH_2Cl_2	298K		N(eq): 13.87 H(eq): 4.62 N(ax): 14.37 H(ax): 10.75	133

Table 2.2 Continued

Substances	solvent	Temp.	g value	a value(G)	Ref.
$\begin{array}{c} \text{S}-\text{N}-\text{Ar} \\ \\ \text{O}\cdot \end{array}$	CH ₃ CN	293K	2.006 ₀	N(t): 13.4 N(t,d): 13.9 H: 7.9	This work
	CHCl ₃	293K	2.005 ₆	N(t): 13.5 N(t,d): 14.5 H: 9.2	This work
$\begin{array}{c} (\text{CO})_3\text{FeC}_6\text{H}_7-\text{N}-\text{Ar}' \\ \\ \text{O}\cdot \end{array}$	DMSO C ₆ H ₆	293K	g(1)= 2.006 ₉ g(2)= 2.006 ₆	N(1): 13.7 H(1): 4.0 N(2): 13.9 H(2): 12.7	This work
	C ₆ H ₆	293K	g(1)= 2.006 ₇ g(2)= 2.006 ₄	N(1): 13.5 H(1): 3.3 N(2): 13.8 H(2): 12.3	This work
$\begin{array}{c} \text{C}_6\text{H}_{11}-\text{N}-\text{Ar}' \\ \\ \text{O}\cdot \end{array}$	C ₆ H ₆	300K	2.005 ₅	N: 14.0 H(CH): 7.6	135
$\begin{array}{c} \text{S}-\text{N}-\text{Ar}' \\ \\ \text{O}\cdot \end{array}$	CH ₃ CN	293K	2.005 ₉	N(t): 13.5 N(t,d): 13.6 H: 7.7	This work

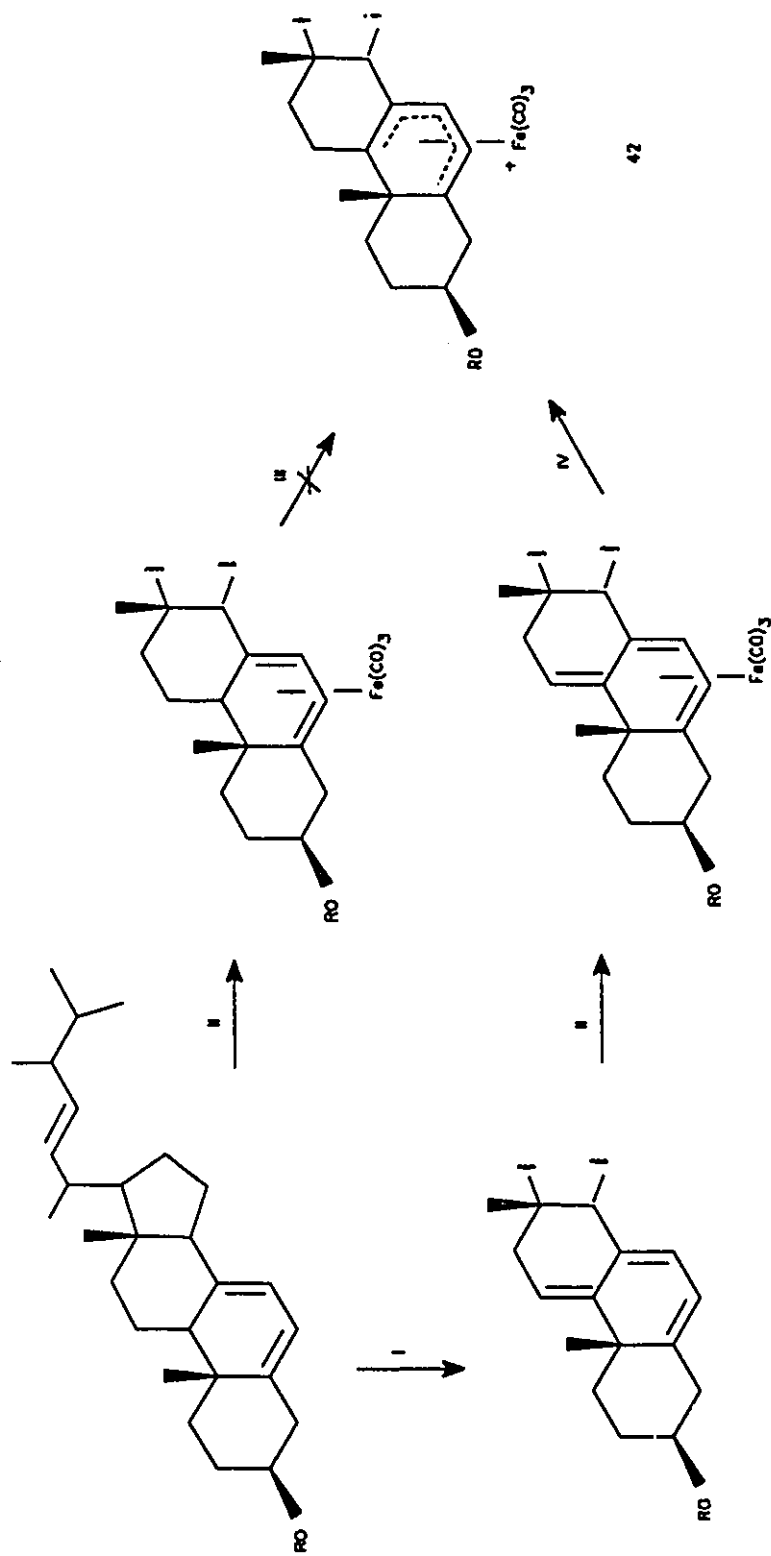
^a Ar = durenyl; S = steroidal group; Ar' = pentamethylphenyl.

organometallic fragment which hinders the approach of the trityl cation which is normally used as the hydride abstracting agent. Instead, a multi-step route has been developed which involves initial oxidation of ergosterol to 9,11-dehydroergosterol; complexation of the $\text{Fe}(\text{CO})_3$ moiety to the 5,6,7,8-diene unit and subsequent protonation at C-11 yields the required cation **42**, as shown in Scheme 2.1.

Nucleophilic attack on metal-complexed polyenyls generally occurs at one of the termini of the delocalized system;¹¹⁵ indeed, nucleophilic attack by the nitrosoarene on the $[(\text{pentadienyl})\text{Fe}(\text{CO})_3]^+$ cation **43** is an entirely reasonable mechanism to account for the observations of Cais *et al.*^{105,106} They reported that the initially formed radical **44** can be reduced to the corresponding amine **45** and the latter molecule, which is diamagnetic, was readily characterized by NMR spectroscopy.

2.3.1 Assignments of the ESR Spectra

The ESR data we have obtained are collected in Tables 2.1 and 2.2. These Tables also contain some relevant literature data. The initial task is to assign the various spectra. By analogy with the results of Cais *et al.*, the radical which would be expected is that shown as **41**, that is, the cyclohexadiene iron tricarbonyl system substituted at the formerly cationic carbon by the group NOAr, where Ar

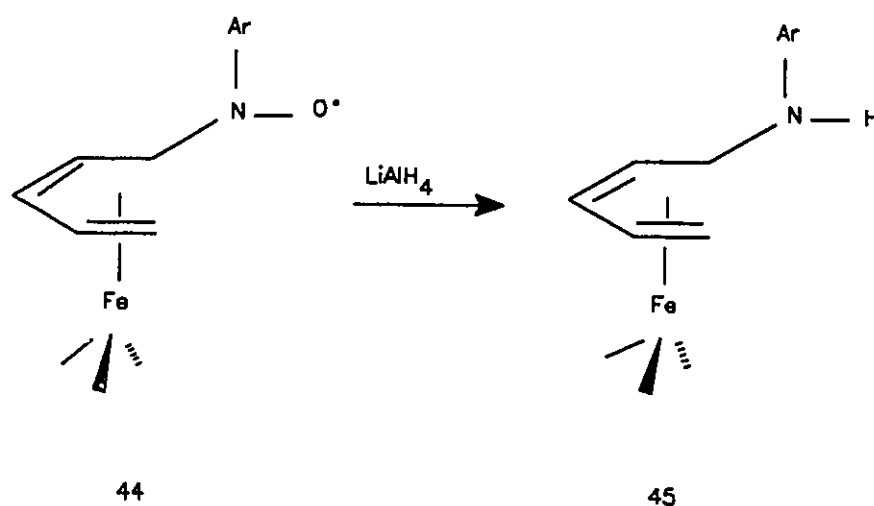
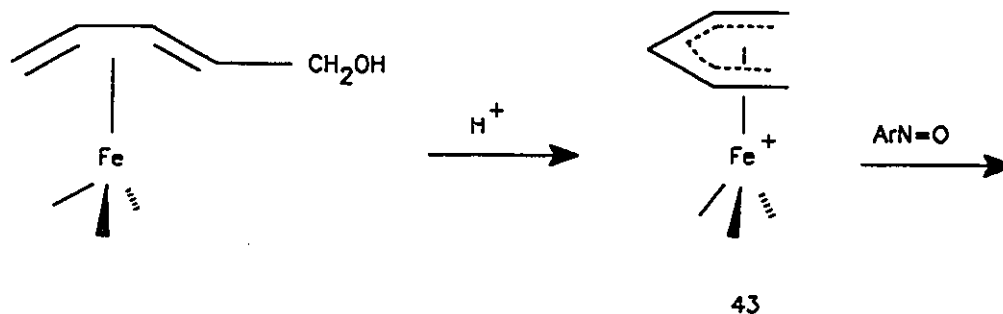


Scheme 2.1 Synthetic route to the steroidal cation 42. (I) Mercuric acetate/acetic acid.

(II) $(\text{Benzylideneacetone})\text{Fe}(\text{CO})_3$. (III) $[(\text{C}_6\text{H}_5)_3\text{C}]^+ \text{BF}_4^-$. (IV) HPF_6^- .

varies according to the identity of the nitrosoarene used. In Table 2.1 the hyperfine coupling constants obtained from the spectra resulting from the reaction of **40** with nitrosobenzene are compared with those reported by Cais and with several organic nitroxide radicals with mixed phenyl and aliphatic substituents. The hyperfine coupling constants of the initial radical from the reactions of **40** in both CH_2Cl_2 and CH_3CN agree closely with those of molecules from the literature possessing analogous structural features and there seems little doubt that the structure of the radical is **41a**, where Ar = phenyl. As noted above, the final spectrum of the reaction in dichloromethane has been identified as the diphenylnitroxide radical.

The six-line spectrum initially obtained from the reaction of **40** with nitrosodurene is entirely consistent with a radical of structure **41b**, with Ar = $\text{C}_6\text{Me}_4\text{H}$. The single proton splitting arises from the hydrogen at the point of attachment to the cyclohexadiene ring. As described above, in DMSO/benzene two six-line spectra are observed. They differ substantially in the hydrogen coupling constant — 3.3G compared with 12.3G. It is suggested that these two spectra arise from different rotamers of the same radical depending on the orientation of the NOAr group. There is ample precedent for slowed rotation in nitroxides containing such bulky substituents as durene or pentamethylbenzene.¹¹⁶ Simulation of the spectra indicate that the two isomers are present in a ratio of approximately 4:1. The angular dependence of the β -hydrogen coupling constants



of nitroxide radicals has been discussed by Chapelet-Letourneux *et al.*¹¹⁶ These workers examined the spectra of a variety of radicals with both alkyls and saturated ring substituents and suggested a relationship of the form $a_H = B \cos^2 \theta$ between the hyperfine coupling constant and the angle made between the C—H bond and the axis of the p orbital containing the unpaired electron. By calculating an average value of B from the literature data¹³³ we can see that a hyperfine

coupling constant of 12.3G gives an angle of 46° while a coupling constant of 3.3G yields a value of 69° .

There are data in the literature which support this assignment of the isomers. Thus Suehiro *et al.*¹¹³ have trapped substituted 1,4-cyclohexadienyl radicals (the present results refer to the 1,3-isomer) and report a_H values of 6-8G for the proton on the adjacent carbon atom. Kanimori *et al.*¹¹⁷ report additional radicals of this type and discuss the hydrogen coupling constants in terms of the angle between the C — H bond and the p orbital on the nitrogen. It may be noted that the reported hyperfine coupling constants in these cases are close to the average of the values we find for the two isomers [$1/2(3.3+12.3) = 7.8G$]. A further paper by Konaka *et al.*¹¹⁸ reports the observation of line width alternations for nitroxide spectra obtained with nitrosodurene. This observation is attributed to restricted rotation because of the bulkiness of the duryl group. The present observation is therefore consistent with more extreme steric restrictions. It may be taken as excellent proof that the iron tricarbonyl group remains attached to the nitroxide radical.

By analogy with the results with nitrosobenzene, it would have been expected that the more complex spectra which were obtained from the decomposition of the above radicals would correspond to the nitroxide radical with a phenyl group and a duryl group as substituents. However, the spectrum cannot be fitted to the hyperfine coupling constants expected for this radical. It appears

more complex and we suspect that it may be a mixture of isomeric radicals differing in the relative orientations of the phenyl and duryl radicals. Again, this implies that the iron tricarbonyl group remains attached to the radical.

The analysis of the spectra obtained from the reaction of **40** with nitrosopentamethylbenzene is identical to that for nitrosodurene. The angles derived from the proton coupling constants are also very similar. We have been unable to analyse the more complex spectra and similar reasons based on mixtures of isomeric radicals are suggested.

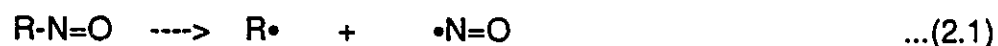
In a similar manner, the ESR spectra derived from the reactions of the steroidal cation **42** with the various nitrosoarenes can be assigned in a relatively straightforward manner. The initial spectrum in each case shows hyperfine couplings appropriate for the presence of the ArN fragment and also a single hydrogen on the steroidal carbon adjacent to the nitrogen. However, in each of the final spectra it is clear that the hydrogen atom is no longer bonded to the aforementioned carbon. In the nitrosopentamethylbenzene case, for example, ultimately we see merely the triplet splitting from the nitrogen.

2.3.2 Mechanistic Considerations

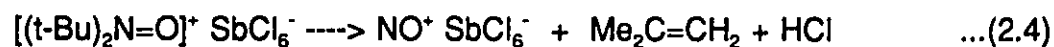
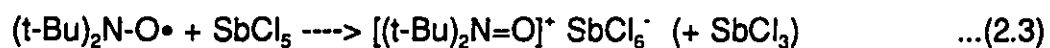
The initial stages of these reactions are directly analogous to those studied by Cais which involved the attack of nitroso compounds on pentadienyl- or

cycloheptadienyl $\text{Fe}(\text{CO})_3$ cations. One of the suggested mechanisms involved nucleophilic attack at the cationic carbon to give an oxo-ammonium ion which suffers one-electron reduction to give the nitroxide radical. There are some variations possible on this theme — reduction may occur before addition of the nitroso moiety or the reactive species may be a triplet ferricinium complex — but the end result is the same. It is assumed that a second molecule of nitroso compound acts as the one-electron reducing agent.

The subsequent reactions are rather more speculative but a reasonable scheme can be devised based on reactions which have literature precedents. We note first that the homolytic decomposition of nitroso compounds according to Equation (2.1) has been shown by Chatgililoglu and Ingold¹¹⁹ to be thermodynamically improbable as a thermal reaction, although it proceeds readily photochemically. However, Bilkis and Shein¹²⁰ have demonstrated that the analogous reaction involving the radical anion occurs readily, as in Equation (2.2).

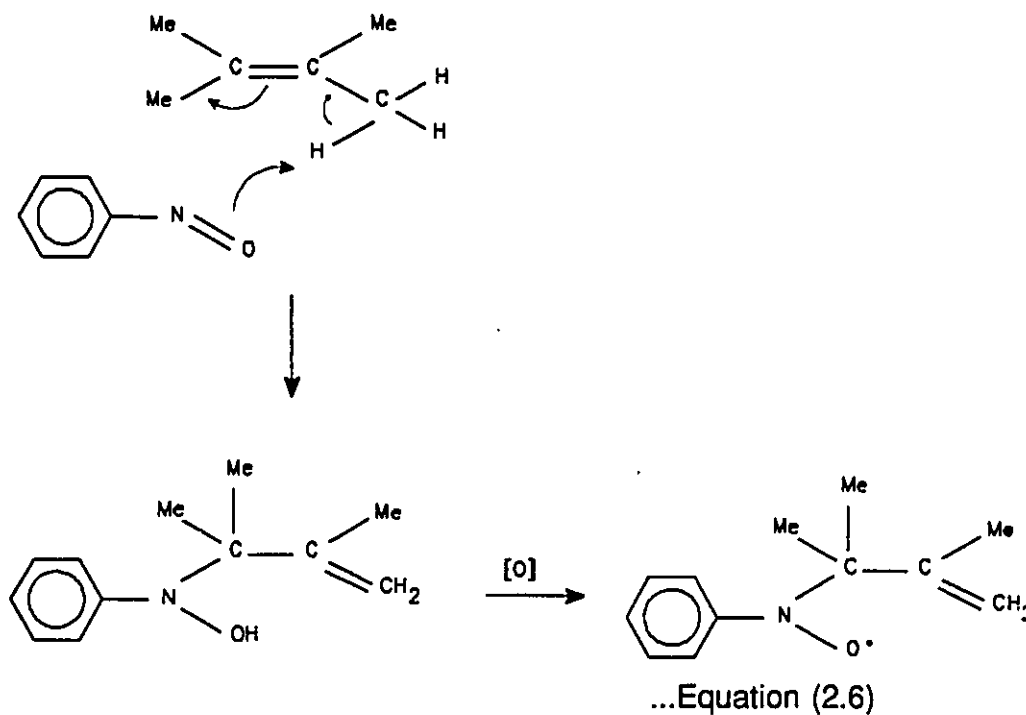
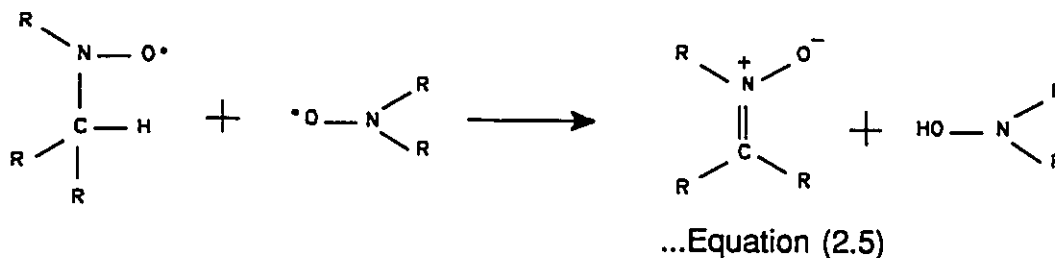


More relevant, perhaps, is the report¹²¹ that dialkyl nitroxides react with SbCl_5 giving N,N-dialkyl-N-oxoammonium salts; these in turn yield NO^+ , as in Equations (2.3) and (2.4).



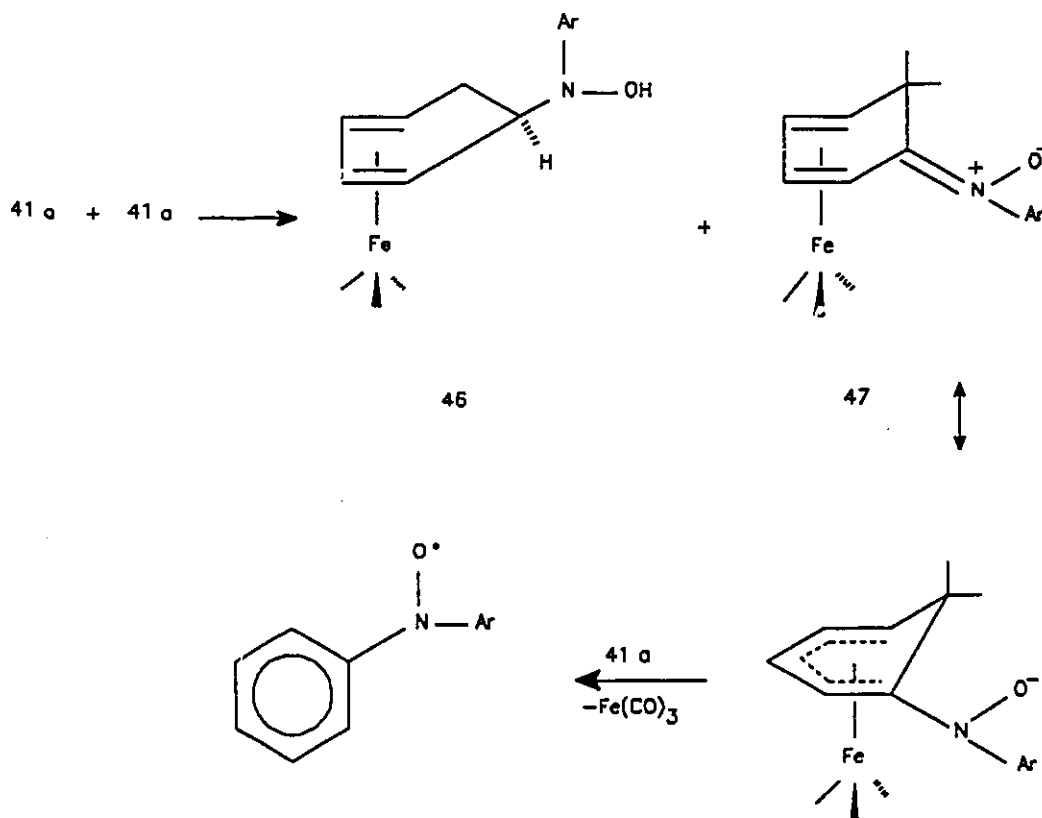
Thus, a not unreasonable initial postulate is that fragmentation of the radical cation arising from the one-electron reduction of the initially formed adduct of nitrosobenzene and **40** yields NO^+ and the phenyl radical; this in turn can be trapped by nitrosobenzene to form diphenylnitroxide. One should note, however, that analogous reactions with $\text{C}_6\text{Me}_5\text{NO}$ and $\text{C}_6\text{HMe}_4\text{NO}$ would then be expected to give rise to the corresponding diarylnitroxides, i.e. $(\text{C}_6\text{Me}_5)_2\text{NO}^\bullet$ and $(\text{C}_6\text{HMe}_4)_2\text{NO}^\bullet$, but these are not observed in reactions with **40**. In fact, there is another possible route to $\text{Ph}_2\text{NO}^\bullet$ which involves dehydrogenation of the cyclohexadienyl(phenyl)-nitroxide **41a**. [We mention parenthetically that the reaction of $t\text{-BuNO}$ with cation **40** yields not only the expected nitroxide but also $\text{C}_6\text{H}_5\text{-}(t\text{-Bu})\text{NO}^\bullet$ which must arise *via* dehydrogenation of a cyclohexadienyl intermediate.] In this context, we next recall information on the self-reactions of nitroxides. These have been extensively studied by Ingold and his collaborators^{122,123,124} and also by Golubev *et al.*¹²⁵ Several different products can be formed depending on the nitroxide substituents but the typical reaction involves dimerization followed by hydrogen atom transfer to give a reduced product, often a hydroxylamine, and an oxidized product, frequently a nitron, as in Equation (2.5).

Furthermore, the mechanism of the "ene" reaction of nitroso compounds with olefins involves initial formation of a C-N bond followed by hydrogen atom transfer to give a hydroxylamine; subsequently there occurs oxidation of the hydroxylamine to a nitroxide by a second molecule of nitroso compound, as in Equation (2.6).¹²⁶⁻¹²⁸



One could follow these literature precedents and postulate a disproportionation of radical **41a** with a second nitroxide radical to give the hydroxylamine **46** and a neutral product **47**; subsequent hydrogen abstraction by another molecule of **41a** and loss of the $\text{Fe}(\text{CO})_3$ fragment would then yield $\text{Ph}_2\text{NO}\cdot$. The formation of the aromatic ring would provide the thermodynamic driving force for such a reaction. Of course, the $\text{Fe}(\text{CO})_3$ moiety binds strongly to diene units but

is generally less firmly attached to arene rings; consequently, the radicals detected at the end of the reaction sequence are those of the non-complexed diarylnitroxide and the metal is left as a residue at the bottom of the tube.



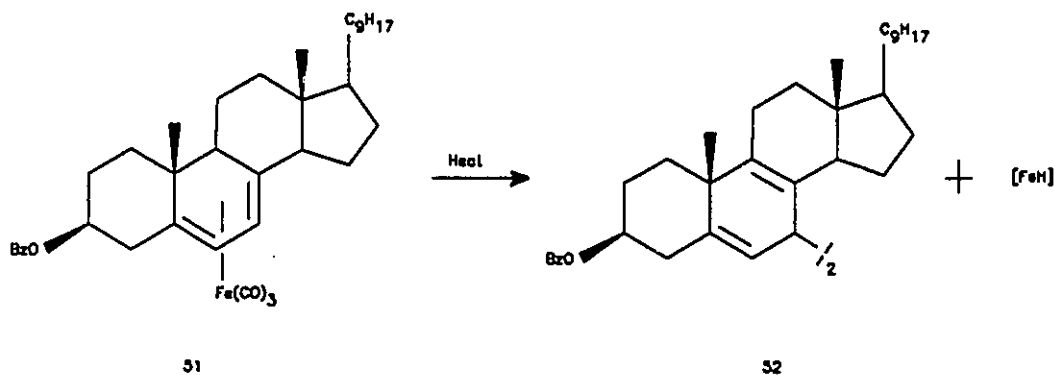
To summarize, therefore, the reaction of **41** with nitrosobenzene in acetonitrile yields the radical **41a**, $Ar = C_6H_5$; in contrast, in dichloromethane the disproportionation reaction becomes significant. This leads to the corresponding hydroxylamine and nitronium; the latter can then suffer hydrogen atom abstraction by another molecule of **41a** so that eventually there is complete conversion to diphenylnitroxide.

With nitrosodurene (and also with C_6Me_5NO) the initial reaction in CH_3CN/CH_2Cl_2 follows the pattern established for nitrosobenzene. Disproportionation occurs but the steric bulk of the polymethylated arene is sufficient to prevent free rotation and so a mixture of $Ph(Ar)NO$ isomers is detectable on the ESR time-scale. In the DMSO/benzene mixtures two isomers are observed for the initial cyclohexadienyl radical **41b** (**41c**). We speculate that these too can disproportionate but that in this solvent mixture the equilibrium favors the nitroxide radicals rather than the hydroxylamines. The existence of this equilibrium is, however, sufficient eventually to convert all of the cyclohexadienyl nitroxide to the more favored isomer.

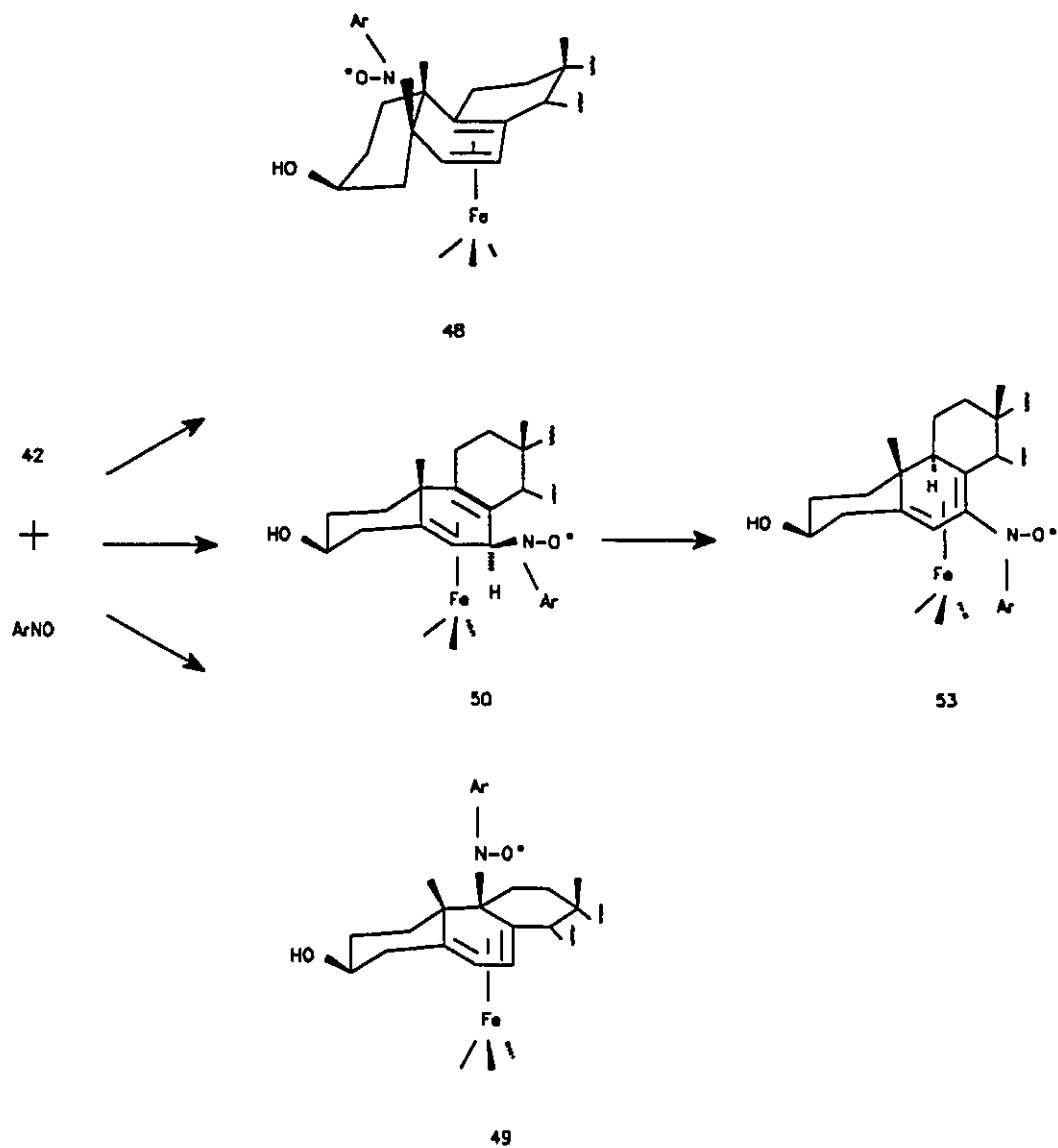
2.3.3 Reactions of ArNO with the Steroidal Cation, 42

By analogy with the reactivity pattern established for the unsubstituted $[(cyclohexadienyl)Fe(CO)_3]^+$ cation, **40**, one would anticipate initial nucleophilic attack by the nitrosoarene at a terminus of the delocalized system, that is at C-5 or C-9. Furthermore, in accord with the known chemistry of such iron complexes¹⁴ the incoming nucleophile will approach from the distal side relative to the metal carbonyl unit. That is, attack will occur on the β face of the steroid. In principle, the two sites of attack are readily differentiable since binding to the C-5 position, as in **48**, should produce a radical showing weak coupling to the olefinic hydrogen at C-6 (and possibly even to the 4α and 4β protons). In contrast,

if the ArNO were to attack at C-9, as in **49**, one should see essentially a simple triplet since there is no alkene hydrogen at C-8. The result of the experiment revealed that attack had occurred at neither C-5 nor C-9. The initial ESR spectrum from the reaction of C_6Me_5NO (Figure 2.5a) shows the expected 1:1:1 triplet with $a_N = 13.5G$ and also a doublet splitting (7.7G) clearly indicating the presence of a single hydrogen only two bonds away from the nitrogen. Apparently, the steric problems engendered by the placement of an aryl nitroso moiety at positions C-5 or C-9 render the C-7, as in **50**, site a more attractive target (see Scheme 2.2). In seeking a precedent for bond formation at the 7-position, we note that the pyrolysis of ergosteryl benzoate iron tricarbonyl, **51**, is reported to yield the dimeric product **52** in which radical coupling has occurred at the 7-position.¹²⁹



In Figures 2.6a, 2.6b and 2.6c we present energy-minimized conformers which were calculated by using the program MACROMODEL.¹³⁰ It is readily apparent that incorporation of the attacking nucleophile can place a bulky aryl group in rather unfavorable positions with respect to the steroidal methyl substituents at C-10 and at C-13. When the nitrosoarene attacks on the β face at



Scheme 2.2 Possible sites of reaction of nitrosoarenes with the steroidal cation

C-5 the A/B rings are forced into a *cis*-fusion and the methyl must bend so as to avoid the new functional group. Similarly, attack at C-9 leads to steric problems but, as shown in Figure 2.6c, attachment at C-7 is relatively unencumbered. It is interesting to note that the energy-minimized structure of the initial adduct at C-7, i.e., **50**, there is a dihedral angle of 33° between the arene ring plane and the C-H bond; this translates as a 57° angle made by the *p* orbital on nitrogen and the C-H bond. Gratifyingly, the experimental hyperfine interaction to the H-7 nucleus is 7.9G which corresponds to an angle of 56° .

This initial product **50** leaves the $\text{Fe}(\text{CO})_3$ fragment attached to a 1,4-cyclohexadiene system and, as is commonly the case with such non-conjugated diene complexes,¹³¹ a subsequent 1,3-hydrogen transfer occurs to generate the favored isomer **53** in which double bond conjugation is achieved. In this latter isomer the extra hyperfine coupling from the nearby hydrogen is lost. The net result of the whole process is to introduce a functional group at the 7-position of the steroid. Future work will focus on the reduction of the nitroxide radical to the more synthetically versatile amino function.

In contrast to the behaviour described above for nitrosoarenes, the corresponding reactions with *t*-BuNO exhibit a rather novel effect. The final product of the reaction with either **40** or **42** is $(t\text{-Bu})_2\text{NO}\cdot$ but the ESR spectrum of this radical exhibits fascinating behaviour in that its intensity varies in an oscillatory manner with time. We will discuss these in the following chapter.

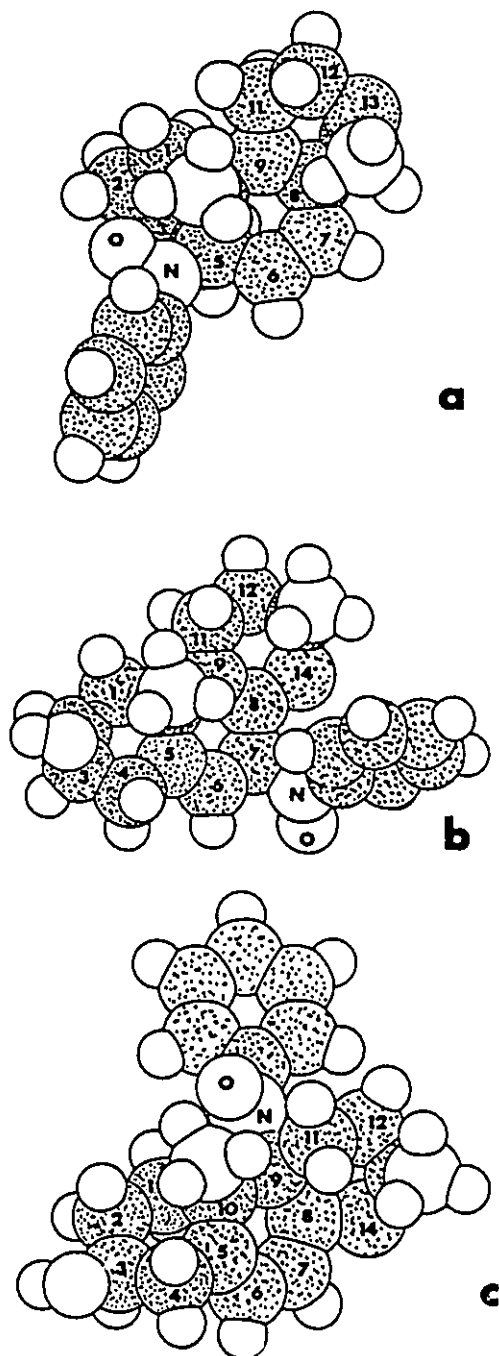


Figure 2.6 (a) Space-filling model of **48** in which attachment of the ArNO fragment at C-5 causes unfavorable interaction with the methyl group at C-10. (The view is from the β face. For clarity, the α -Fe(CO)₃ group and the D ring of the steroid are not shown.) (b) Space-filling model of **50** in which attachment of the ArNO fragment at C-7 causes no problematic steric interactions with the methyl groups. (c) Space-filling model of **49** in which attachment of the ArNO fragment at C-9 causes unfavorable interactions with the methyl groups at C-10 and at C-13.

2.4 Future work

The reactions of $[(\eta^5\text{-C}_6\text{H}_7)\text{Fe}(\text{CO})_3]^+$ with bulky nitroso compounds, such as nitrosodurene and nitrosopentamethylbenzene, result in two rotamers which showed different orientation of the $\text{ArNO}\cdot$ group on the ESR time scale. The angle between the $\text{C}-\text{H}_\beta$ bond and the axis of the p orbital containing the unpaired electron has been calculated from the hyperfine coupling constants using the equation $a_H = B \cos^2\theta$. It is impossible to get crystals of the radical $(\eta^5\text{-C}_6\text{H}_7)\text{Fe}(\text{CO})_3(\text{Ar})\text{N}-\text{O}\cdot$ to obtain the evidence of the structure, therefore, one could grow crystals of a closely analogous molecule, such as $(\eta^5\text{-C}_6\text{H}_7)\text{Fe}(\text{CO})_3(\text{Ar})\text{C}=\text{O}$, with a view to obtaining X-ray data that could clarify this point.

The analogous reactions with the steroidal cation, **42**, lead to initial attack not at one of the termini of the delocalized system but rather at the central carbon, i.e., at C-7. Subsequent hydrogen migration leads to the (5,7-diene) $\text{Fe}(\text{CO})_3$ complex bearing the aryl nitroxide at the 7-position. Future work could focus on the reduction of the nitroxide radical to the more synthetically versatile amino function which could then be analyzed by NMR spectroscopy.

CHAPTER THREE

THE REACTION OF $[(\eta^5\text{-cyclohexadienyl})\text{Fe}(\text{CO})_3]^+ \text{BF}_4^-$ WITH 2-METHYL-2-NITROSOPROPANE: AN UNEXPECTED OSCILLATING REACTION

3.1 *Introduction*

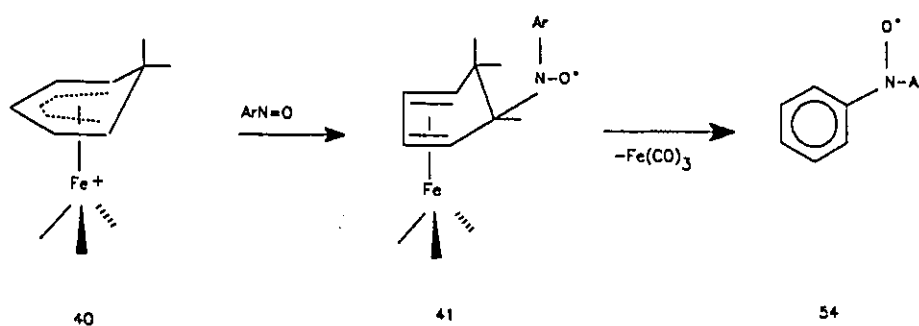
Oscillating chemical reactions¹³⁶ (especially those which involve dramatic colour changes) have attracted considerable attention in recent years not only because of their intrinsic beauty and visual fascination but also because they pose challenging problems to kineticists. As exemplars of non-linear processes they are also relevant to biological problems related to the formation of dissipative structures, to morphogenesis and to the growth of organisms.¹³⁷ The actual oscillatory reactions occurring in biological systems are, however, in general poorly understood and not closely related to the systems studies by inorganic chemists. Many of the commonly demonstrated reactions are derived from the now classic observations of Belousov, Zhabotinski and their colleagues such as the reaction of bromates with malonates in the presence of a ferrous/ferric redox system.¹³⁸ Since that time, a number of variations on this theme have been developed and designed oscillatory chemical systems are now possible.¹³⁹ However, our

involvement in this field was entirely serendipitous. In continuation of our ESR studies¹⁴⁰ of organometallic nitroxide radicals derived from the interaction of metal carbonyl stabilized cations such as **40** with nitrosoarenes (which give organometallic nitroxides **41** and diarylnitroxides **54**), we treated the cation $[(\eta^5\text{-cyclohexadienyl})\text{Fe}(\text{CO})_3]^+$, **40**, with *tert*-BuNO with the expectation of observing the simple radical **41**. However, the ESR spectrum exhibited as its major feature a simple triplet signal readily attributable to the well-known bis(*tert*-butyl)nitroxide radical, (*tert*-Bu)₂N-O•. Even more surprising was the observation that the intensity of this triplet resonance showed oscillatory behaviour with time, sometimes appearing and disappearing up to eight times. We here describe a set of experiments in which we attempt to delineate the factors controlling the formation of the various radical products. We also note the very different rates of oscillation when the concentrations of the reactants are changed.

3.2 Results and Discussion

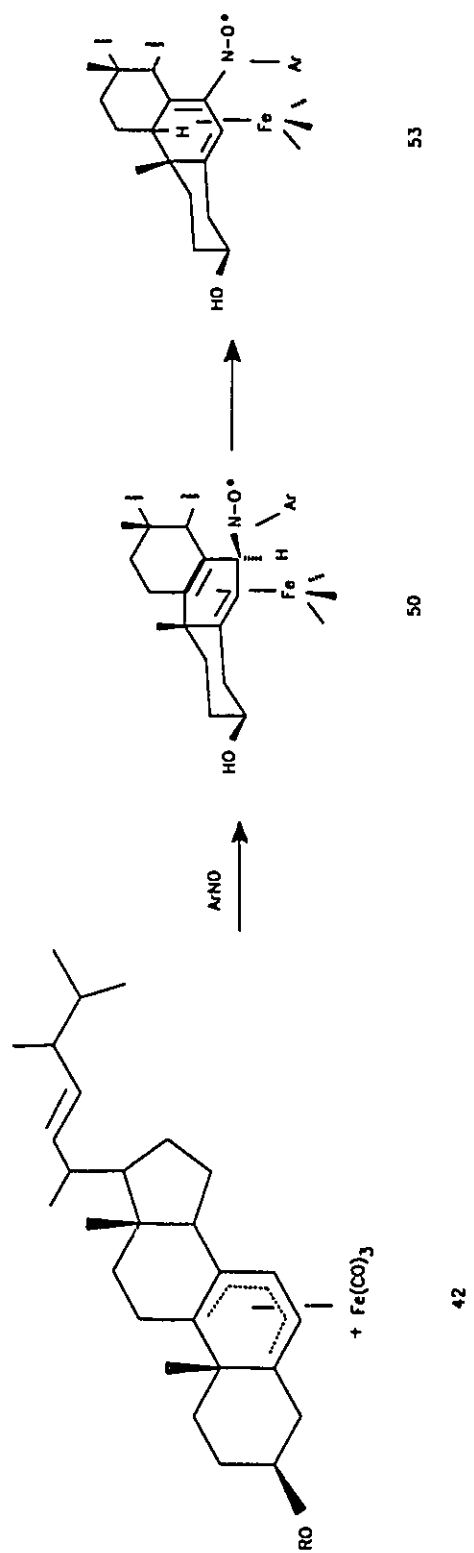
We have recently reported¹⁴⁰ that the reactions of nitroso-arenes with the $[(\eta^5\text{-cyclohexadienyl})\text{Fe}(\text{CO})_3]^+$ cation, **40**, initially produce the organometallic nitroxides, **41**, and ultimately yield the diarylnitroxides, **54**, as shown in Scheme 3.1. In some instances, the initial unconjugated nitroxide can undergo hydrogen migration to yield a more stable second radical in which the carbon-carbon double

bonds are now conjugated. Thus, the $\text{Fe}(\text{CO})_3$ -stabilized steroidal cation **42** gives the nitroxide radicals **50** and **53** successively, as in Scheme 3.2. These observations are in accord with the earlier reports by Cais concerning the reactions of nitroso-arenes with ferrocenyl and related cations.^{105,106}



Scheme 3.1 The reaction of **40** with nitrosoarenes.

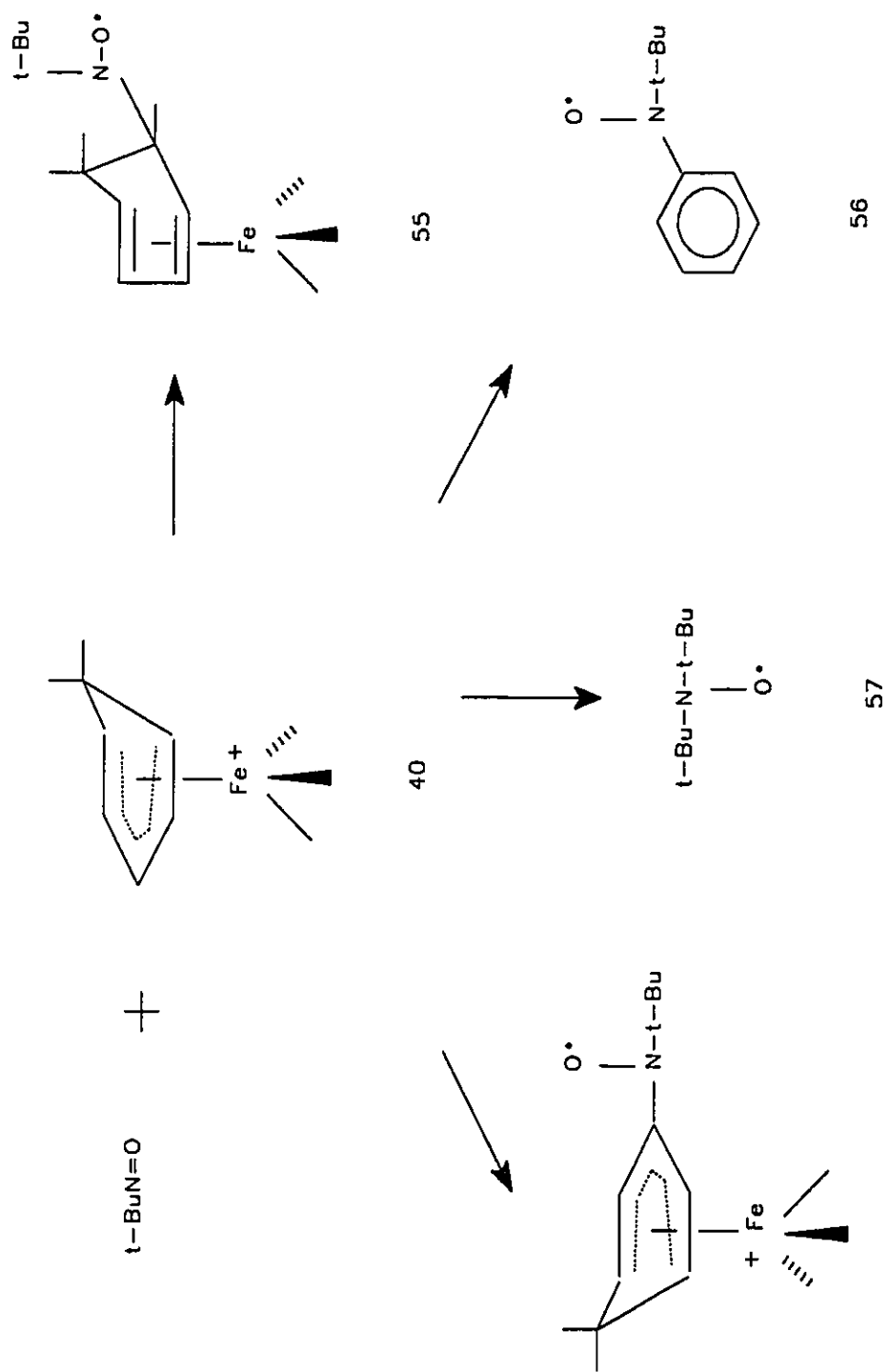
In continuation of this work, we treated the cation **40** with 2-methyl-2-nitrosopropane in the expectation of observing formation of the organometallic radical **55** in which the aryl substituent in **41** had merely been replaced by a *tert*-butyl group. However, this anticipated radical is only a minor, short-lived product and in many cases is not detectable at all. The major products **56**, **57** and **58** were characterized by their ESR spectra. Scheme 3.3 depicts the experimental and simulated ESR spectra of *tert*-butyl(phenyl)nitroxide, **56**, ($g = 2.005_8$) which exhibits the usual triplet ($a_{\text{N}} = 13.1 \text{ G}$) as well as smaller hyperfine couplings to the *ortho* (1.7 G), *meta* (0.85 G) and *para* (1.7 G) hydrogens of the



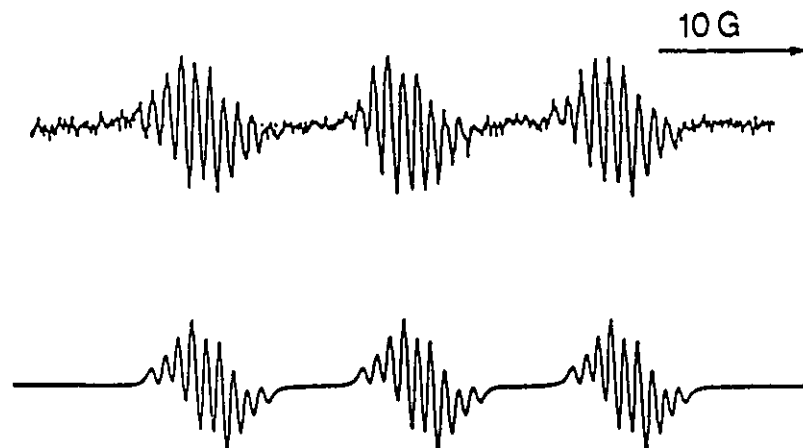
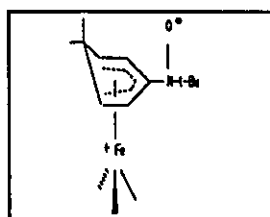
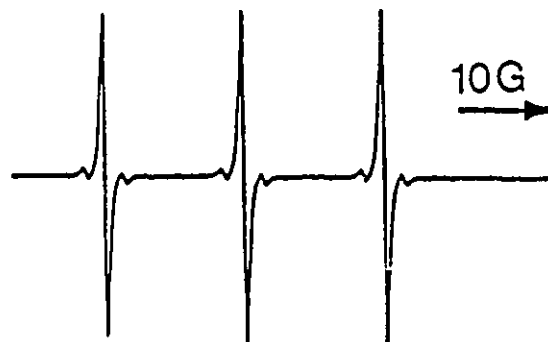
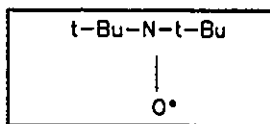
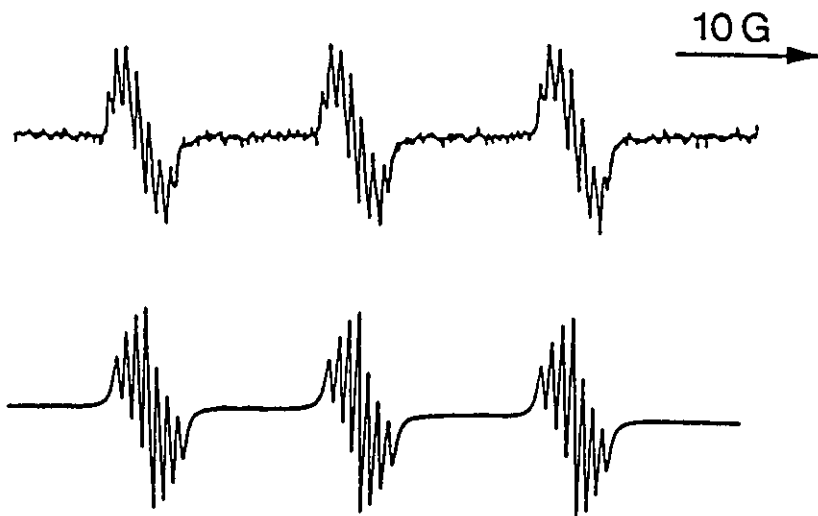
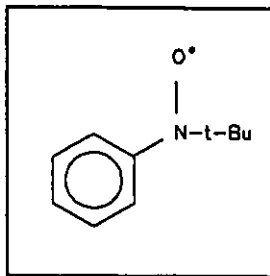
Scheme 3.2 The rearrangement of a steroidal nitroxide.

phenyl ring. The simulation and comparison with the literature data¹⁴¹⁻¹⁴⁶ confirm the assignment of the structure of **56**. Likewise, the bis(*tert*-butyl)nitroxide radical **57** has been prepared by many synthetic procedures and its ESR parameters are well known.¹⁴⁷⁻¹⁴⁹ The structure of **58** is less trivial to establish. The radical is clearly a nitroxide ($g = 2.006_g$; $a_N = 15.3$ G) which also shows hyperfine interactions to two *ortho* (1.44 G) and two *meta* (0.72 G) protons. This leads one to assign **58** as a (cyclohexadienyl)-nitroxide but, in order to maintain its overall radical character, the cyclohexadienyl moiety must have an even -electron count; these criteria are all satisfied by structure **58** in which the cyclohexadienyl cation is stabilized by complexation to an $\text{Fe}(\text{CO})_3$ fragment. In fact, as shown in Scheme 3.4, the formation of **58** can be rationalized in a straightforward manner merely by invoking hydrogen migration in the initially formed radical **55**.

Nevertheless, the most striking feature of the experiments is the oscillatory behaviour of **57**. Typically, as shown in Figure 3.1, when 3.0×10^{-2} mmol of the cation **40** and a 24-fold excess of 2-methyl-2-nitrosopropane were allowed to react in dichloromethane, the (*tert*-Bu)₂N-O· radical, **57**, appears for the first time 10 minutes after mixing the reactants and then disappears within 4 minutes. After a silent period of 17 minutes, **57** reappears and disappears over approximately 5 minutes. The time-scale of the waxing and waning of the peak intensity of **57** is clearly shown in Figure 3.1. Thus, at a scan rate of 1 gauss per second, the components of the triplet (which should of course have equal intensity) are manifestly changing.



58 Scheme 3.3 The ESR spectra of the products arising from the reaction of 40 with $t\text{-BuNO}$.



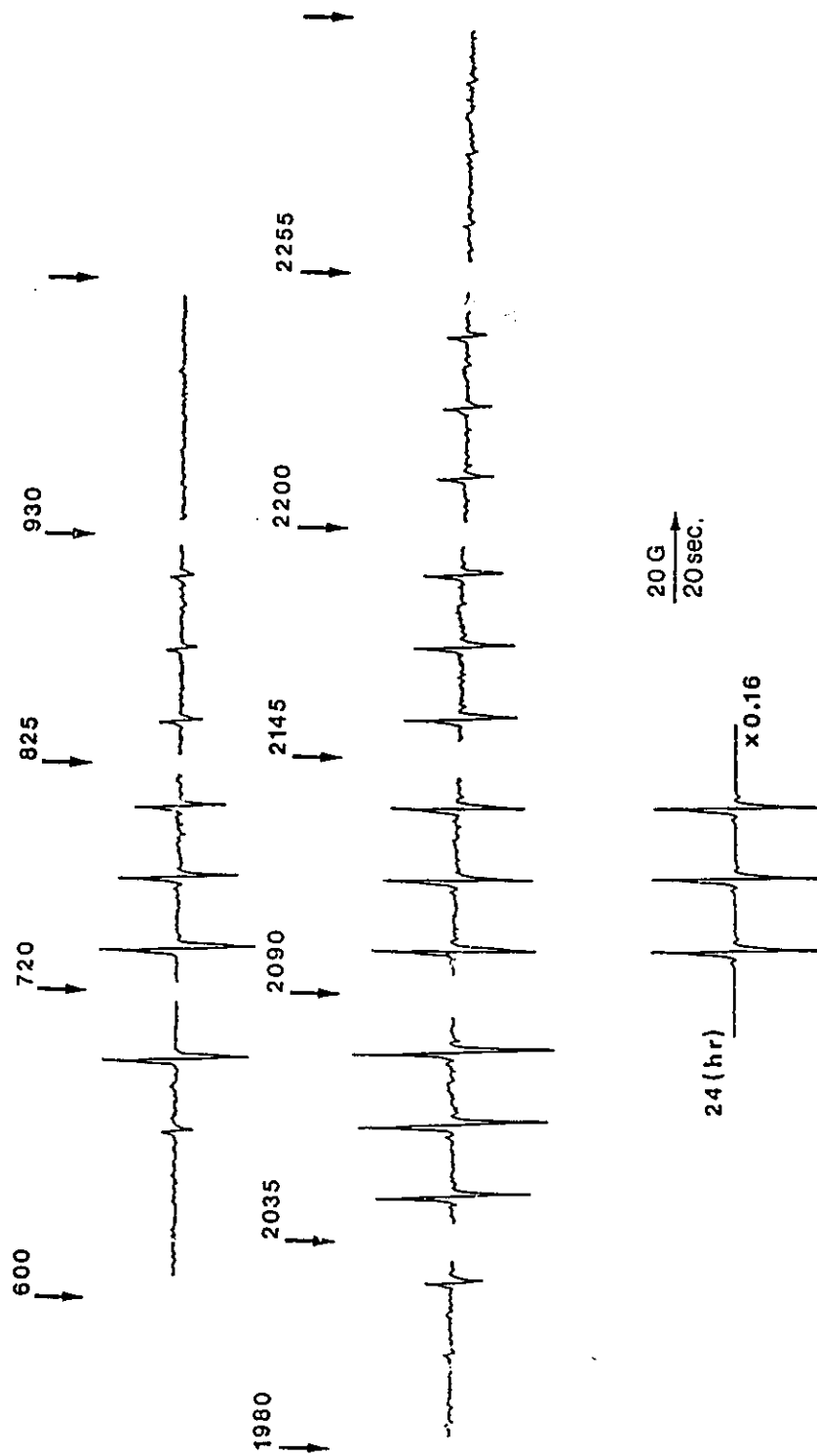


Figure 3.1 The time-dependent ESR spectra observed when 3×10^{-2} mmol of 40 react with a 24-fold excess of t-BuNO. The initial time values are quoted in seconds from the start of the reaction.

In contrast, Figure 3.2 shows the result of mixing **40** (1.6×10^{-2} mmol) with a 15-fold excess of *tert*-BuNO in acetonitrile which exhibits slowly oscillating behaviour for **57**, while **58** appears only after 6 hrs. In this particular case, $(tert\text{-Bu})_2\text{N-O}\cdot$ appears and disappears within the first 30 minutes; this radical subsequently reappears, disappears again after 6 hours and finally reappears after 20 hrs.

Another example appears as Figure 3.3 which shows the spectra resulting when 2.0×10^{-2} mmol of **40** and a 3-fold excess of the nitroso compound are mixed in CH_2Cl_2 . Within 2 minutes one sees both **56** and **57**. After 8 minutes, the $(tert\text{-Bu})_2\text{N-O}\cdot$ has disappeared leaving only *tert*-butyl(phenyl)nitroxide, **56**. After 75 minutes only a very weak $(tert\text{-Bu})_2\text{N-O}\cdot$ signal is detectable but the next day the triplet attributable to **57** is once again very strong.

To summarize a large number of experiments, we note that oscillations are observed in acetonitrile or dichloromethane solvent but not in toluene. The radical products observed depend to some extent on the relative concentrations of the reactants. When the 2-methyl-2-nitrosopropane is present in greater than 20-fold excess, the reaction at room temperature in dichloromethane as solvent gives only the $(tert\text{-Bu})_2\text{N-O}\cdot$ radical. If the concentration of *tert*-BuNO is only in the range of 3 - 15 times that of the organometallic cation **40** then the radicals **56** and **58** can also be observed. The delay time before the onset of the $(tert\text{-Bu})_2\text{N-O}\cdot$ signal varies from zero to 40 minutes; oscillations are not observed below -20°C . The

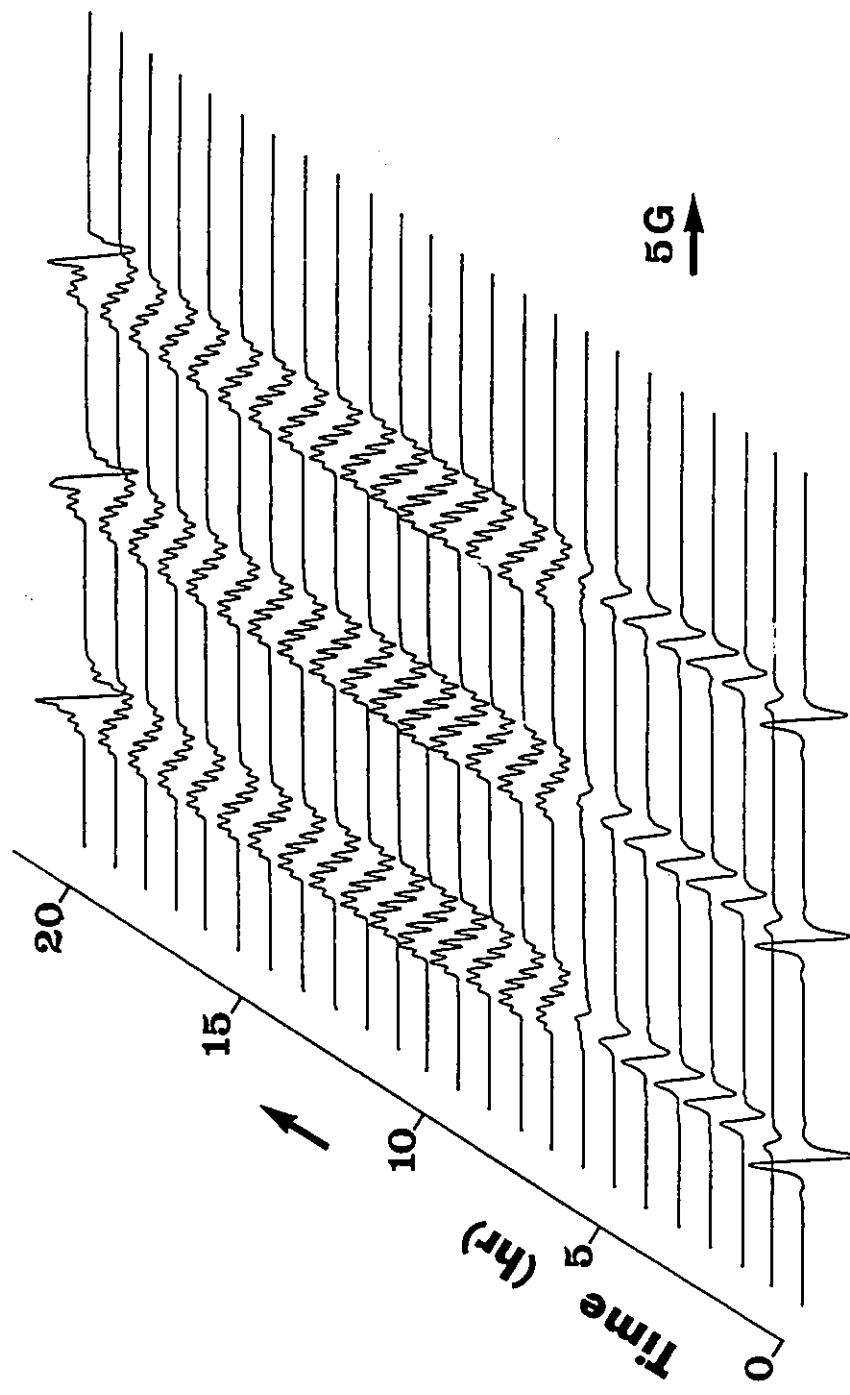


Figure 3.2 ESR spectra for the reaction of 1.6×10^{-2} mmol of **40** with a 15-fold excess of t-BuNO.

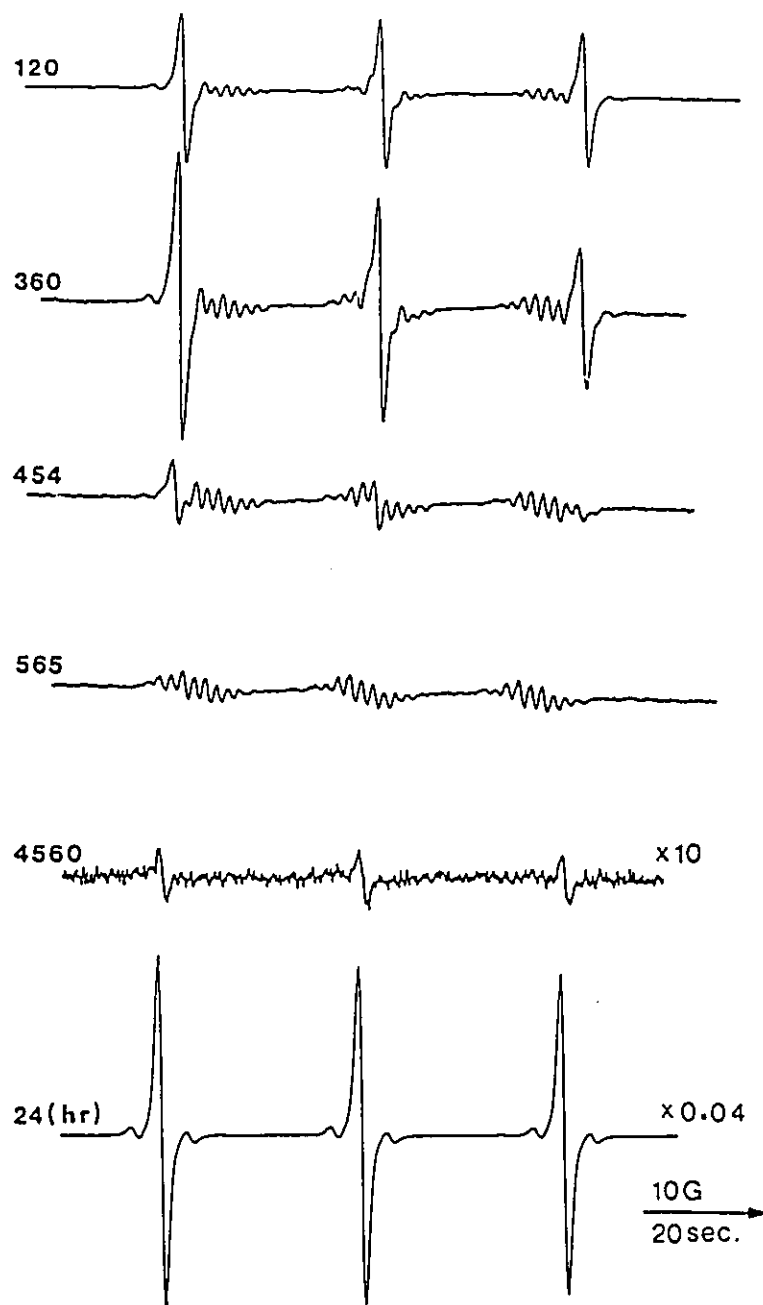


Figure 3.3 ESR spectra arising from the reaction of 2×10^{-2} mmol of **40** and a 3.5-fold excess of t-BuNO. The initial time values are quoted in seconds from the start of the reaction.

time from appearance to disappearance of **57** ranges from 4 minutes to 10 hours, while the ESR silent period between oscillations ranges from 15 minutes to one hour. Finally, it appears that high concentrations of reactants and a large excess of *tert*-BuNO lead to more rapid oscillations. In all cases, the period of the oscillations lengthens with time and the final persistent spectrum is that of bis(*tert*-butyl)nitroxide radical **57**. We have been unable to observe oscillatory behaviour using spectroscopic techniques other than ESR, e.g., uv-visible spectroscopy nor in the NMR regime (no evidence of CIDNP). This is perhaps not surprising since the concentrations of radical species are likely to be small compared to those of diamagnetic species. Visually during the course of the reaction there is a steady change of colour from bluish-green to yellowish-green. It was observed that during the course of the ESR experiment there was some evolution of gas and the possibility was considered that the oscillatory behaviour could be an artifact brought about by removal of solution from the ERS cavity by the gas bubbles produced; however, this was shown not to be the case. The reaction was also run on a vacuum line to allow collection of the gas evolved. The major component proved to be carbon monoxide with smaller amounts of carbon dioxide (which appeared quite intense due to the higher extinction coefficient) and also methylene chloride (the solvent used). The rotational structure observed in the gas phase IR spectra allowed unambiguous identification of these species. There are several conditions necessary for the observation of chemical oscillations.

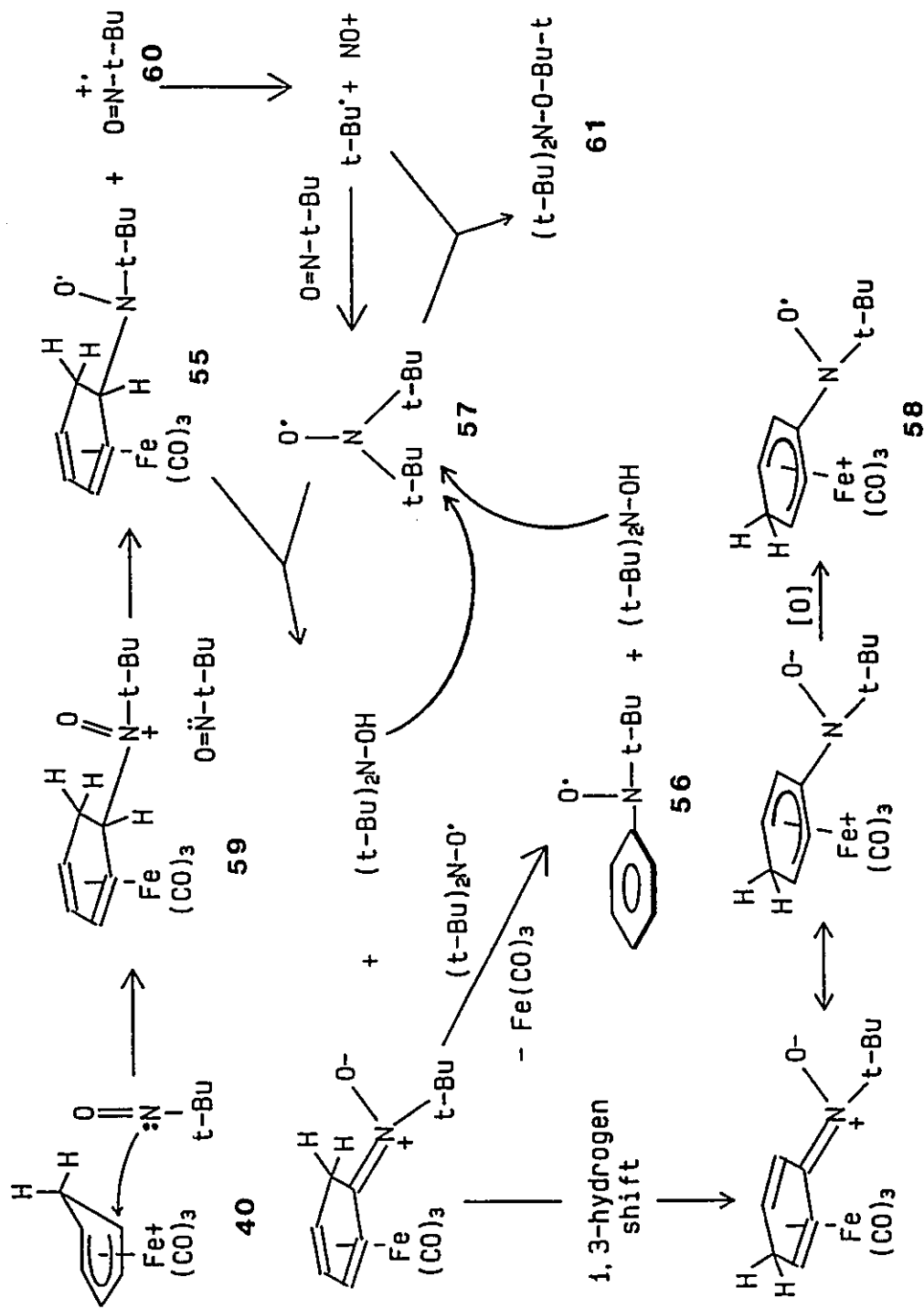
There has to be some positive feedback mechanism such that production of the oscillating species becomes more rapid as the reaction proceeds. There also has to be some reaction removing the oscillating species, which is therefore usually an intermediate rather than a final product. The following scheme fulfills these conditions.

Scheme 3.4 depicts a possible (speculative) mechanism to account for the observed radical products. In particular, we emphasize that the $(tert\text{-Bu})_2\text{N-O}\cdot$ radical is produced and destroyed in separate steps, as required for an oscillatory mechanism. It is proposed that initial nucleophilic attack by a molecule of $tert\text{-BuNO}$ on the cation **40** leads to an oxo-ammonium cation **59**. (We note that an analogous cation has been observed in the reaction of $(tert\text{-Bu})_2\text{N-O}\cdot$ with SbCl_5 ;¹⁵⁰ upon warming, the oxo-ammonium cation $[(tert\text{-Bu})_2\text{N=O}]^+$ decomposes to yield isobutene, NO^+ $[\text{SbCl}_6]^-$ and HCl .) We then suggest that **59** can suffer one-electron reduction by $tert\text{-BuNO}$ thus forming the nitroxide radical **55** and the $[(tert\text{-BuNO})^+]$ radical cation, **60**, which can fragment to give the nitrosonium ion and a $tert$ -butyl radical. This latter radical is well known to combine with $tert\text{-BuNO}$ to produce the stable $(tert\text{-Bu})_2\text{N-O}\cdot$ radical, **57**.¹⁵¹ It has been pointed out previously¹⁵¹ that in the presence of excess $tert$ -butyl radicals **57** reacts to produce tri- $tert$ -butylhydroxylamine, **61** $(t\text{-Bu})_2\text{NO-Bu-t}$; such an ESR-silent product is obviously a possibility here. Since one of the products is $tert$ -butyl(phenyl)nitroxide, **56**, clearly it is necessary to dehydrogenate the

cyclohexadienyl ring in **55**; such a process can be brought about by successive hydrogen abstractions by **56** to give the corresponding hydroxylamine, *i.e.*, $(tert\text{-Bu})_2\text{N-OH}$. We noted previously that the oscillating species is normally an intermediate rather than (as in this case) a final product. However, the reactions described here all use excess nitroso compound so the $(tert\text{-Bu})_2\text{N-O}\cdot$ radical, **57**, remains after the other reagent has been completely consumed. Under these conditions, the criteria for an oscillatory system can still be satisfied.

We further propose that the radical cation **58** might arise *via* the 1,3-hydrogen shift process depicted in Scheme 3.4. Such 1,3-shifts are formally symmetry-forbidden but in this case there exists the possibility of the migration occurring *via* a metal hydride intermediate; we cannot rule out the possible intervention of catalytic traces of acid. Moreover, we have previously reported that nitroso-arenes can attack the central carbon of a complexed cyclohexadienyl cation¹⁴⁰ thus rendering unnecessary the hydrogen migration process; that is, **58** could arise directly from **40**.

The serendipitous observation of this novel oscillating system sent us searching for literature precedents. While we found much elegant experimental and theoretical work on a variety of reaction types, we were unable to find any close analogues to this particular chemical oscillator. However, we did discover that some years ago Turcsanyi¹⁵² had proposed that a nitroxide / hydroxylamine system could in principle give rise to oscillatory behaviour under appropriate



Scheme 3.4 A speculative mechanism for the reaction of **40** with $t\text{-BuNO}$.

conditions. We have repeated Turcsanyi's calculations using a kinetics program written for this purpose¹⁵³ and have confirmed his results. A crucial component of any proposal to account for oscillatory behaviour is the existence of a feed-back mechanism by which a previous intermediate product can be regenerated. In this case, the important factor would appear to be the recycling of $(tert\text{-Bu})_2\text{N-O}\cdot$ by oxidation of the $(tert\text{-Bu})_2\text{N-OH}$, entirely analogous to the regeneration of the nitroxide intermediate in Turcsanyi's mechanistic scheme. The hydroxylamine $(tert\text{-Bu})_2\text{N-OH}$, like many such species, is very readily converted to the corresponding nitroxide radical. A suitable candidate to effect this oxidation is the cationic starting material **40**.

A referee has raised the interesting point that these observations may not be of the conventional oscillatory type but instead may best be characterized as "oligo-oscillatory" or "undershoot-overshoot kinetics".^{39,154} In oligo-oscillation, different component processes are responsible for each extremum, while in true oscillation (no matter how strongly damped) the chemistry is the same in each cycle.

In closing, it is of interest to note that the central feature of Turcsanyi's reaction scheme is that a molecule exists in three oxidation states, separated by one-electron transfers. It is the concentration of the middle oxidation state which oscillates, with the feedback mechanism being provided by oxidation or reduction reactions of the outer oxidation states. In the present case the middle oxidation

state is represented by a nitroxide radical and the other oxidation states by nitroso compounds and hydroxylamines. It is unlikely that this particular combination has great biological significance but carbon analogues can be readily visualized.

3.3 *Future work*

The mechanisms of oscillating reactions are usually very complicated. Typically, the mechanisms of the Belousov-Zhabotinski reaction complex system involve literally dozens of elementary or pseudo-elementary processes. It has taken more than 30 years and hundreds of publications to study the experimental details and the mechanisms of such systems since the first report of the oscillating reaction, and it is still not completely understood. Our system is the first chemical oscillating reaction which involves organometallic complexes. The mechanism we discussed is only preliminary. Future work would certainly involve using a computer to simulate this fascinating system and to construct a suitable model. The model finally selected for a tractable study must be a simplification of the complete mechanism but must still retain enough detail to generate all qualitative observations of experimental significance. Therefore, further studies on both theories and experiments are needed.

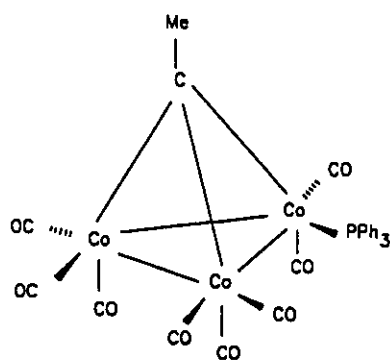
CHAPTER FOUR

HIGH-FIELD NMR STUDY OF VERTEX ROTATION IN $(C_5H_nMe_{5-n})MCo_2(CO)_8CR$ CLUSTERS (M = Mo, W)

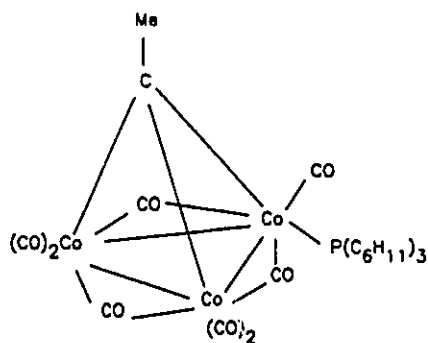
4.1 Introduction

Over the past few years, logical synthetic routes to mixed metal clusters have been developed.¹⁵⁵⁻¹⁵⁷ In particular, tetrahedral systems comprising three transition metal vertices and a capping carbonyl moiety have been intensively studied and it is now possible to focus on the structural and spectroscopic parameters and also the molecular dynamics of a series of such molecules. Two general synthetic approaches are widely applicable. The first involves the production of a cluster type such as $RCo_3(CO)_9$ which is readily available in multi-gram quantities^{158,159} and which undergoes facile substitution of a tricarbonylcobalt vertex by an isolobal¹⁶⁰ fragment such as $CpMo(CO)_2$,¹⁶¹ $CpNi$ ¹⁶² or $Ru(CO)_3^-$,¹⁶³ as in Scheme 4.1. The second general route proceeds *via* the reaction of a metal-carbyne complex with a molecule containing (or capable of generating) a metal-metal triple bond.^{155,164}

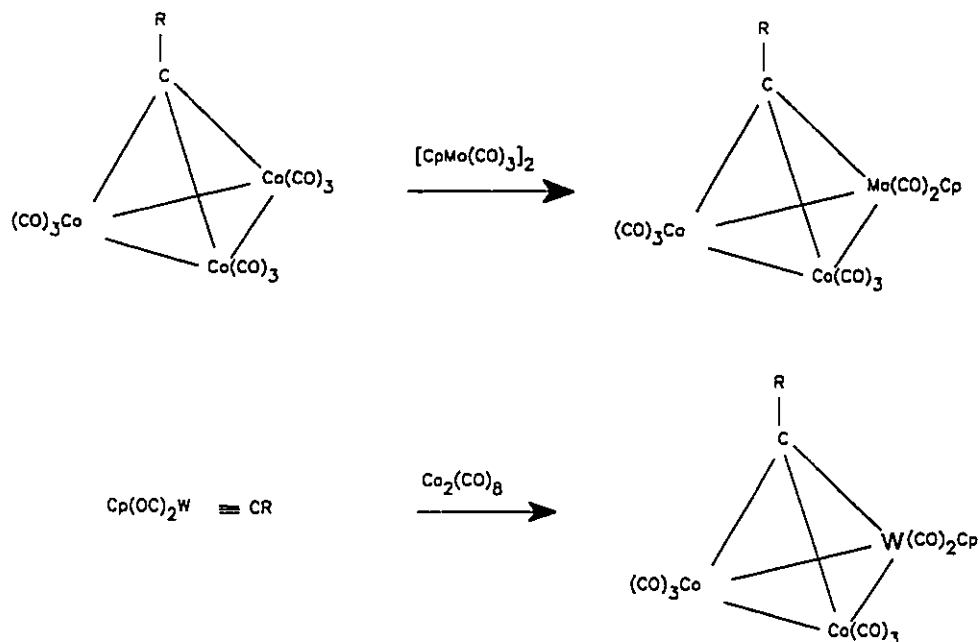
In small clusters the fluxionality of ligands (and even of vertices^{165,166}) is well established.¹⁶⁷ Typically, $RCo_3(CO)_8L$ complexes are known in which the carbonyl ligands are found only in terminal positions, as in **62**, or in both terminal and bridging environments, as in **63**. In these latter cases the solution infrared spectra exhibit more ν_{CO} stretching vibrations than can be assigned to a single structure.^{168,169} However, on the NMR time scale, these exchange processes are so fast as to yield only an averaged ^{13}CO resonance in most cases. With the advent of very high field spectrometers, it is occasionally possible to slow such exchange processes on the NMR time scale and so establish the molecular structure. To take a particularly fine example, we note that the C_s symmetry of $H_2Os_3(CO)_9CCO$ in solution was first demonstrated by ^{13}C NMR spectroscopy which revealed a 2:1:2:2:2 pattern for the CO's at low temperature;¹⁷⁰ subsequently, X-ray crystallography was used to show that the molecule adopted the same structure in the solid state.¹⁷¹



62



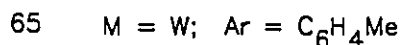
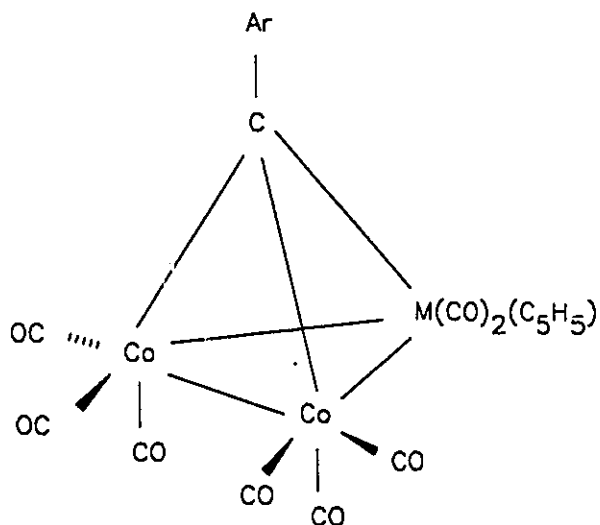
63



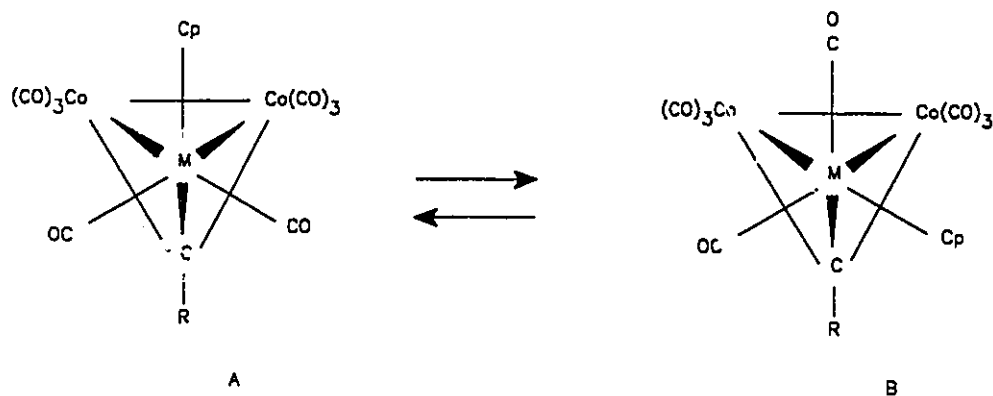
Scheme 4.1 Synthetic routes to mixed-metal clusters

The molecules $(\text{C}_5\text{H}_5)\text{MoCo}_2(\text{CO})_8\text{C}-\text{C}_6\text{H}_5$, **64**, and $(\text{C}_5\text{H}_5)\text{WCo}_2(\text{CO})_8\text{C}-\text{C}_6\text{H}_4\text{CH}_3$, **65**, have been characterized X-ray crystallographically;^{172,173} the structures are almost identical and show that (a) all carbonyls are terminal (b) the cyclopentadienyl ring is positioned below the trimetallic plane (*i.e.*, *distal* to the capping group) and (c) the plane of the aryl ring is parallel to the cobalt-cobalt vector. However, as was pointed out by both sets of authors, the solution infrared data exhibited too many carbonyl stretching vibrations to be assigned solely to the structure of the crystalline form. Furthermore, the observation of an infrared band at $\sim 1875\text{ cm}^{-1}$ was interpreted as implying the presence of an isomer with semi-bridging carbonyl ligands. The comment was also made¹⁷³ that rotational

isomerism attributable to different orientations of the $\text{CpM}(\text{CO})_2$ fragment relative to the Co_2C triangular face should be considered (see Scheme 4.2).



To clarify the conformational behavior of these molecules, we undertook a 125 MHz ^{13}C NMR study of a series of $\text{R-CCo}_2(\text{CO})_6\text{M}(\text{CO})_2\text{Cp}$ clusters, where $\text{M} = \text{Mo}$ or W , in which the bulk of the substituents in the cyclopentadienyl ring could be modified. As the apical substituent we chose the isopropyl ester functionality since its potentially diastereotopic methyl groups could be used as a probe for chiral systems such as conformation **B** in Scheme 4.2.¹⁷⁴

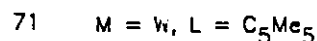
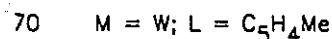
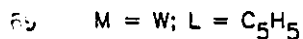
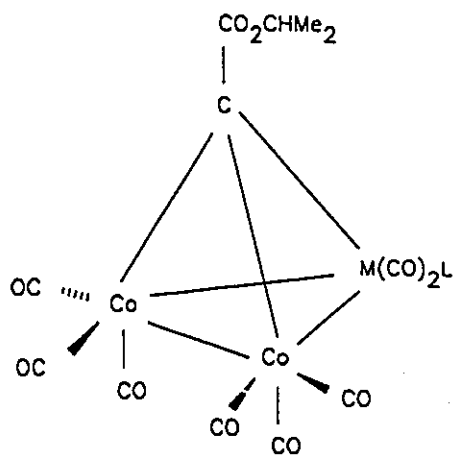


Scheme 4.2 Rotation of a $\text{CpMo}(\text{CO})_2$ vertex relative to a triangular face.

4.2 Results and Discussion

4.2.1 ^{13}C NMR and Infrared Spectroscopy

In connection with our earlier studies on chiral mixed metal clusters,¹⁷⁵ Karen Sutin had prepared $(\text{C}_5\text{H}_5)\text{MoCo}_2(\text{CO})_8\text{C}-\text{CO}_2\text{CHMe}_2$, **66**, and recorded its ^{13}C NMR spectrum over the temperature range $+30^\circ\text{C}$ to -90°C . The metal carbonyl resonances appear as a single peak at room temperature on an 80 MHz spectrometer, but at -50°C on a 250 MHz instrument the peak broadens and splits into a 2:6 pattern with shifts characteristic of carbonyls bonded to molybdenum and cobalt, respectively. The -90°C ^{13}C spectrum recorded at 11.7 Tesla (500 MHz for ^1H , 125 MHz for ^{13}C) is shown as trace (a) in Figure 4.1. Clearly, two isomers are present in solution. The major component has a cobalt carbonyl peak at 203 ppm



and a molybdenum carbonyl resonance at 221 ppm; the integrated intensity ratio is 3:1, corresponding to Co₂(CO)₆ and Mo(CO)₂ fragments. The minor component likewise exhibits a 6:2 ratio of cobalt to molybdenum carbonyls but now the latter resonance is found at 230 ppm — a region more typical of bridging or semi-bridging bonded carbon monoxide ligands on molybdenum.¹⁷⁶ As shown in trace (b) of Figure 4.1, similar behavior is exhibited by the monomethylcyclopentadienyl analogue, **67**, but the pattern is completely reversed for the pentamethylcyclopentadienyl complex, **68**. Figure 4.1 also shows the 125 MHz ¹³C NMR spectra of the corresponding tungsten clusters, and again the (C₅H₅)WCo₂(CO)₈CR, **69**, and (C₅H₄Me)WCo₂(CO)₈CR, **70**, molecules favor the

structure with high field tungsten carbonyls (at 208 ppm) while in the $(C_5Me_5)WCo_2(CO)_8CR$ system, **71**, the low field (high frequency) tungsten carbonyl peak predominates. In these latter molecules, the carbonyl resonances assigned to the $W(CO)_2$ fragment are unambiguously distinguished from those of the $Co(CO)_3$ groups not only by their characteristic chemical shifts but also by the observation of satellite peaks attributable to coupling to the ^{183}W nuclei ($I = 1/2$; 14% abundant).

It is a commonly observed phenomenon that carbonyl ligands which find themselves in bridging environments exhibit a marked high frequency shift relative to situations in which they are terminally bonded to the same metal. Typically, $Fe(^{13}CO)_3$ moieties in clusters resonate at approximately 215 ppm but a carbonyl which bridges two Fe atoms can be deshielded by more than 30 ppm; analogous data exist for bridging carbonyls bonded to a variety of other metals.^{177,178} The evidence thus suggests that, in the clusters **66** through **71**, the predominant conformation adopted by those molecules containing unsubstituted or mono-substituted cyclopentadienyl groups is one in which the carbonyl ligands bonded to molybdenum or tungsten possess only terminal carbonyls; in contrast, with the much more bulky pentamethylcyclopentadienyl group, the CO's attached to the Group 6 metal apparently adopt a bridging or semi-bridging position in the predominant isomer.

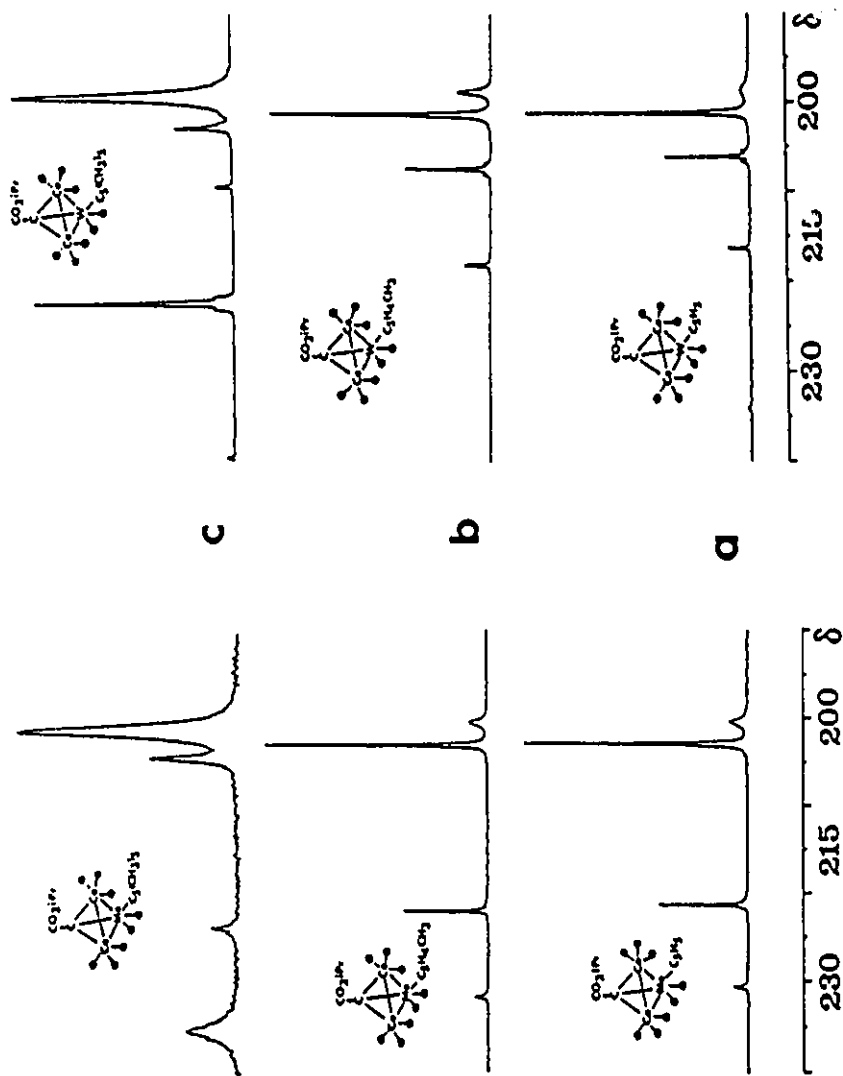


Figure 4.1 Low-temperature 125.7-MHz ^{13}C NMR spectra in the metal carbonyl region for (a) 66 and 69, (b) 67 and 70, and (c) 68 and 71.

The low-temperature ^{13}C NMR spectrum of $\text{Ph-CCo}_2(\text{CO})_6\text{Mo}(\text{CO})_2(\text{C}_5\text{H}_5)$, **64**, is in accord with the pattern observed for all the other complexes bearing unsubstituted cyclopentadienyl rings. That is, the predominant isomer exhibits a Mo-carbonyl resonance at 223 ppm while in the minor isomer the corresponding peak is found at 232.5 ppm. Again, the major constituent has terminal carbonyls on molybdenum in accord with the structure found X-ray crystallographically in the solid state. These arguments are buttressed by infrared data on $\text{Ph-CCo}_2(\text{CO})_6\text{Mo}(\text{CO})_2(\text{C}_5\text{H}_5)$. As previously reported by Vahrenkamp and shown again in Figure 4.2, the infrared spectrum in CH_2Cl_2 exhibits many ν_{CO} bands, including a weak absorbance at $\sim 1875\text{ cm}^{-1}$ which suggests the existence of a semi-bridging carbonyl. This feature is entirely absent when the infrared spectrum of **64** is recorded as a KBr pellet. In an entirely analogous fashion, the solution and solid state infrared spectra of $(\text{C}_5\text{H}_4\text{Me})\text{WCo}_2(\text{CO})_6\text{C-CO}_2\text{-}i\text{Pr}$, **70**, demonstrate (see Figure 4.2) the existence of a small fraction of the semi-bridged isomer in solution but a single all-terminal structure in the solid state. The situation is quite different for the pentamethylcyclopentadienyl complexes **68** and **71** for which the semi-bridging situation is favored both in solution and in the solid phase.

Before postulating viable structures for the two isomers detectable on the NMR time scale, we must examine the evidence provided by the other NMR probes that have been built into the molecules. We note initially that the ^{13}C ring carbon resonances are split at low temperature into the same intensity ratios as

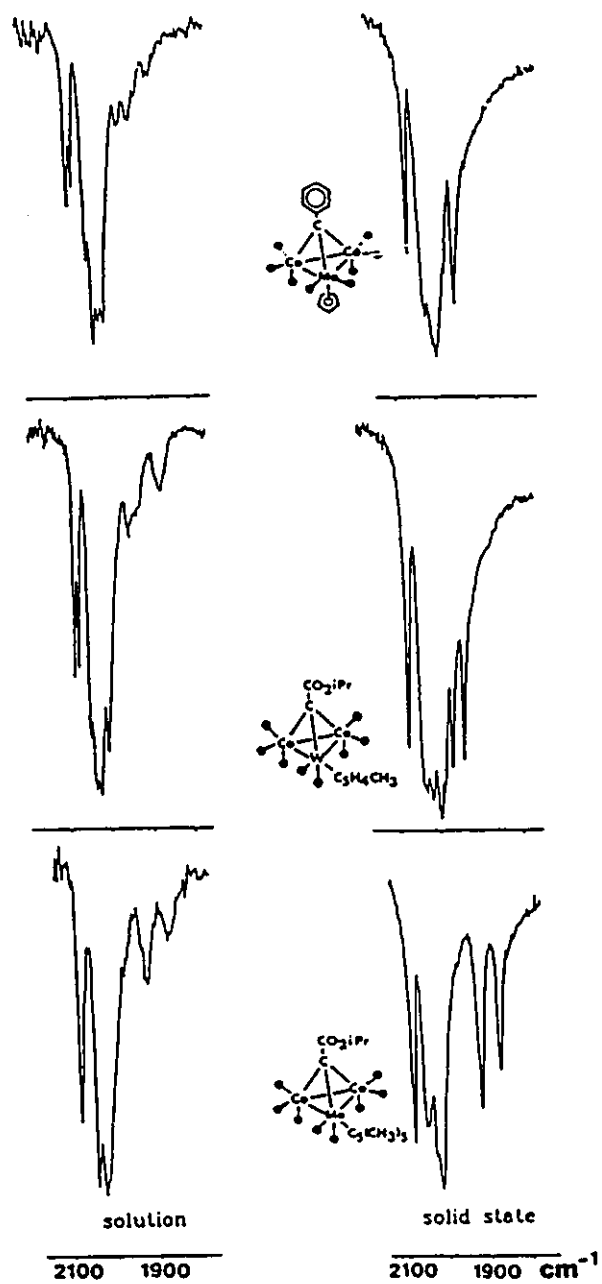
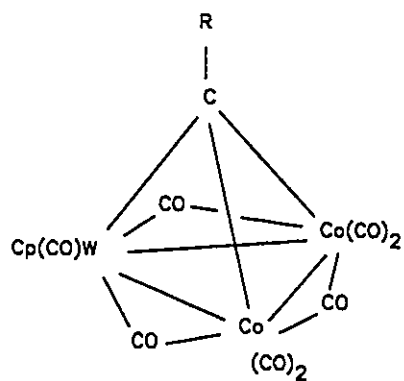
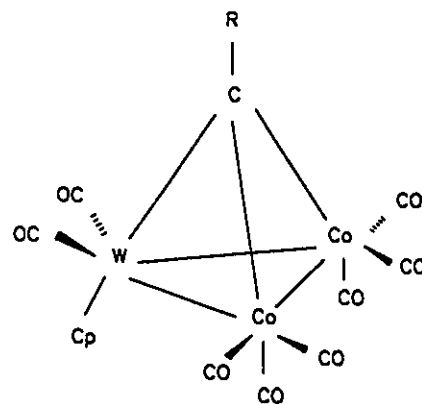


Figure 4.2 Sections of the infrared spectra of the clusters **64**, **70**, and **68** in solution in methylene chloride and in solid state as KBr pellets.

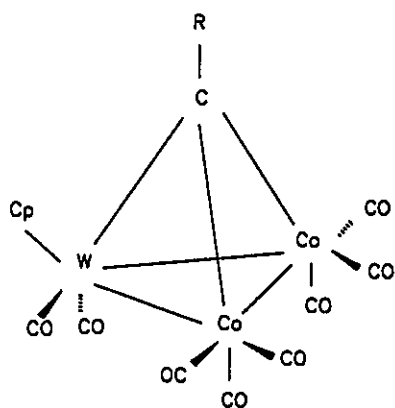
are the carbonyls. We can thus associate a given set of cyclopentadienyl peaks with a particular isomer. It is also particularly significant that, although we see two sets of resonances in either the ^1H or ^{13}C spectra for the methyl groups of the isopropyl ester substituent, these signals are never split into diastereotopic pairs,¹⁷⁹ that is, the molecules adopt *achiral* conformations. We can, therefore, eliminate rotamers of the $\text{CpM}(\text{CO})_2$ vertex (for example, conformer **B** in Scheme 4.2) which place the cyclopentadienyl group in a *gauche* position with respect to the Co_2C triangle. [This assumption is only valid if there is no very low energy process that equilibrates enantiomeric *gauche* conformers. It is noteworthy that a *gauche* orientation for a $\text{CpM}(\text{CO})_2$ unit has been crystallographically characterized in $(\text{C}_5\text{H}_5)\text{W}(\text{CO})_2\text{Fe}_2(\text{CO})_6(\mu\text{-CO})\text{C-C}_6\text{H}_4\text{Me}$; in that case the ^{13}CO region shows only a single resonance but no low temperature data were reported.¹⁸⁰] Moreover, we can also see that structures involving three bridging carbonyls, such as **72**, are not viable candidates since the observed ratio of cobalt carbonyls to molybdenum or tungsten carbonyls is inconsistent with such a formulation. The most reasonable structures for the isomers observable by NMR are those which place the cyclopentadienyl rings either below (*distal* to the carbonyl cap) or above the trimetallic plane (*proximal* to the cap), as in **73** or **74**, respectively, and which preserve the mirror symmetry of the molecule.



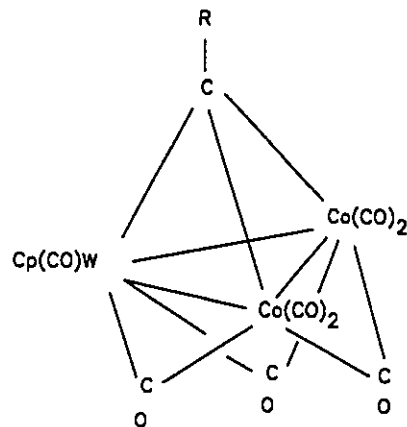
72



73



74



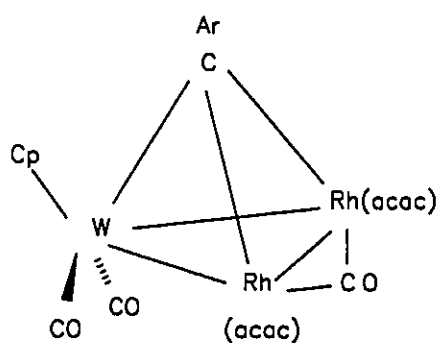
75

4.2.2 Vertex rotation and CO exchange

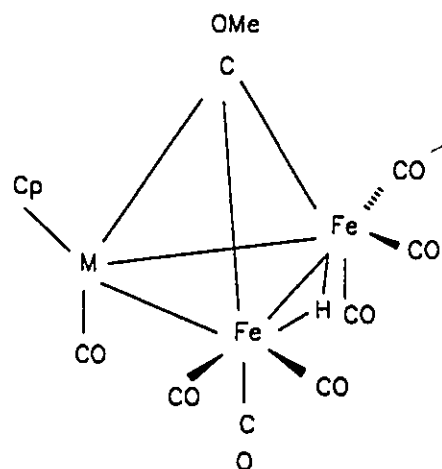
Karen Sutin grew crystals of $(C_5Me_5)MoCo_2(CO)_8C-CO_2-iPr$, **68**, and solved the structure shown in Figure 4.3. The crucial differences relate to the orientation of the $Cp^*Mo(CO)_2$ moiety which is now positioned such that the C_5Me_5 ring is

proximal with respect to the carbonyl capping unit. Moreover, the molybdenum carbonyls, which are clearly terminal and linear in **64** and **65**, are semi-bridging in **68**.

It is interesting to speculate on the reasons for the preferred orientation of the bulky pentamethylcyclopentadienyl ring in a site *proximal* to the carbonyl cap. One might suggest that the enhanced electron-donating capability of the pentamethylated ring causes a build-up of charge on the molybdenum or tungsten atom; this in turn can best be alleviated by siphoning off the excess electron density to the tricarbonylcobalt centers *via* semi-bridging carbonyls. In this vein, we note that in $(C_5H_5)W(CO)_2Rh_2(acac)_2(\mu-CO)C-C_6H_4Me$, **76**, the cyclopentadienyl group is *proximal* and the semi-bridging tungsten carbonyls appear to be trying to compensate for the electron deficiency at the rhodium centers.¹⁷³



76



77

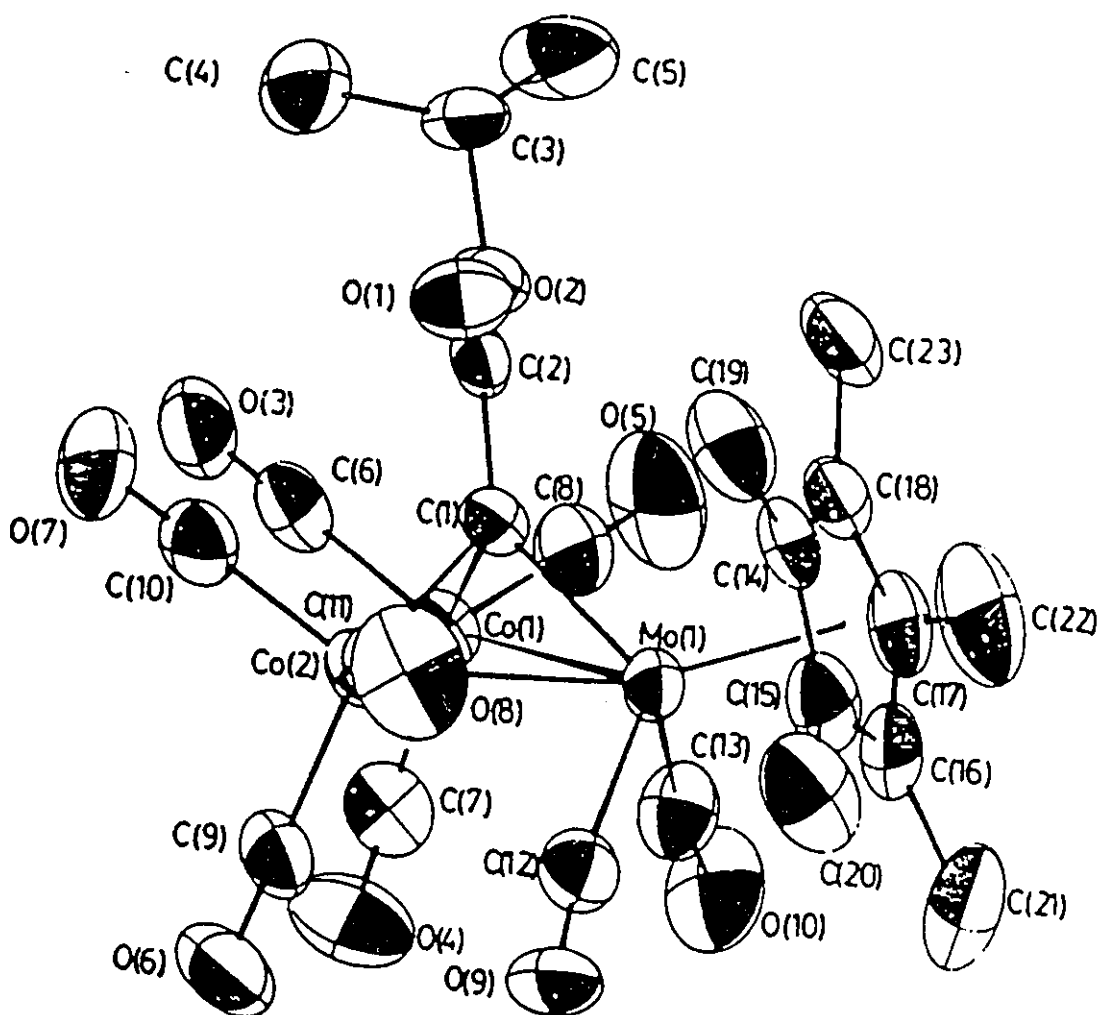


Figure 4.3 View of (C₅Me₅)MoCo₂(CO)₈CCO₂-i-Pr (68), showing the atom numbering scheme.

Therefore, we know that in solution the predominant conformers of $(C_5H_5)MCo_2(CO)_8C-R$, *i.e.*, **64**, **65**, **66**, **69**, and of $(C_5H_4Me)MCo_2(CO)_8C-R$, *i.e.*, **67**, **70**, are of type **73** whereby the cyclopentadienyl group is oriented below the plane of the three metals and all the carbonyls are clearly terminal, as in the solid state.¹⁸¹ In contrast, conformation **74** is found in both phases for the analogous C_5Me_5 clusters **68** and **71**. Nevertheless, since the room temperature NMR spectrum shows only an averaged ^{13}CO environment, it is obviously incumbent upon the molecule to spend at least part of its time in a conformation which facilitates the transfer of carbonyl ligands from one metal vertex to another. This criterion may best be satisfied by a conformation such as **75** which could be attained from **74** with only minor adjustments. Fluxionality of axial ligands has been invoked in $RCo_3(CO)_7(diphos)$ and related molecules^{175,182} in which the *diphos* ligand occupies two equatorial sites and so blocks the conventional merry-go-round.¹⁶⁷ Moreover, Farrugia has shown that in $Fe_2M(\mu-H)(\mu_3-COCH_3)(CO)_7(\eta-C_5H_5)$, **77**, where $M = Co$ or Rh , the single carbonyl bound to cobalt or rhodium is axially positioned and can undergo exchange with the carbonyls on the iron atoms.^{183,184} (In some ways this process resembles the intermetallic carbonyl migration in $(C_5H_5)_3Rh_3(CO)_3$ reported some years ago by Shapley.¹⁸⁵) McGlinchey and his coworkers have already reported¹⁷⁵ that the barriers to intermetallic carbonyl scrambling in tetrahedral $CpMCo_2(CO)_8CR$ systems are of the order of 9-10 kcal mol⁻¹ and such values fit in well with the barriers to rotation of the

(C₅H_{5-n}Me_n)Mo vertices in (RC≡CR)Cp₂M₂(CO)₄ clusters;¹⁸⁶⁻¹⁸⁸ it is interesting to speculate whether these two fluxional processes are interdependent. Since the CO ligands can only be transferred from metal to metal when they can adopt a bridging or semi-bridging bonding mode, it seems not unreasonable to postulate that the ability of the carbonyl ligands to migrate over the triangle of metals is controlled by the ease of rotation of the CpM(CO)₂ vertex.

To investigate the viability of the hypothesis that the intermetallic migration of carbonyls is controlled by the barrier to CpM(CO)₂ vertex rotation, we recorded the variable temperature ¹³C spectra of (C₅H₄Me)MoCo₂(CO)₈CCO₂CHMe₂, **67**, and Figure 4.4 shows the behavior of the metal carbonyl resonances over the range 203-293K. It is clear that rotation of the CpMo(CO)₂ vertex must interconvert the Mo-CO peaks at δ 204.1 and 200.9. Moreover if the migration of the carbonyl ligands between molybdenum and cobalt centers can only occur when the molybdenum vertex adopts a particular conformation (for example, a gauche rotamer), then the rate constant for intermetallic carbonyl exchange cannot exceed the rate of vertex rotation. Thus, the simulated spectra shown in Figure 4.4 were obtained by using the same rate constant for proximal-distal interconversion as for intermetallic carbonyl migration at any given temperature; gratifyingly, the agreement is excellent. An Arrhenius plot of these data yield an activation energy barrier of 8.8 ± 0.3 kcal mol⁻¹. We are therefore drawn to the conclusion that these two fluxional processes are indeed correlated.

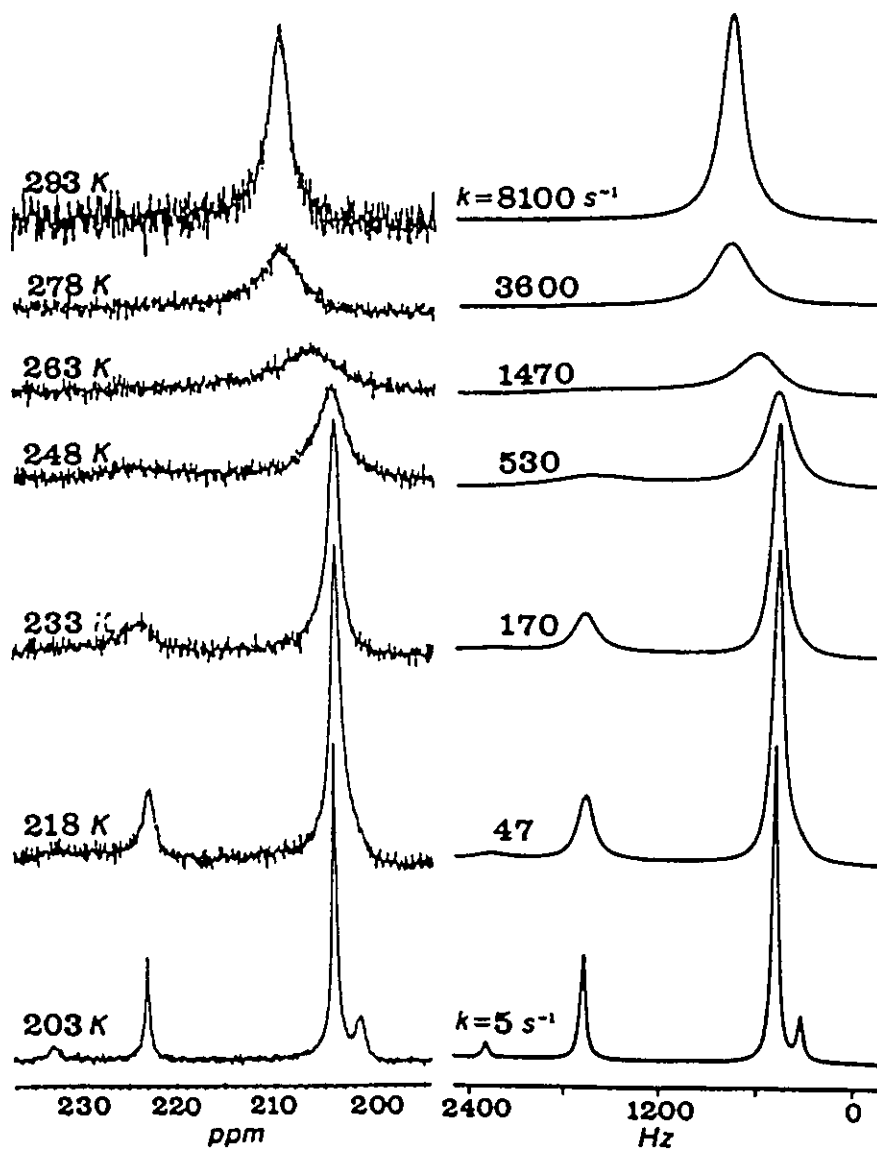
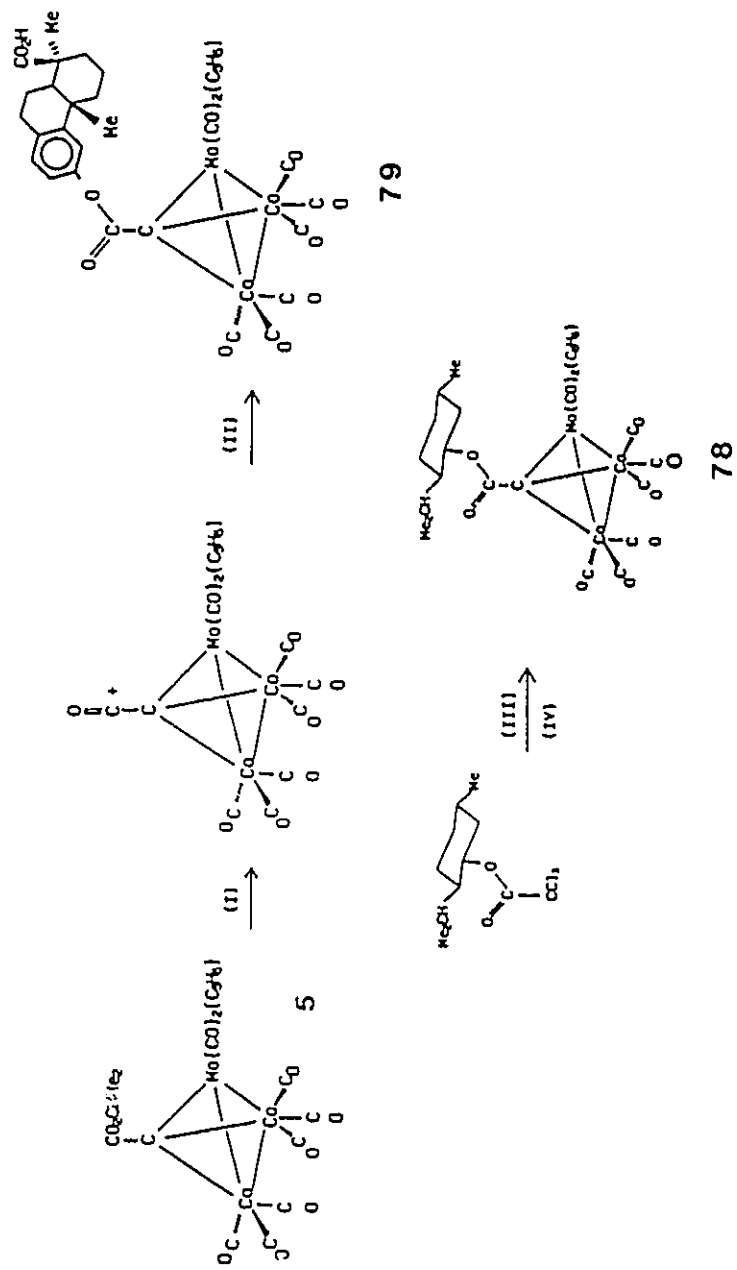


Figure 4.4 Experimental and simulated 62.86-MHz ^{13}C variable-temperature NMR spectra of **67** in the metal carbonyl region.

4.2.3 Chiral Clusters

The fluxional processes discussed above involve either rotation of a $\text{CpM}(\text{CO})_2$ vertex or the intermetallic migration of carbonyls between molybdenum (or tungsten) and cobalt vertices. However, the mirror symmetry of clusters of the type **73** and **74** precludes the detection of slowed carbonyl exchange between $\text{Co}(\text{CO})_3$ moieties;¹⁸⁹ that is, such a fluxional process is hidden because the cobalt environments are equivalent. To break this symmetry it is necessary to incorporate a chiral substituent and thus render diastereotopic the two $\text{Co}(\text{CO})_3$ sites. McGlinchey *et al.* have previously reported¹⁹⁰⁻¹⁹⁴ the syntheses of a series of such clusters in which the capping carbonyl group bears a chiral substituent derived from a natural product such as a steroid or a terpene. Scheme 4.3 shows the synthetic routes to the clusters $(\text{C}_5\text{H}_5)\text{MoCo}_2(\text{CO})_8\text{C-R}^*$, **78** and **79**, in which the chiral units are derived from menthol and from podocarpic acid (a naturally occurring diterpene, readily available from the New Zealand rimu tree¹⁹⁵), respectively. These clusters are now not only inherently chiral but also bear relatively bulky ester substituents.

The establishment of the rotameric structures of these clusters allows one to assign unambiguously a given $\text{Co}(\text{CO})_3$ resonance to a molecule in which the cyclopentadienyl ring is positioned either *distal* or *proximal* to the cap. Figure 4.5 shows the variable-temperature ^{13}C NMR spectra of **78** in the cobalt carbonyl region.



Scheme 4.3

Synthetic routes to the chiral clusters **78** and **79**.

(I) $\text{H}^+\text{PF}_6^-(\text{EtCO})_2\text{O}$ (II) podocarpic acid (III) $\text{Co}_2(\text{CO})_8$ (IV) $\text{Cp}_2\text{Mo}_2(\text{CO})_6$

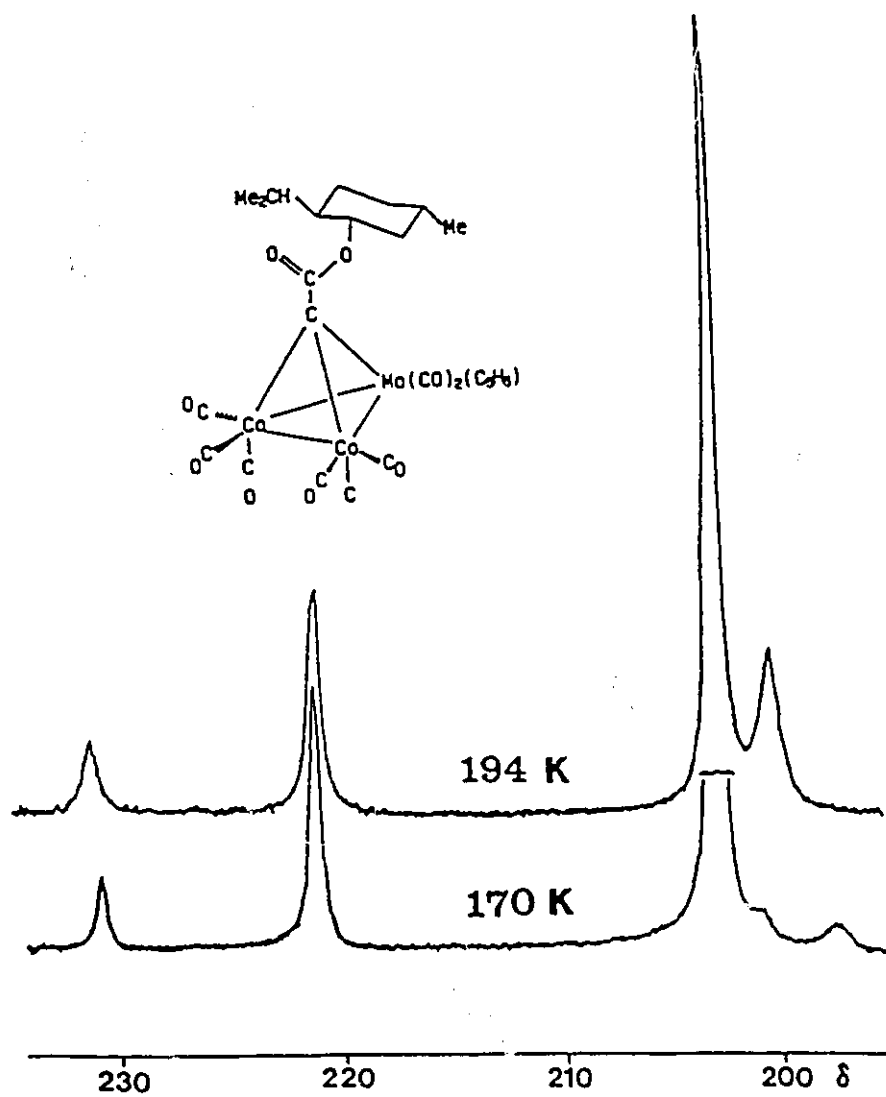


Figure 4.5 Variable-temperature 125.7-MHz ^{13}C NMR spectra in the metal carbonyl region for 78.

It is readily apparent that at the lowest accessible temperature the $\text{Co}(\text{CO})_3$ resonances **of the minor isomer only** are split into two equally intense peaks. The Gutowsky-Holm approximation yields a ΔG^\ddagger_{180} value of $\approx 8.6 \pm 0.5 \text{ kcal mol}^{-1}$. The podocarpate complex **79** behaves similarly in that the minor $\text{Co}(\text{CO})_3$ peaks broadens out but does not yield a fully resolved limiting spectrum; apparently ΔG^\ddagger is somewhat lower than for **78**. These observations must mean that carbonyl exchange between the two cobalt centers has been slowed on the NMR time scale and the diastereotopic nature of these vertices is now evident. Since we know that in this rotamer the cyclopentadienyl unit is oriented *proximally* to the carbonyl cap one might conclude that the bulky menthol (or slightly less bulky podocarpate) fragment is constrained to lie over the cobalt-cobalt bond, as depicted in the CHEMX model¹⁹⁶ shown in Figure 4.6. In the predominant isomer of **78** or **79**, where the cyclopentadienyl ring is *distal* and the chiral capping unit is free to rotate, the cobalt vertices are, of course, still diastereotopic but their chemical shift differences may be smaller than they are in the minor rotamer where the chiral group is held closer to these metals.

In summary, therefore, it has been shown that the fluxional behavior of clusters of the $\text{CpMCo}_2(\text{CO})_8\text{C-R}$ type, where $\text{M} = \text{Mo}$ or W and Cp bears zero, one or five methyl substituents, can be rationalized in terms of restricted rotation of the $\text{CpM}(\text{CO})_2$ vertex such as to give isomers in which the cyclopentadienyl ring lies either *proximal* or *distal* with respect to the carbonyl capping group. In either

case, the Cp ring is bisected by a molecular mirror plane thus rendering the $\text{Co}(\text{CO})_3$ vertices equivalent unless the capping group is made chiral in which case slowed exchange of CO's between cobalts is observable.

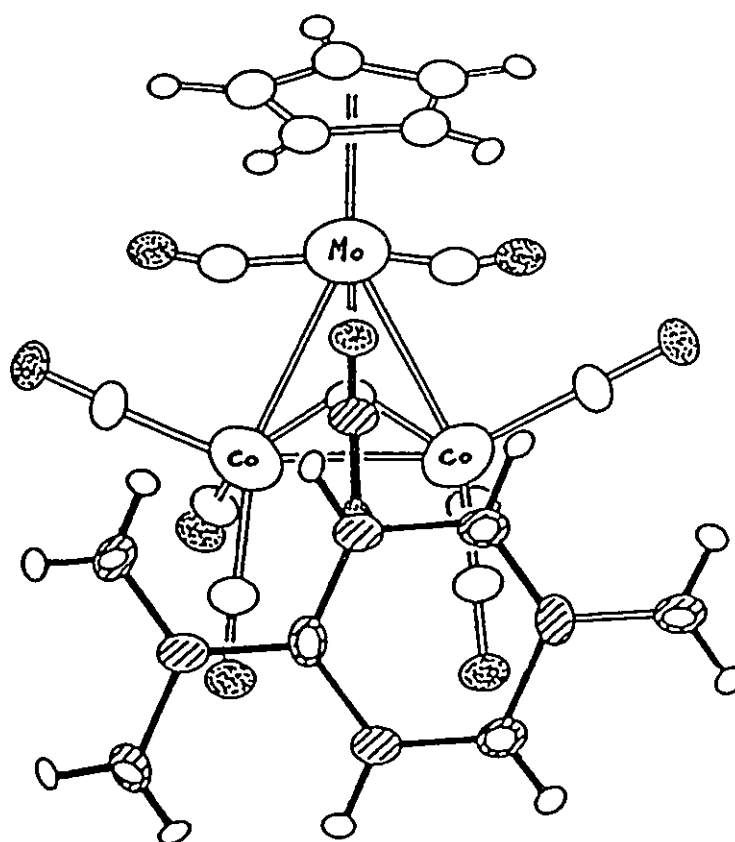


Figure 4.6 CHEMX model of the cluster **78** in which the C_5H_5 ligand is proximal to the capping group and the bulky menthol substituent lies over the cobalt-cobalt vector.

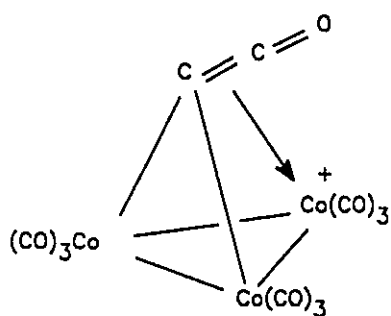
CHAPTER FIVE

VARIABLE-TEMPERATURE 1- AND 2-DIMENSIONAL ^{13}C NMR STUDIES ON $\text{CH}_3\text{CCo}_3(\text{CO})_8\text{P}(\text{cyclo-C}_6\text{H}_{11})_3$: THE MECHANISM OF CARBONYL MIGRATION

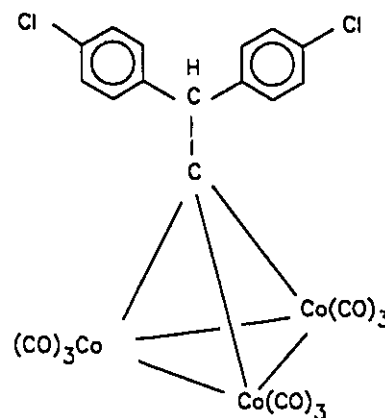
5.1 Introduction

The fluxional behavior of carbonyl ligands on metal cluster surfaces has attracted much attention for a considerable number of years. Some very fine experimental data have emerged; especially notable are the ingenious and elegant experiments carried out to elucidate the carbonyl scrambling mechanisms in heavy metal clusters.^{65,98} Moreover, the thought-provoking ideas of Johnson and Benfield may give us cause to re-evaluate our models of fluxionality in metal clusters.¹⁹⁷ Nevertheless, the situation is much less clear for carbonyl-capped tricobalt systems in which not only local rotation of $\text{Co}(\text{CO})_3$ vertices but also intermetallic carbonyl migrations have such low barriers that the ^{13}C NMR spectrum in solution is almost invariably a single line even at very low temperatures. Very recently, the nine-fold degeneracy of the carbonyl ligands in $[\text{Co}_3(\text{CO})_9\text{C-C=O}]^+$, **80**, and in $\text{Co}_3(\text{CO})_9\text{C-CH}(\text{C}_6\text{H}_4\text{Cl})_2$, **81**, has been split to give in each case a 6:3 pattern at

low temperature.^{198,199} Although these results yield valuable structural information, they do not provide unequivocal answers to mechanistic questions.

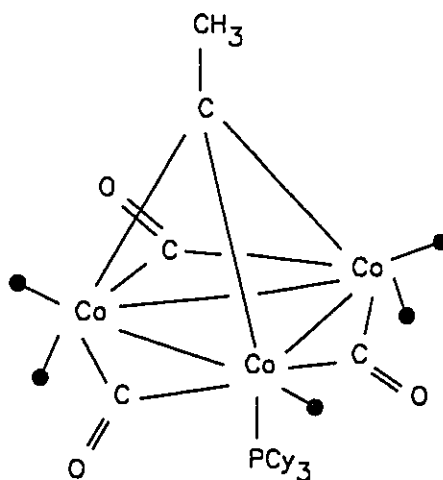


80



81

To our knowledge, the only other carbonyl-tricobalt cluster showing well-defined fluxional behavior is $\text{CH}_3\text{CCo}_3(\text{CO})_8\text{P}(\text{cyclo-C}_6\text{H}_{11})_3$ which has the triple-bridged structure **63** in the solid state.²⁰⁰ ^{13}C NMR measurements on **63** at 25 MHz suggested²⁰¹ that the low temperature limiting spectrum would yield a 1:2:1:2:2 pattern for the carbonyl resonances, consistent with the solid state structure. These data prompted us to initiate a study using high field instrumentation which might allow a more complete analysis of the molecular dynamics of this system. We now report the variable-temperature one- and two-dimensional ^{13}C NMR spectra of **63** obtained at 11.7 tesla (500 MHz for protons; 125.7 MHz for carbon-13 nuclei).

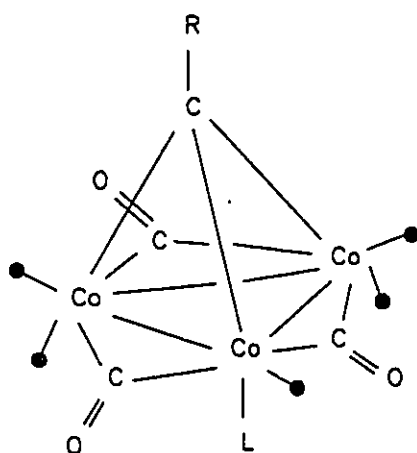


63

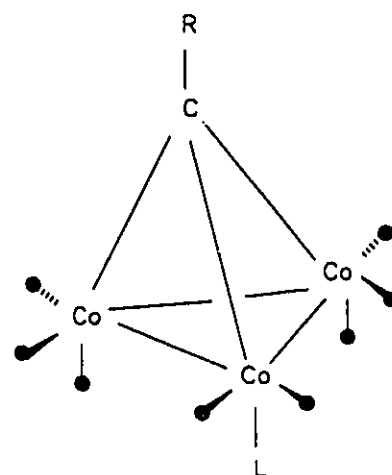
5.2 Results and Discussion

It has been established that the factors which affect the equilibrium between the bridged and non-bridged isomers **82** and **83** are rather subtle.²⁰² Nevertheless, it is generally true that bulky electron-donating phosphines favor the triple-bridged structure **82** which has been characterized crystallographically for the case where $L = P(\text{cyclo-C}_6\text{H}_{11})_3$, **63**.²⁰⁰ Matheson and Robinson attempted to quantify the equilibrium ratios of **82:83** by using variable-temperature infrared spectroscopy and they concluded that for $\text{CH}_3\text{-CCo}_3(\text{CO})_8\text{P}(\text{cyclo-C}_6\text{H}_{11})_3$, **63**, this ratio was 88:12 at 195 K.²⁰¹ We now report the ^{13}C NMR spectra of **63** as shown in Figure 5.1. These measurements confirm the preliminary report that the fluxionality of this

complex can be slowed on the NMR time-scale at low temperature. However, we found no NMR evidence which indicated the presence of any other isomer (such as **83**). The relative intensities make assignment of the carbonyl peaks trivial except for the resonances at δ 200.4 and δ 198.8; these are clearly the terminal ligands (**D** and **E**) on the cobalts which do not bear the phosphine ligand. Although one cannot unequivocally assign a given resonance to the **D** site or the **E** environment, it turns out that this distinction is not crucial to the mechanistic argument.



82



83

Before attempting to simulate the set of variable-temperature experimental spectra shown in Figure 5.2 one must, of course, select a chemically reasonable scenario which ultimately equilibrates all the sites. The simple merry-go-round process,²⁰³ shown in Scheme 5.1, will eventually equilibrate the **A**, **B**, **C** and **D** environments.

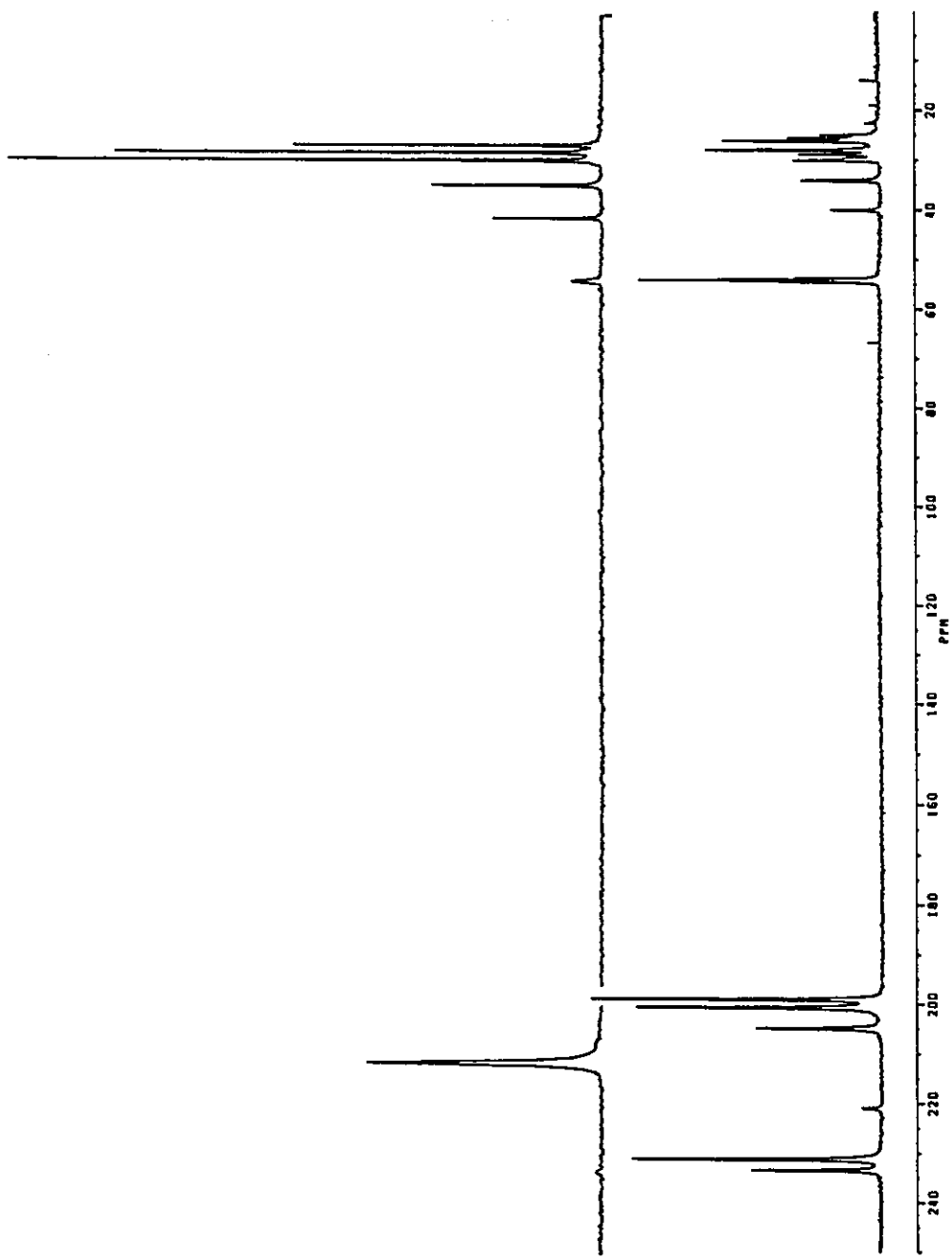


Figure 5.1 ^{13}C NMR spectra of $\text{CH}_3\text{CCO}_3(\text{CO})_8\text{P}(\text{cyclo-C}_6\text{H}_{11})_3$, 63, at 183K and 263K.

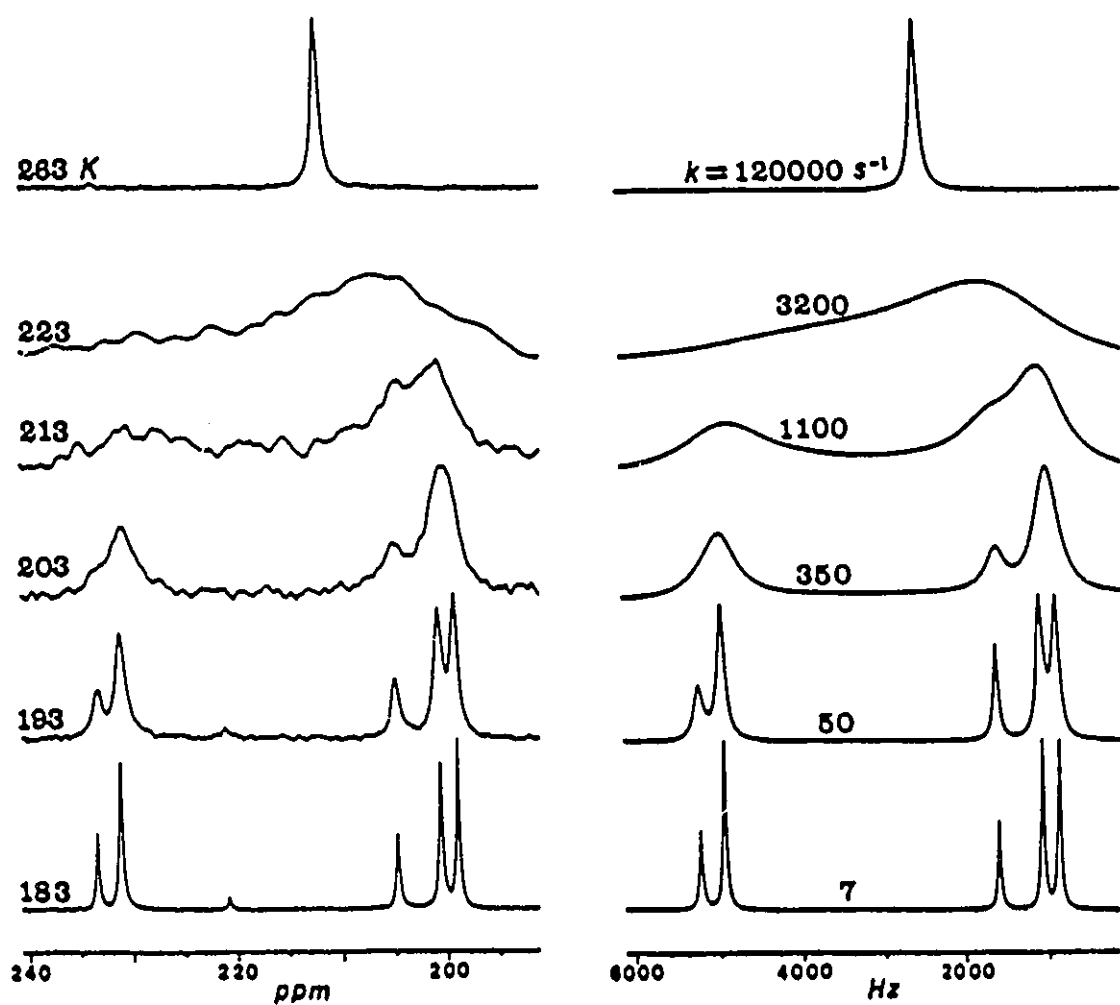


Figure 5.2 Experimental and simulated variable-temperature ^{13}C NMR spectra of $\text{CH}_3\text{CCO}_3(\text{CO})_8\text{P}(\text{cyclo-C}_6\text{H}_{11})_3$, **63**, in the metal carbonyl region.

Moreover, at the bridge-opened stage, rapid local rotation allows the axial ligands, viz. **E** and **E'**, to enter the sequence and so scramble all carbonyl sites.

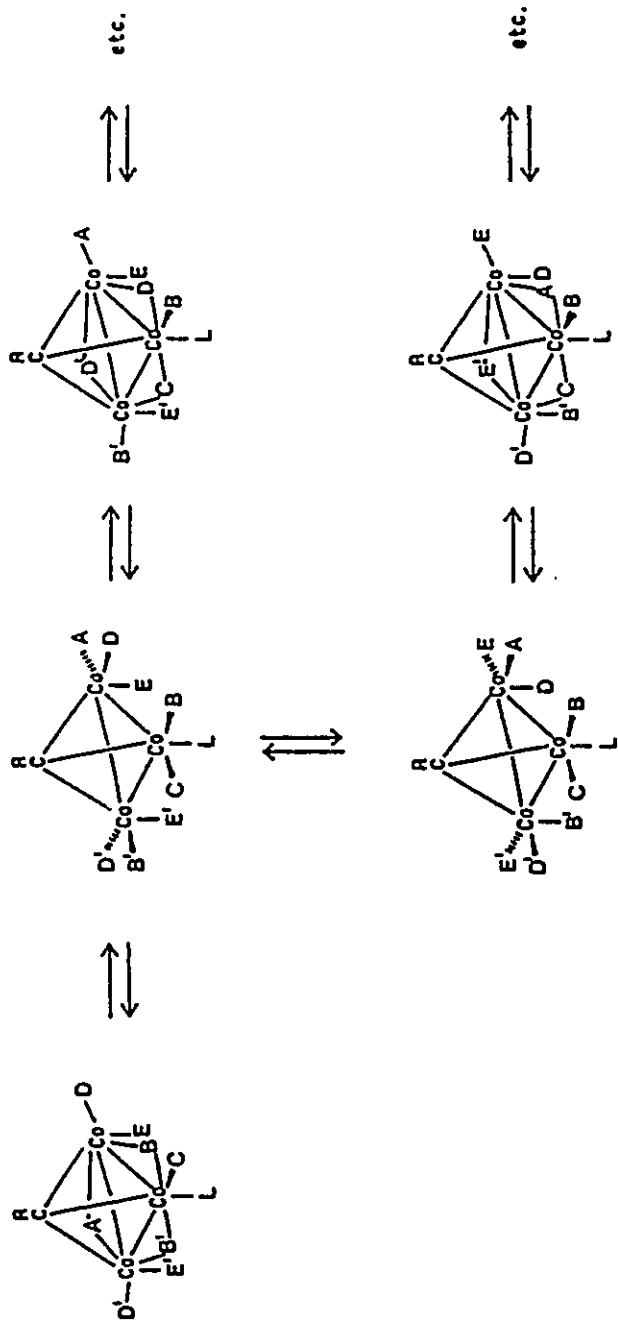
In their early work, Matheson and Robinson proposed an alternative pathway which involved concerted conrotatory movement by $\approx 100^\circ$ of each cobalt vertex so as to interconvert the bridged and non-bridged configurations.²⁰¹ This proposal would require the tricyclohexylphosphine ligand to oscillate between axial and equatorial positions. Such a process, in conjunction with local rotation of each cobalt vertex would allow each carbonyl access to all the other sites. However, we are less enthusiastic about moving the extremely bulky tricyclohexyl-phosphine ligand from its axial position and instead prefer the simple merry-go-round process.

However, we wish to make the following points: (i) if the merry-go-round could operate rapidly *without the intermediacy of a completely non-bridged isomer* we should see rapid exchange among the **A**, **B**, **C** and **D** environments and a subsequent slower collapse of peak **E**; (ii) in contrast, if the rate-determining step is the formation of the all-terminal isomer **83** (and local rotation of each $\text{Co}(\text{CO})_3$ vertex has a very low barrier) then the rate for **D** \leftrightarrow **E** exchange will be *twice as fast* as the interconversions **A** \leftrightarrow **D**, **A** \leftrightarrow **E**, **B** \leftrightarrow **D**, **B** \leftrightarrow **E**, **A** \leftrightarrow **B** or **B** \leftrightarrow **C**. That is, each time the bridges open, half of the nuclei in the **B** environment exchange with **C** while the other 50% equilibrate with **A**, **D** and **E**; concomitantly, the single **A** nucleus also scrambles with **B**, **D** and **E**. But, and this is the crucial point, the entire populations of **D** and **E** are immediately rendered equivalent. Note

that the **C** nucleus (which is attached to the same cobalt as the phosphine) cannot move directly onto the other cobalts without passing through one of the **B** sites. Hence, $A \rightleftharpoons C$ exchange must have the smallest rate constant. In light of these considerations, the experimental spectra in Figure 5.2 were simulated by using the exchange matrix shown in Table 5.1 for which the rate constant for $D \rightleftharpoons E$ interconversion was twice that for the others. Gratifyingly, there is an excellent correspondence between the experimental and calculated spectra and the resulting Arrhenius plot yields a value of 11.6 ± 0.3 kcal mol⁻¹ for the activation energy. In the preliminary study²⁰¹ already referred to, the activation energy for carbonyl scrambling was estimated from a single coalescence temperature but such an approach is not valid for a multi-site exchange process with unequal populations.

Table 5.1. Exchange Matrix for Carbonyl Fluxionality in **63**.

	A	B	C	D	E
A	—	k	0	k	k
B	k	—	k	k	k
C	0	k	—	0	0
D	k	k	0	—	$2k$
E	k	k	0	$2k$	—



Scheme 5.1 Proposed scrambling mechanism for the CO ligands of 63; rapid local rotation can occur at the bridge-opened stage.

Although the line-shape simulations discussed above were in excellent agreement with the experimental spectra and any deviation from the exchange matrix in Table 5.1 (*e.g.*, $\mathbf{D} \leftrightarrow \mathbf{E} = 3k$) led to a significantly worse fit, we decided to seek independent evidence which might shed light on our mechanistic proposals. We therefore chose to look for direct evidence of the proposed mechanistic pathway and selected the 2D-EXCHANGE pulse sequence (NOESY)²⁰⁴ for this purpose. The NOESY sequence, *viz.*,

$$\pi/2 - t_1 - \pi/2 - \tau_m - \pi/2 - t_2$$

differs from the standard COSY experiment by the addition of a mixing time (τ_m) which provides an opportunity for a nucleus undergoing chemical exchange to migrate to another site. The experimental problem is to find an appropriate combination of mixing times and temperatures to detect different stages of the fluxional process. If the rate constant, k , is much less than $1/T_1$, then the frequency-labelled z magnetization will disappear before the nucleus has a chance to migrate;²⁰⁵ in this particular instance, the presence of the quadrupolar cobalt nuclei reduces the carbonyl T_1 's to less than 100ms. On the other hand, we cannot raise the temperature to such a value that the rate constant causes us to lose the chemical shift difference between the exchanging sites. Figure 5.3a shows the result of an experiment carried out at 183 K but using a rather short mixing time of seven milliseconds. The only detectable process under these conditions is the $\mathbf{D} \leftrightarrow \mathbf{E}$ exchange. Use of a slightly longer mixing time ($\tau_m = 10$

ms) reveals a network of exchanging spins but not of $A \rightleftharpoons C$, as shown by the cross-peaks indicated in Figure 5.3b. These experiments provide clear qualitative evidence that the exchange between the **D** and **E** sites is the fastest process while the $A \rightleftharpoons C$ interchange is the slowest one. In principle, one could attempt to quantify the 2D-EXCHANGE data as has been elegantly described by Orrell et al.²⁰⁶ The experimental problem in this particular case is that, even at high field, the temperature range over which the chemical shifts remain distinct is only about 20° and so it is difficult to obtain good variable-temperature data.

It is also of interest to view the low frequency (high-field) region of the ¹³C spectra of **63** which depict the resonances of the tricyclohexylphosphine ligand; as the temperature is lowered, these peaks exhibit clear decoalescence behavior. As shown in Figures 5.4 and 5.5, the C(1) and C(4) peaks are split 2:1, while the C(2) and C(3) resonances each yield 2:2:2 patterns. This is readily explicable in terms of the crystal structure of **63** which reveals effective C_s symmetry. At low temperature the local three-fold symmetry of the phosphine ligand is broken as rotation about the phosphorus—cobalt bond becomes slow on the NMR time-scale. We see from Figure 5.6 (which depicts the conformation of **63** as established by X-ray crystallography²⁰⁰) that, as expected, the three cyclohexyl rings adopt chair conformations in which the phosphorus is positioned equatorially. Two of these cyclohexyl groups are related by the molecular mirror plane while the third ring straddles this plane. The former two rings are oriented such that one half of each

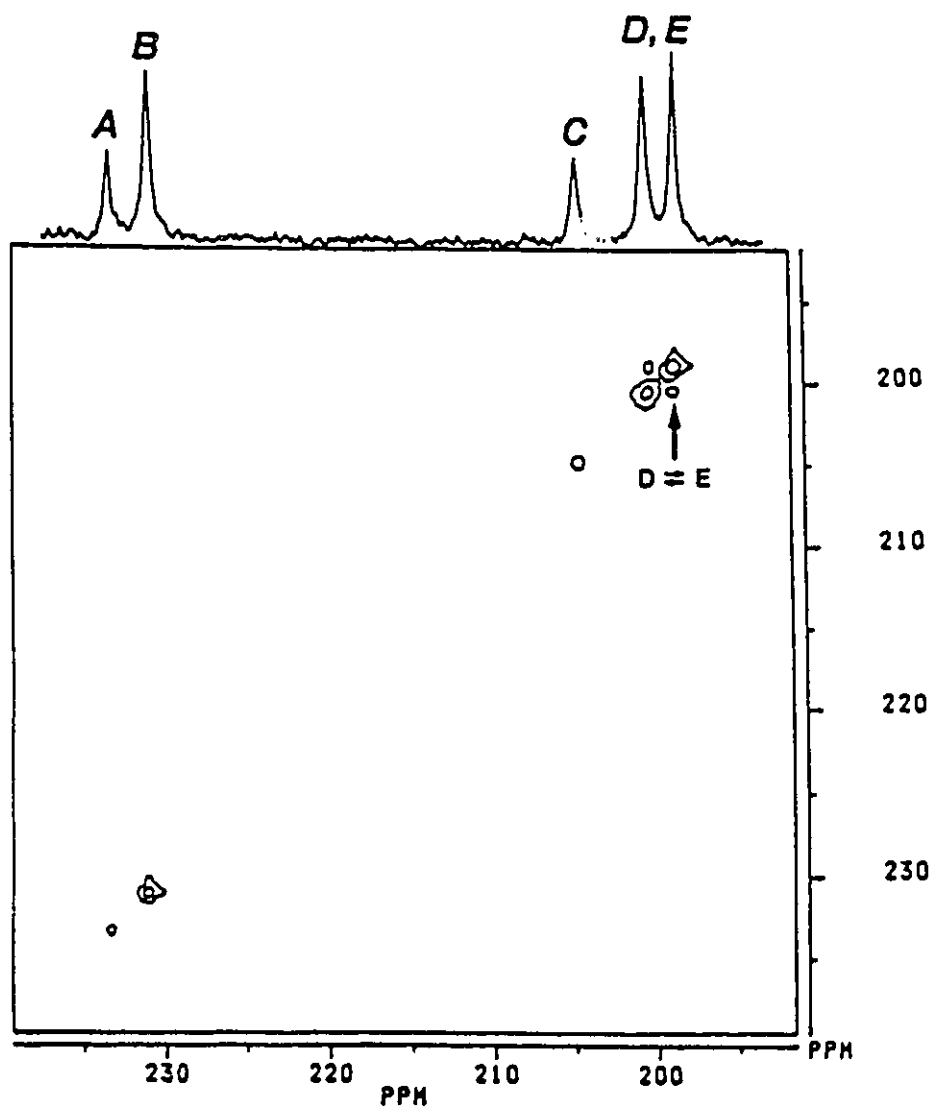


Figure 5.3(a) Contour plot representations of NOESY experiments at -90°C ; the mixing time (τ_m) is 7 ms.

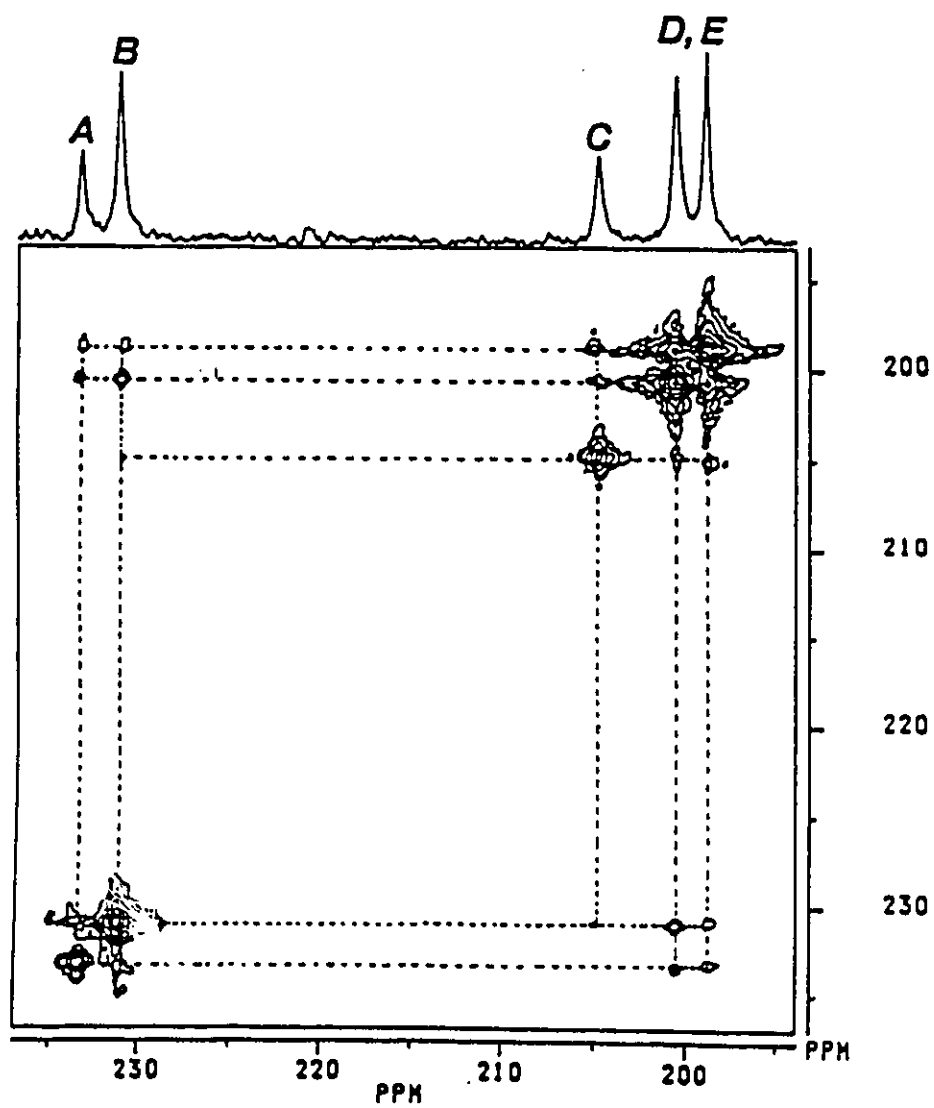


Figure 5.3(b) Contour plot representations of NOESY experiments at -90°C ; the mixing time (τ_m) is 10 ms.

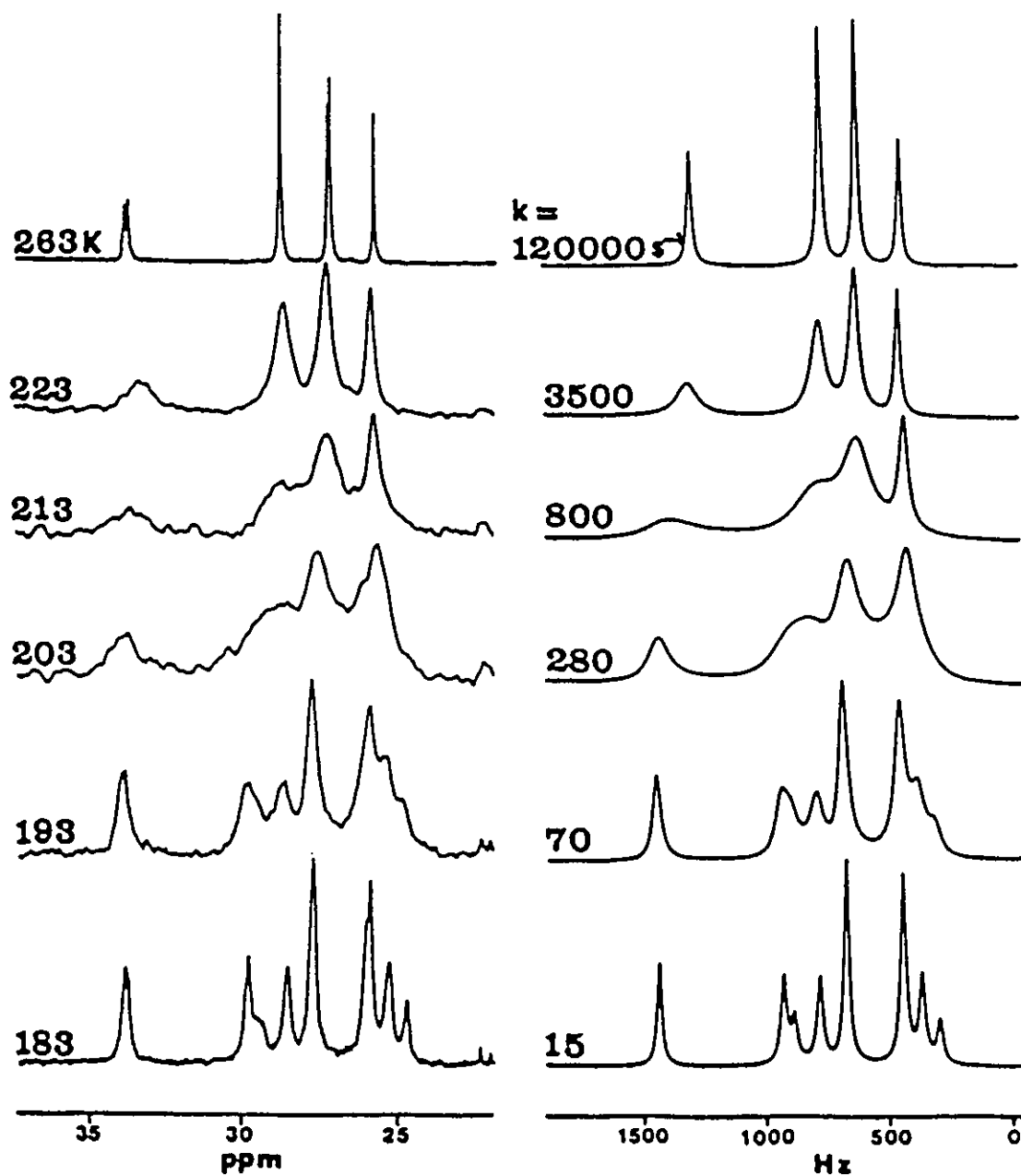


Figure 5.4 Experimental and simulated variable-temperature ^{13}C NMR spectra of $\text{CH}_3\text{CCo}_3(\text{CO})_8\text{P}(\text{cyclo-C}_6\text{H}_{11})_3$, **63**, in the cyclohexyl ring region.

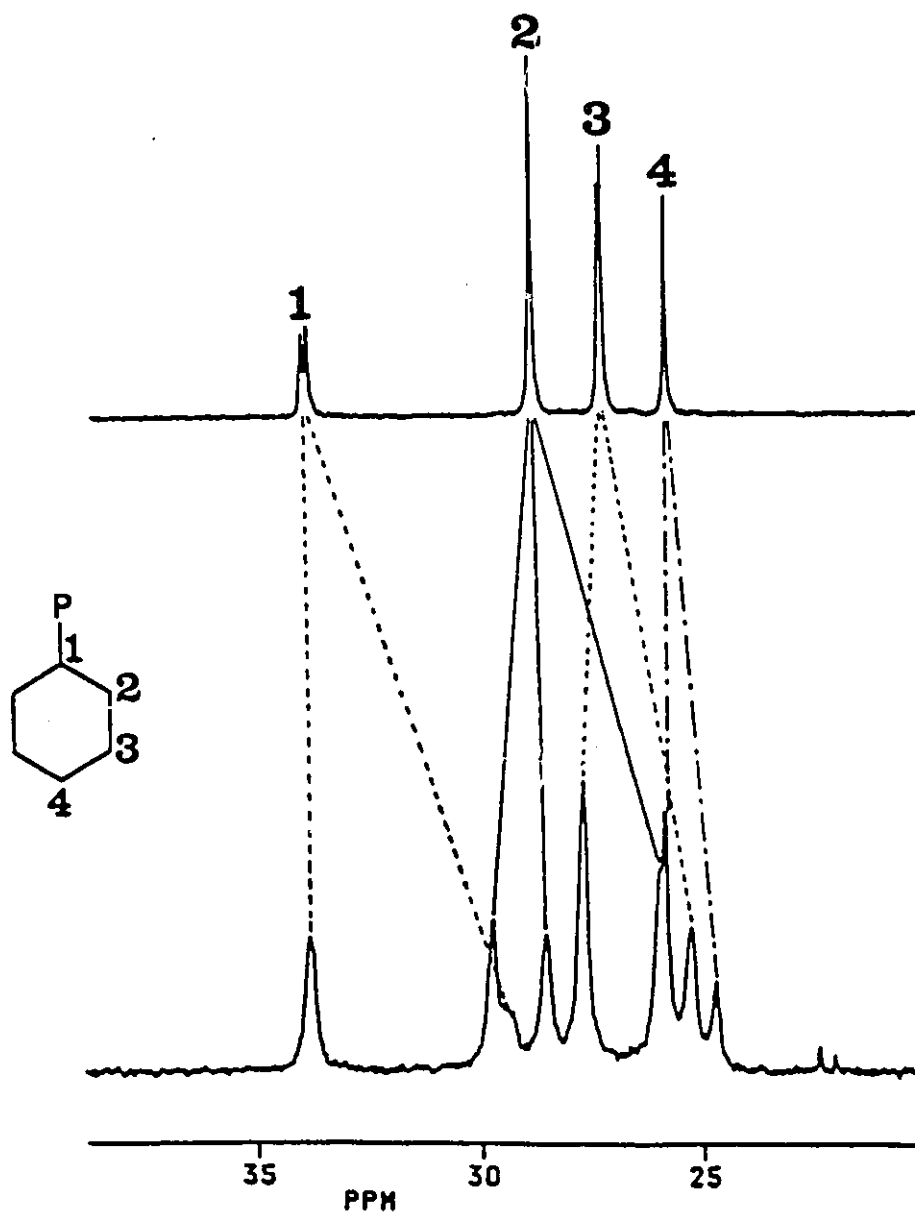


Figure 5.5 Peak coalescence pattern for the cyclohexyl carbons of 63.

cyclohexyl fragment is *proximal* with respect to the tricobalt plane while the other edge of each ring is *distal*. Moreover, as shown in Figure 5.6, the axial proton at C(1) in the unique ring points inward toward the pseudo three-fold Co—P axis while the corresponding axial H(1) atoms are directed outwards in the other two cyclohexyl rings. Thus, simple rotation through 120° about the cobalt-phosphorus axis does not suffice to interconvert all the C(2) and C(3) sites; rotation about the C(1)-P bonds is also required. Of course, these rings cannot flip to the other chair since the conformations are locked in place by the enormous P(C₆H₁₁)₂ groups in the equatorial positions.

Figure 5.5 shows the simulations of the variable-temperature spectra and yields a barrier of 10.8 ± 0.4 kcal mol⁻¹. One is tempted to propose that the rather similar values of ΔG^\ddagger for carbonyl migration and for phosphine rotation are not mere coincidence. Undoubtedly the very large cone angle of tricyclohexylphosphine ($\approx 180^\circ \pm 10^\circ$) causes steric problems and may severely restrict rotation not only of the phosphine but also of the cyclohexyl rings in the triply-bridged isomer **63**. Molecular modelling studies on tricyclohexyl-phosphine itself suggest that rotation of a single ring is difficult and that correlated rotations of the rings are favored.²⁰⁷ It is indeed possible that bridge opening to an isomer such as **83** provides release of steric strain and so facilitates phosphine rotation. Thus, the two fluxional processes, *viz.*, carbonyl migration and phosphine rotation **may** be correlated but such a scenario is certainly not mandatory.

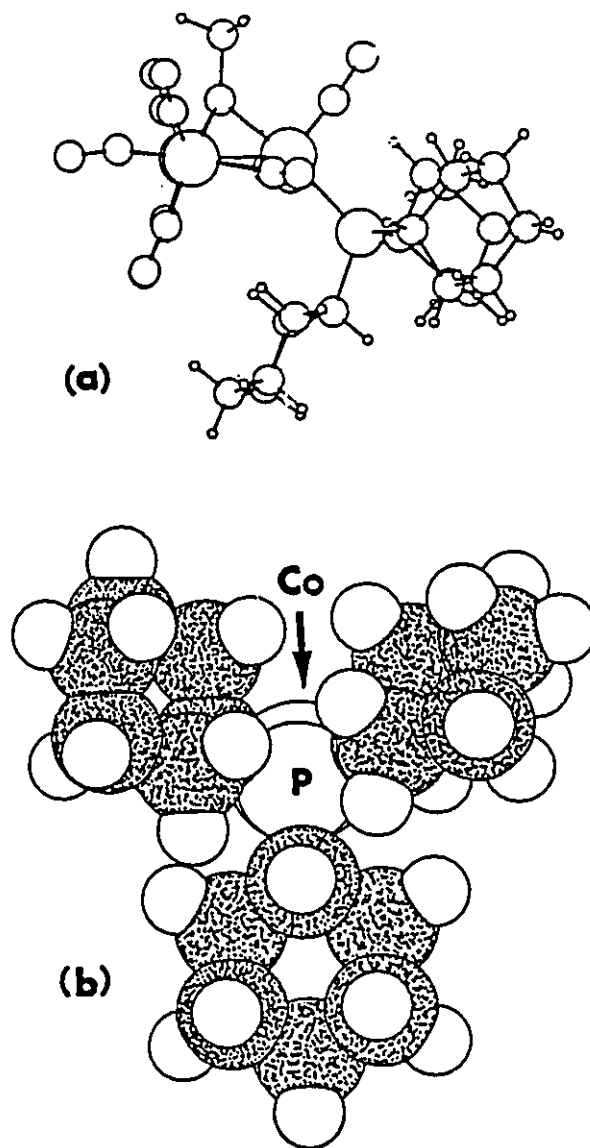
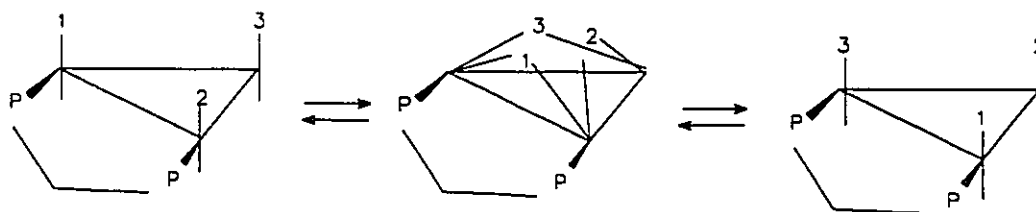
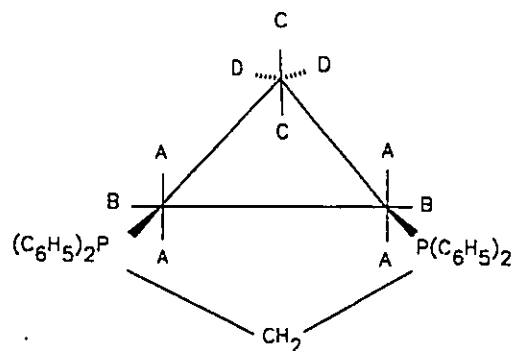


Figure 5.6 Views of the X-ray crystal structure of **63**; (a) shows the chair conformations of the cyclohexyl rings while (b) is a view along the phosphorus—cobalt bond showing the relative orientations of the rings. [The atom coordinates are taken from Ref. 200.]

To conclude, we have shown that the exchange mechanism in **63** occurs via a completely bridge-opened structure in which local rotation of $\text{Co}(\text{CO})_3$ vertices is rapid; thus these two carbonyl migration processes can be simulated by a single set of rate constants at a given temperature. To put these results in perspective, we note that in $\text{Fe}(\text{CO})_3\text{Co}_2(\text{CO})_6\text{S}$ the local rotation of the $\text{Fe}(\text{CO})_3$ vertex can be slowed on the NMR time-scale but rotation of the cobalt fragments can not.²⁰⁸ This has been rationalized with the aid of molecular orbital calculations at the extended Hückel level.²⁰⁹ Interestingly, in $\text{CpMo}(\text{CO})_2\text{Co}_2(\text{CO})_6\text{CR}$ clusters (which have all-terminal ground state structures) the rate of carbonyl migration between molybdenum and cobalt centers is controlled by the rate of $\text{CpMo}(\text{CO})_2$ vertex rotation^{210(a)}.

5.3 *Future work*

The results obtained for the two research projects discussed in the preceding chapters allowed us to successfully draw some specific conclusions regarding the fluxional behavior of trimetallic organotransition metal clusters. Future work could focus on other trimetallic clusters, such as $\text{Ru}_3(\text{CO})_{10}(\text{dppm})$, in which the bidentate ligand, bis(diphenylphosphino)methane, bridges two ruthenium atoms in the equatorial plane. The X-ray crystal structure showed that all the carbonyls are terminal. Thus, the ^{13}C NMR spectrum yields a 4:2:2:2 splitting



pattern as previously reported by Cotton *et al.*^{210(b)} They studied the variable-temperature ¹³C NMR spectra of Ru₃(CO)₁₀(dppm) and all the peaks coalesced at 111°C. They proposed two carbonyl exchange mechanisms. The first exchanges A and B, while the second (higher energy) exchanges C or D with A or B and involves the concerted formation of three bridges on one face of the triangle of ruthenium atoms, as shown in the Scheme above. We wish to raise two points here. (1). The line shape analysis at temperature as high as 111°C may be somewhat unreliable since the compound is known to decompose above this temperature. (2). The mechanism they proposed to exchange C, D with A, B has

been shown by EHMO calculations to have a very high barrier. Actually, it is rather trivial to understand this by calculating the distances between the CO's. In this intermediate, the three CO's are only 1.4 Å away from each other, which causes the very high energy barrier.

An experiment to verify this could be 2D-EXCHANGE which would allow us to avoid raising the temperature and thus provide direct evidence for the exchange mechanism.

To follow up this work, one could carry out EHMO investigations on these and other related migration mechanisms.

CHAPTER SIX

EXPERIMENTAL

All reactions were carried out under an atmosphere of dry nitrogen employing conventional benchtop and glovebag techniques. All solvents were dried according to standard procedures before use.²¹¹

ESR spectra were recorded on a Bruker ER-100D instrument operating at X-band frequency with 100KHz modulation. Spectral simulations were carried using the ESR program on the Bruker ASPECT 2000 computer. The g values were calculated from a knowledge of the microwave frequency and the magnetic field, the latter having been calibrated by use of DPPH. The ESR samples were prepared on a vacuum line. The two reactants were degassed three times separately before mixing in an ESR tube which was then sealed. The reaction mixture was kept in liquid nitrogen prior to the recording of the ESR spectra. The concentrations of the reagents used were in the range 0.005-0.02M.

¹³C NMR spectra were recorded on ¹³CO enriched samples at 125.7 MHz by using a Bruker AM 500 spectrometer equipped with a 5 mm dual frequency ¹H/¹³C probe. ¹H NMR spectra were recorded using Bruker AM 500, AC 200 and Varian EM390 spectrometers. ¹H and ¹³C chemical shifts are reported relative to

tetramethylsilane. Where necessary, peaks attributable to the minor isomer are marked with an asterisk (*). Carbon-13 2D spectra were obtained at -90°C by using the standard NOESY pulse sequence, D1 - 90° - D0 - D9 - 90° - FID. Spectra were acquired by using 16 scans for each of 256 FID's that contained 1024 points in the F2 dimension covering a spectral width of 6024 Hz. Delay D1 was 0.15 s, delay D0 was 3 μs, delay D9 was 10 ms and the 90° pulse width was 5.7 μs. The F1 dimension was zero filled to 512 points and a Gaussian window function was applied in both dimensions during Fourier transformation using a line broadening factor (LB) of 50 and a Gaussian broadening factor (GB) of zero. NMR simulations were carried out by using the multisite EXCHANGE program generously provided by Professor R. E. D. McClung (University of Alberta at Edmonton).

Molecular modelling studies were conducted by using the CHEMX modelling package.²¹² Infrared data were obtained on a Nicolet 7199 FTIR spectrometer using either NaCl solution cells or KBr pellets. Mass spectra were obtained with a double-focusing VG ZAB-E mass spectrometer under positive ion fast atom bombardment (FAB+) and negative ion fast atom bombardment (FAB-) conditions. Analytical data are from Guelph Chemical Laboratories, Guelph, Ont.

Cyclohexa-1,3-diene, nitrosobenzene, and 2-methyl-2-nitropropane were purchased from Aldrich and were used without further purification.

Acetoxymercuridurene was synthesized following published procedures.²¹³

10g of durene was dissolved in 50ml of methanol, and 23.73g of mercuric acetate was introduced. Enough acetic acid (9ml) was added and the solution was refluxed for a week. Acetoxymcuridurene was soluble in the hot reaction mixture; the solution was filtered from the insoluble diacetoxymcuridurene and cooled. The crude product was crystallized from methanol.

Acetoxymcuripentamethylbenzene was synthesized in a similar method of acetoxymcuridurene.²¹³ 10g of pentamethylbenzene was dissolved in 50 ml of methanol, and 21.4 g of mercuric acetate and 8 ml of acetic acid were added. The solution was refluxed for 7 days. Acetoxymcuripentamethylbenzene was filtered from the hot reaction mixture and crystallized from chloroform.

Nitrosodurene, 5, was synthesized using the method of Smith and Taylor.²¹⁴ The acetoxymcuridurene (5.04 g) was dissolved in chloroform (25 ml); the solution was cooled in an ice-bath and stirred. A mixture of hydrochloric acid (3.75 ml, concd.) and acetic acid (5 ml) was added. NOCl gas was then introduced to the solution for 30 min. and the reaction mixture was stirred for another 30 min. The chloroform solution extracted with water, warmed to dissolve all the product, extracted three more times, treated with 2.5 ml of methanol, filtered, concentrated by distillation, and cooled. The crystallized product was obtained as white needles.

Nitrosopentamethylbenzene, 6, was synthesized in a similar method to nitrosodurene. 10 g of acetoxymcuripentamethylbenzene was dissolved in 50

ml of chloroform; the solution was cooled in an ice-bath and stirred. A mixture of hydrochloric acid (5 ml, concd.) and acetic acid (10 ml) was added. NOCl gas was then introduced to the solution for 30 min. and the reaction mixture was stirred for another 20 min. The reaction mixture was washed with water (mercury salt recovered) and filtered. The solid was recrystallized from chloroform. The green filtrate, evaporated and cooled, deposited more nitrosocompound. The substance was recrystallize from chloroform twice. The crystallized product was obtained as white needles.

(Benzylideneacetone)iron tricarbonyl was synthesized following the literature procedure.²¹⁵

$C_6H_7Fe(CO)_3^+BF_4^-$ (**40**) was prepared by heating cyclohexa-1,3-diene with an $Fe(CO)_3$ precursor, namely, (benzylideneacetone)iron tricarbonyl under reflux for 24h in toluene. The reaction mixture was cooled, filtered through celite and the solvent removed by rotary evaporation. Subsequent chromatographic separation on a silica column and elution with a 1:1 mixture of hexane and toluene afforded the appropriate complex (60% yield) as previously reported by Birch.²¹⁶ The complex was then treated with $Ph_3C^+ BF_4^-$ in CH_2Cl_2 and the cationic complex **40** was obtained as a yellow precipitate upon addition of ether.

The steroidal cation **42** was synthesized in a similar fashion from its $Fe(CO)_3$ complex. The experimental details and NMR spectroscopic data refer to ref. 217.

$\text{Co}_3(\text{CO})_9\text{C-CO}_2\text{-}i\text{-Pr}$ was prepared according to the literature method,¹⁷⁵ and ^{13}C enrichment was carried out as previously described.¹⁷⁵

$(\text{C}_5\text{H}_5)\text{MoCo}_2(\text{CO})_8\text{C-CO}_2\text{-}i\text{-Pr}$ (66) was prepared according to the method of Mlekuz *et al.*²¹⁸ ^{13}C NMR δ 247.0 (apical C), 207.9 (all CO's), 177.7 (ester CO), 92.3 (C_5H_5 ring), 69.3 (CHMe_2), 22.1 (CHMe_2); at 193 K, δ 230.5*, 221.2 (Mo-CO's), 202.8, 200.2* (Co-CO's), 94.0*, 90.1 (C_5H_5 rings).

$(\text{C}_5\text{H}_4\text{Me})\text{MoCo}_2(\text{CO})_8\text{C-CO}_2\text{-}i\text{-Pr}$ (67). A solution of $\text{Co}_3(\text{CO})_9\text{C-CO}_2\text{-}i\text{-Pr}$ (0.30 g, 0.56 mmol) and $[(\text{C}_5\text{H}_4\text{Me})\text{Mo}(\text{CO})_3]_2$ (0.15 g, 0.29 mmol) were heated under reflux in 20 mL THF during 8 h. Progress of the reaction was followed by TLC on Kieselgel (eluent ether/petroleum ether 15/85); the desired product **67** gave a green spot at $R_f = 0.47$. Chromatography on silica gel (100/200 mesh) yielded dark green crystals of **67** (0.080 g, 0.13 mmol; 23%): mp 92°C; IR ((CH_2Cl_2)) ν_{CO} 2087(m), 2076(m), 2050(s), 2028(s), 2006(s), 1961(w), 1938(m), 1666 (ester) cm^{-1} ; IR (KBr) ν_{CO} 2074(m), 2018(s), 2001(s), 1974(m), 1952(m), 1920(m), 1661 (ester) cm^{-1} . ^{13}C NMR δ 247.2 (apical C), 208.3 (all CO's), 184.5 (ester CO), 106.5 (Cp ring C-Me), 91.3, 89.5 (Cp ring CH's), 69.4 (CHMe_2), 22.1 (CHMe_2), 14.1 Cp Me; at 183 K, δ 231.8*, 222.2 (Mo-CO's), 203.1, 200.6* (Co-CO's), 106.5, 91.4, 89.5, 106.5*, 95.1*, 92.5*, ($\text{C}_5\text{H}_4\text{Me}$ rings). Anal. Calcd for $\text{C}_{19}\text{H}_{14}\text{Co}_2\text{MoO}_{10}$: C, 37.04; H, 2.29. Found: C, 37.07; H, 2.04.

$(\text{C}_5\text{Me}_5)\text{MoCo}_2(\text{CO})_8\text{C-CO}_2\text{-}i\text{-Pr}$ (68) was prepared according to the method of Sutin *et al.*¹⁷⁵ ^{13}C NMR δ 248.8 (apical C), 209.9 (all CO's), 178.5 (ester CO),

106.1 (C_5Me_5 ring), 69.0 ($CHMe_2$), 22.1 ($CHMe_2$), 10.2 (C_5Me_5 ring); at 193 K, δ 235.0, 223.5* (Mo-CO's), 204.1*, 200.9 (Co-CO's), 105.3, 104.8* (C_5Me_5 rings), 12.0, 10.2 (C_5Me_5 rings).

(C_5H_5)WCo₂(CO)₈C-CO₂-*i*-Pr (69). Analogously to the preparation of 67, Co₃(CO)₉C-CO₂-*i*-Pr (1.64 g, 3.04 mmol) and [(C_5H_5)W(CO)₃]₂ (2.10 g, 3.04 mmol) were heated under reflux in 100 mL THF during 43 h. to give brown crystals of 69 (0.055 g, 0.08 mmol; 3%): mp 99°C; IR ((CH₂Cl₂) ν_{CO} 2087(m), 2077(m), 2040(s), 2025(s), 2006(s), 1956(w), 1933(w), 1879(w), 1668 (ester) cm⁻¹; IR (KBr) ν_{CO} 2076(m), 2019(s), 1998(s), 1970(m), 1947(m), 1921(w), 1661 (ester) cm⁻¹. ¹³C NMR δ 202.6 (all CO's), 90.5 (C_5H_5 ring), 69.3 ($CHMe_2$), 22.1 ($CHMe_2$); at 193 K, δ 216.3*, 206.0 [J(¹⁸³W-¹³C) = 165 Hz] (W-CO's), 201.0, 198.6* (Co-CO's). Anal. Calcd for C₁₈H₁₂Co₂WO₁₀: C, 31.33; H, 1.75. Found: C, 31.42; H, 1.93.

(C_5H_4Me)WCo₂(CO)₈C-CO₂-*i*-Pr (70). Analogously to the preparation of 69, Co₃(CO)₉C-CO₂-*i*-Pr (1.00 g, 1.85 mmol) and [(C_5H_4Me)W(CO)₃]₂ (1.30 g, 1.87 mmol) were heated under reflux in 150 mL THF during 24 h. to give brown crystals of 70 (0.101 g, 0.14 mmol; 8%): IR ((CH₂Cl₂) ν_{CO} 2086(m), 2076(m), 2048(s), 2024(s), 2005(s), 1953(w), 1931(m), 1875(w), 1662 (ester) cm⁻¹; IR (KBr) ν_{CO} 2076(m), 2031(s), 1997(s), 1970(m), 1941(m), 1661 (ester) cm⁻¹. ¹³C NMR δ 202.9 (all CO's), 185.0 (ester CO), 106.5 (Cp ring C-Me), 91.6, 90.9 (Cp ring CH's), 69.2 ($CHMe_2$), 22.1 ($CHMe_2$), 13.8 Cp Me; at 193 K, δ 218.1*, 207.3 [J(¹⁸³W-¹³C) = 164 Hz] (W-CO's), 201.2, 198.7* (Co-CO's), 105.8, 90.7, 89.3, 105.8*, 94.5*, 92.5*,

(C_5H_4Me rings). Anal. Calcd for $C_{19}H_{14}Co_2WC_{10}$: C, 32.41; H, 2.00. Found: C, 32.36; H, 2.23.

(C_5Me_5)WCo₂(CO)₈C-CO₂-*i*-Pr (71). Analogously to the preparation of 69, Co₃(CO)₉C-CO₂-*i*-Pr (1.17 g, 2.17 mmol) and [(C_5Me_5)W(CO)₂]₂ (0.83 g, 1.10 mmol) were heated under reflux in 35 mL THF during 24 h. to give dark green crystals of 71 (0.055 g, 0.07 mmol; 3%): mp 173°C; IR ((CH₂Cl₂) ν_{CO} 2081(s), 2044(s), 2023(s), 1915(m), 1856(w), 1656 (ester) cm⁻¹; IR (KBr) ν_{CO} 2080(s), 2042(s), 2009(s), 1905(m), 1858(m), 1665 (ester) cm⁻¹. ¹³C NMR δ 239.7 (apical C), 205.4 (all CO's), 182.2 (ester CO), 104.1 (C_5Me_5 ring), 69.0 (CHMe₂), 22.0 (CHMe₂), 10.1 (C_5Me_5 ring); at 193 K, δ 222.3, 209.3* [J(¹⁸³W-¹³C) = 165 Hz] (W-CO's), 202.7*, 199.2 (Co-CO's), 105.3, 104.8* (C_5Me_5 rings), 12.0, 10.2 (C_5Me_5 rings).. Anal. Calcd for C₂₃H₂₂Co₂WO₁₀: C, 36.34; H, 2.92. Found: C, 36.10; H, 3.02.

(C_5H_5)MoCo₂(CO)₈C-Ph (64) was prepared analogously to the method used for 66 to yield the compound previously synthesized by Beurich and Vahrenkamp.¹⁷² ¹³C NMR δ 251.0 (apical C), 208 (all CO's), 160.7 (*ipso*-C in phenyl ring), 128.2, 127.6 (*ortho* and *meta* CH's), 126.5 (*para* CH), 92.5 (C_5H_5 ring); at 193 K, δ 232.2*, 222.7 (Mo-CO's), 203.2, 201.0* (Co-CO's), 94.0*, 90.1 (C_5H_5 rings). ¹³C solid state NMR δ 224 (broad, CO's undergoing exchange), 159 (*ipso*-C, 128 (CH's in phenyl ring), 90.1 (C_5H_5 ring).

(C_5H_5)MoCo₂(CO)₈C-CO₂-menthyl (78) was prepared according to the method of Blumhofer and Vahrenkamp.²¹⁹ ¹³C NMR at 194 K, δ 230.8*, 221.3 (Mo-

CO's), 202.8, 200.2* (Co-CO's); at 170 K, δ 202.8, 201.0*, 197.6* (Co-CO's).

(C₅H₅)MoCo₂(CO)₈C-CO₂-podocarpate (79). The isopropyl ester **66** (0.545 g, 0.91 mmol) was stirred with 8.6 mL propionic anhydride in a two-necked 100 mL flask. To this flask was added 0.21 mL of a 65% aqueous solution of HPF₆. After five minutes, the resulting black crystals were filtered under nitrogen and rinsed twice with 2.5 mL aliquots of CH₂Cl₂ to yield [(C₅H₅)MoCo₂(CO)₈C=C=O]⁺ [PF₆]⁻ (0.436 g, 0.619 mmol; 68%) as described previously.²²⁰ This salt was placed in a flask with podocarpic acid (0.197 g, 0.72 mmol) in 10 mL methylene chloride. This slurry was then solubilized by the addition of 3 mL ether. Immediately the contents of the flask dissolved and turned green. The product **79** was separated by chromatography on silica gel but traces of the podocarpic acid remained. The ¹³C NMR spectrum at ambient temperature exhibited a single carbonyl peak at 208.6 ppm; at 188 K, δ 229.5*, 220.1 (Mo CO's), 201.8, 199.5* (Co CO's); at 170 K, the δ 199.5 resonance broadens to give two poorly resolved peaks of equal intensity.

CH₃CCo₃(CO)₈P(cyclo-C₆H₁₁)₃, 63, was prepared following the method of Matheson et al.^{202b} and was enriched by stirring a methylene chloride solution of **63** under an atmosphere of ¹³CO for one week. At -90°C, the ¹³C NMR spectrum of **63** shows: δ 233.24 [1], 230.95 [2], 204.68 [1], 200.44 [2], 198.76 [2], (Co-carbonyls), 39.95 (CH₃), 33.82 [2], 29.41 [1] (C-1), 29.77 [2], 28.57 [2], 25.89 [2] (C-2), 27.73 [4], 25.29 [2] (C-3), 25.89 [2], 24.72 [1] (C-4). At -10°C, δ 211.46 (Co-

carbonyls), 40.95 (CH₃), 34.38 d (C-1), 29.33 (C-2), 27.73 d (C-3), 26.28 (C-4). The ¹³C assignments for the tricyclohexylphosphine ligand follow those given by Rügger for a series of platinum complexes for which ³¹P-coupled doublets are visible for C-1 and C-3.²²¹

REFERENCES

1. J. H. MacNeil, A. C. Chiverton, S. Fortier, M. C. Baird, R. C. Hynes, A. J. Williams, K. F. Preston and T. Ziegler, *J. Am. Chem. Soc.*, **113**, 9834 (1991).
2. J. E. Wertz and J. R. Bolton, *Electron Spin Resonance: Elementary Theory and Practical Applications*, McGraw-Hill, New York, 1972.
3. A. Carrington and A. D. McLachlan, *Introduction to Magnetic Resonance*, Harper & Row, New York, 1967.
4. E. Konig, *Electron Paramagnetic Resonance, in Physical Methods in Advanced Inorganic Chemistry*, Ed. H. A. O. Hill and P. Day, Wiley-Interscience, London, 1968.
5. H. Fischer and J. Bargon, *Accounts Chem. Res.*, **2**, 110 (1969); M. Cocivera and A. M. Trozzolo, *J. Am. Chem. Soc.*, **92**, 1772 (1970); G. L. Closs and A. D. Trifunac, *ibid.*, **92**, 2183, 2186 (1970); G. C. Closs, C. E. Doubleday and D. R. Paulson, *ibid.*, **92**, 2185 (1970); A. R. Leplay, P. M. Cook and G. F. Willard, *ibid.*, **92**, 1101 (1970); H. R. Ward, R. C. Lawler, H. Y. Loken and R. A. Cooper, *ibid.*, **91**, 4928 (1969).
6. E. G. Janzen and B. J. Blackburn, *J. Am. Chem. Soc.*, **91**, 4481 (1969).
7. Species other than nitroxides, of course, have been used as spin labels.

8. J. F. W. Keana, *Chem. Rev.*, **78**, 37 (1978).
9. (a) S. P. Makarov, A. Y. Yakubovich, S. S. Dubov and A. N. Medvedev, *Doklady Akad. Nauk SSSR*, **160**, 1319 (1965).
(b) E. G. Rozantsev and E. N. Guryanova, *Izv. Akad. Nauk SSSR, Ser. Khim.*, 979 (1966).
10. E. G. Janzen, *Chem. Eng. News*, **43**, 50 (1965).
11. E. G. Janzen, *Acc. Chem. Res.*, **4**, 31 (1971).
12. C. Lagercrantz, *J. Phys. Chem.* **75**, 3466 (1971).
13. D. Rehorek, *Z. Chem.*, **20**, 325 (1980).
14. K. Torssell, *Tetrahedron*, **26**, 2759 (1970).
15. M. L. Hair and J. R. Harbour, *Adv. Chem. Ser.*, **184**, 173 (1980).
16. D. Rehorek and H. Hennig, *Can. J. Chem.*, **60**, 1565 (1982).
17. M. P. Crozet, J. Muzart, P. Pale and P. Tordo, *J. Organomet. Chem.*, **124**, 191 (1983).
18. D. Rehorek, *Z. Chem.*, **20**, 325 (1980).
19. E. G. Janzen and B. J. Blackburn, *J. Am. Chem. Soc.*, **90**, 5909 (1968).
20. E. G. Janzen and J. L. Gerlock, *J. Am. Chem. Soc.*, **91**, 3109 (1969).
21. E. G. Janzen and J. L. Gerlock, *Nature*, **222**, 867 (1969).
22. A. Mackor, Th. A. J. W. Wajer and Th. J. de Boer, *Tetrahedron*, **24**, 1623 (1968).
23. S. Forshult, C. Lagercrantz and K. Torssell, *Acta Chem. Scand.*, **23**, 522 (1969).

24. S. Terabe, K. Kuruma and R. Konaka, *J. Chem. Soc. Perkin II*, 1252 (1973)
25. R. Konaka, S. Terabe, T. Mizuta and S. Sakata, *Can. J. Chem.*, **60**, 1532 (1982).
26. A. B. Sullivan, *J. Org. Chem.*, **31**, 2811 (1966).
27. G. T. Knight and B. Pepper, *Tetrahedron*, **27**, 6201 (1971).
28. R. Sridhar and R. A. Floyd, *Can. J. Chem.*, **60**, 1574 (1982).
29. L. H. Sutcliffe and A. Zilnyk, *J. Chem. Soc., Faraday Trans. I*, **81**, 1215 (1985).
30. R. J. Field and R. M. Noyes, *Accounts Chem. Res.*, **10**, 214 (1977).
31. (a) I. Prigogine, and G. Nicolis, *J. Chem. Phys.*, **46**, 3542 (1967); (b) P. Glansdorff, and I. Prigogine, "*Thermodynamic Theory of Structure, Stability and Fluctuations*", Wiley-Interscience, New York, N.Y., 1971.
32. R. J. Field and R. M. Noyes, *J. Am. Chem. Soc.*, **94**, 8649 (1972)
33. K. R. Sharma and R. M. Noyes, *J. Am. Chem. Soc.*, **97**, 202 (1975)
34. P. Gray, J. F. Griffiths and R. J. Moule, *Faraday Symp. Chem. Soc.*, **9**, 103 (1974), and the references therein.
35. B. P. Belosov, *Sb. Ref. Radiats. Med.*, 1958, Medgiz, Moscow, 145 (1959).
36. (a) A. M. Zhabotinsky, *Dokl. Akad. Nauk SSSR*, **157**, 392 (1964); (b) *Biofizika*, **9**, 306 (1964).
37. A. M. Zhabotinsky, "*Oscillatory Processes in Biological and Chemical systems*" (Science Publ., Moscow, 1967), p. 149; A. N. Zaikin and A. M.

- Zhabotinsky, *Nature*, **225**, 535 (1970).
38. I. R. Epstein, *Chem. Eng. News*, **March**, 24 (1987).
 39. J. Higgins, *Industrial Eng. Chem.*, **59**, 19 (1967).
 40. R. Markby, I Wender, R. A. Friedel, F.A Cotton and H. W. Sternberg, *J. Am. Chem. Soc.*, **80**, 6529 (1958).
 41. W. T. Dent, L. A. Duncanson, R. G. Guy, H. W. G. Reed and B. L. Shaw., *Proc. Chem. Soc.*, 169 (1961).
 42. R. Ercoli, E. Santambrogio and G. Tettamanti-Casagrande, *Chim. Ind. (Milano)* **44**, 1344 (1962).
 43. G. Bor, L. Marko and B. Marko, *Acta. Chim. Acad. Sci. Hung.* **27**, 395 (1961).
 44. D. Seyferth, J. E. Hallgren and P. L. K. Hung, *J. Organomet. Chem.*, **50**, 265 (1973).
 45. J. E. Huheey, "*Inorganic Chemistry, Principles of structure and Reactivity*" 2nd Ed. Harper and Row, New York, 1978, pp. 579.
 46. G. Binsch, in "*Dynamic NMR Spectroscopy*", ed. L. M. Jackman and F. A. Cotton. Academic Press, New York, 1975, p45.
 47. T. S. Piper and G. Wilkinson, *J. Inorg. Nucl. Chem.*, **3**, 104 (1956).
 48. F. A. Cotton, in "*Dynamic Nuclear Magnetic Resonance Spectroscopy*", ed. L. M. Jackman and F. A. Cotton. Academic Press, New York, 1975, p377.
 49. F. A. Cotton, D. L. Hunter, *J. Am. Chem. Soc.*, **98**, 1413 (1976).

50. A. Cutler, D. Ehntholt, W. P. Giering, P. Lennon, S. Raghu, A. Rosan, M. Rosenblum, J. Tancrede and D. Wells, *J. Am. Chem. Soc.*, **98**, 3495 (1976).
51. I. B. Benson, S. A. R. Knox, R. F. D. Stansfield and P. Woodward, *J. Chem. Soc., Chem. Commun.*, 404 (1977).
52. D. L. Reger and C. Coleman, *J. Organomet. Chem.*, **131**, 153 (1977).
53. D. M. P. Mingos, *J. Chem. Soc. Dalton Trans.*, 1 (1977); D. M. P. Mingos, in "*Comprehensive Organometallic Chemistry*", vol. **3**, p. 1 (1982).
54. R. B. Woodward and R. Hoffmann, "*The Conservation of Orbital Symmetry*", Academic Press, New York, 1970.
55. B. E. Mann, *Chem. Soc. Rev.*, **15**, 167 (1986).
56. A.E. Derome, *Modern NMR Techniques for Chemistry Research*; Pergamon Press, 1987
57. M. J. Hails, B. E. Mann and C. M. Spencer, *J. Chem. Soc., Chem. Commun.*, 120 (1983)
58. M. J. Hails, B. E. Mann and C. M. Spencer, *J. Chem. Soc. Dalton Trans.*, 693 (1985)
59. G. D. Williams, M. C. Lieszkovszky, C. A. Mirkin, G. L. Geoffroy and A. L. Rheingold, *Organomet.*, **5**, 2228(1986).
60. M. Grassi, B. E. Mann, B. T. Pickup and C. M. Spencer, *J. Chem. Soc. Dalton Trans.*, 2649 (1987).

61. M. Grassi, B. E. Mann and C. M. Spencer, *J. Chem. Soc., Chem. Commun.*, 1169 (1985).
62. D. R. Muhandiram and R. E. D. McClung, *J. Magn. Reson.*, **71**, 187 (1987)
63. M. Grassi, B. E. Mann, B. T. Pickup, and C. M. Spencer, *J. Magn. Reson.*, **69**, 92 (1986).
64. R. J. Abraham, J. Fisher and P. Loftus; "*Introduction to NMR Spectroscopy*" John Wiley and Sons, Toronto, 1978
65. B. E. Mann, *Adv. Organomet. Chem.*, **28**, 397 (1986)
66. S. Forsen and R. A. Hoffman, *J. Chem. Phys.*, **39**, 2892 (1963); *ibid* **40**, 1189 (1964).
67. S. Forsen and R. A. Hoffman, *Prog. N.M.R. spectroscopy* **1**, 173 (1966).
68. J. A. Gibson and B. E. Mann, *J. Chem. Soc. Dalton Trans.*, 1021 (1979).
69. F. A. Cotton, D. L. Hunter and P. Lahuerta, *J. Am. Chem. Soc.*, **96**, 4723, 7926 (1974).
70. G. A. Morris and R. Freeman, *J. Magn. Resonance*, **29**, 433 (1978).
71. M. J. Hails, B. E. Mann and C. M. Spencer, *J. Chem. Soc., Chem. Commun.*, 120 (1983)
72. M. J. Hails, B. E. Mann and C. M. Spencer, *J. Chem. Soc. Dalton Trans.*, 693 (1985)
73. M. Grassi, B. E. Mann, B. T. Pickup and C. M. Spencer, *J. Chem. Soc. Dalton Trans.*, 2649 (1987).

74. T. H. Whitesides and R. A. Budnik, *Inorg. Chem.*, **15**, 874 (1976).
75. G. Y. Kiel and J. Takats; *Organometallics*, **6**, 2009(1987).
76. M. Grassi, B. E. Mann and C. M. Spencer, *J. Chem. Soc., Chem. Commun.*, 1169 (1985).
77. D. M. Heinekey and W. A. G. Graham, *J. Am. Chem. Soc.*, **101**, 6115 (1979).
78. R. B. Larrabee, *J. Am. Chem. Soc.*, **93**, 1510 (1971).
79. B. E. Mann, B. F. Taylor, N. A. Taylor and R. J. Wood, *Oganomet. Chem.*, **162**, 137 (1978).
80. D. M. Heinekey and W. A. G. Graham, *J. Am. Chem. Soc.*, **104**, 915 (1982).
81. F. A. Cotton, *Inorg. Chem.*, **5**, 1083 (1966).
82. B. E. Mann, C. M. Spencer; *J. Organomet. Chem.*, **244**, C17-C20 (1983).
83. B. E. Mann, B. T. Pickup; *J. Chem. Soc. Dalton Trans.*, 889 (1989).
84. D. Braga, B. Ros and R. Roulet, *J. Organomet. Chem.*, **286**, C8 (1985).
85. G. E. Hawkes, L. Y. Lian, E. W. Randall, K. D. Sales and S. Aime; *J. Magn. Reson.*, **65**, 173-177 (1985).
86. G. E. Hawkes, E. W. Randall, S. Aime, D. Osella, and J. E. Elliot, *J. Chem. Soc., Dalton Trans.*, 279, (1984).
87. E. W. Abel, T. P. J. Coston, K. G. Orrell, V. Sik, and D. Stephenson, *J. Magn. Reson.*, **70**, 34 (1986).

88. T. Beringhelli, G. D'Alfonso, H. Molinari, B. E. Mann, B. T. Pickup, and C. M. Spencer, *J. Chem. Soc. Chem. Commun.*, 796 (1986).
89. Y. Huang, S. Macura and R. R. Ernst, *J. Am. Chem. Soc.*, **103**, 5327 (1981).
90. J. Jeener, B. H. Meier, P. Bachmann and R. R. Ernst, *J. Chem. Phys.*, **71**, 4546 (1979).
91. J.K. Sanders and B.K. Hunter, *Modern NMR Spectroscopy, a Guide for Chemists*; Oxford University Press, Oxford, 1987
92. R. Benn, *Angew Chem. Int. Ed. Engl.*, **21**, 626 (1982).
93. A. A. Ismail, F. Sauriol, J. Sedman, and I. S. Butler, *Organometallics*, **4**, 1914 (1985).
94. A. A. Ismail, F. Sauriol, J. Sedman, and I. S. Butler, *Inorg. Chem.*, **28**, 1007-1012 (1989).
95. R. Benn, K. Cibura, P. Hoffmann, K. Jonas and A. Ruffhska, *Organometallics*, **4**, 2214 (1985).
96. G. A. Hawkes, L. Y. Lian, E. W. Randall, K. Sales and S. Aime, *J. Chem. Soc. Dalton Trans.*, 225 (1985).
97. G. A. Hawkes, L. Y. Lian, E. W. Randall, K. Sales and S. Aime, *J. Magn. Res.*, **65**, 173 (1985).
98. A. Strawczynski, R. Ros, and R. Roulet, *Helvetica Chimica Acta*, **71**, 867 (1988).

99. A. Strawczynski, R. Ros, and R. Roulet, *Helvetica Chimica Acta*, **71**, 1885 (1988).
100. P. Ewing, L. J. Farrugia and D. S. Rycroft, *Organometallics*, **7**, 859 (1988).
101. L. J. Farrugia, *Organometallics*, **8**, 2410 (1989).
102. W. E. Lindsell, N. M. Walker and A. S. F. Boyd, *J. Chem. Soc. Dalton Trans.*, 675 (1989).
103. R. Benn, H. Grongey, R. Nolte and G. Erker, *Organometallics*, **7**, 777 (1988).
104. M. E. Lappert, C. J. Pickett, P. L. Riley and P. L. W. Yarrow, *J. Chem. Soc. Dalton Trans.*, 805 (1981).
105. M. Cais, P. Ashkenazi, S. Dani, and J. Gottlieb. *J. Organomet. Chem.* **124**, 49 (1977).
106. M. Cais, P. Ashkenazi, and J. Gottlieb. *Rev. Roumaine Chim.* **22**, 545 (1977).
107. S. Lupon, M. Kapon, M. Cais, and F. H. Herbstein. *Angew. Chem. Int. Ed. Engl.* **11**, 1025 (1972).
108. M. I. Rybinskaya, A. Z. Kreindlin, and S. S. Fadeeva., *J. Organomet. Chem.* **358**, 363 (1988).
109. Yu. A. Belousov and T. A. Kolosova. *Polyhedron*. **6**, 1959 (1987).
110. J. F. W. Keana, T. Tamura, D. A. McMillen, and P. C. Jost. *J. Am. Chem. Soc.* **103**, 4904 (1981).

111. R. E. Perrier, C. S. Frampton, R. Faggiani, and M. J. McGlinchey. *J. Organomet. Chem.*, in press.
112. E. T. Strom, A. L. Bluhm, and J. Weinstein. *J. Org. Chem.* **32**, 3853 (1967).
113. T. Suehiro, M. Kamimori, K. Tokumaru, and M. Yoshida. *Chem Lett.* 531 (1976).
114. A. J. Pearson. *Science.* **223**, 895 (1984).
115. S. G. Davies, M. L. H. Green, and D. M. P. Mingos. *Tetrahedron.* **34**, 3047 (1978).
116. G. Chapelet-Letourneux, H. Lemaire, R. Lenk, M-A Marechal, and A. Rassat. *Bull. Chim.* 3963 (1968).
117. M. Kamimori, H. Sakuragi, T. Suehiro. K. Tokumaru, and M. Yoshida. *Bull. Chem. Soc. Jap.* **50** 1195 (1977).
118. R. Konaka, S. Terabe, T. Mizuta, and S. Sakata. *Can. J. Chem.* **60**, 1532 (1982).
119. C. Chatgililoglu and K.U. Ingold. *J. Am. Chem. Soc.* **103**, 4833 (1981).
120. R. L. Bilkis and S. M. Shein. *Tetrahedron.* **31** 969 (1975).
121. V. A. Golubev and G. N. Voronina. *Bull. Akad. Sci. USSR(Eng Trans).***21**, 2024 (1972).
122. D. F. Bowman, T. Gillan, and K. U. Ingold. *J. Am. Chem. Soc.* **93**, 6555 (1971).
123. K. Adamic, D. F. Bowman, T. Gillan, and K. U. Ingold. *J. Am. Chem. Soc.*

- 93, 902 (1971).
124. A. L. Castelhana, D. Griller, and K. U. Ingold. *Can J. Chem.* **60**, 1501 (1982).
 125. V. A. Golubev, G. N. Voronina, and E. G. Rozantsev. *Bull. Akad. Sci. USSR(Eng Trans)*. **21**, 146 (1972).
 126. A. B. Sullivan, *J. Org. Chem.* **31**, 2811 (1966).
 127. G. T. Knight and B. Pepper. *Tetrahedron*. **27**, 6201 (1971).
 128. L. H. Sutcliffe and A. Zilnyk, *J. Chem. Soc. Farad. Trans.* **181**, 1215 (1985).
 129. A. F. Mateos and S. G. Davies, *Anal. Quim.* **75**, 385 (1979).
 130. "MACROMODEL", program developed by W.C. STILL, Columbia University, New York, N.Y.
 131. R. B. King, T. A. Manuel, and F. G. A. Stone, *J. Inorg. Nucl. Chem.* **16**, 233 (1961).
 132. S. K. Wong and J. K. S. Wan, *Can. J. Chem.* **51**, 753 (1973).
 133. M. P. Crozet, J. Muzart, P. Pale, and P. Tordo, *J. Organomet. Chem.* **244**, 191 (1983).
 134. S. Terabe, K. Kuruma and R. Konaka., *J. Chem. Soc. Perkin Trans. 2*, 1252 (1973).
 135. T. Doba, T. Ichikawa, and H. Yoshida, *Bull. Chem. Soc. Jpn.* **50**, 3124 (1977).
 136. I. Prigogine, "From Being To Becoming", W. H. Freeman and Co., (1980)

137. I.R. Epstein, *Chemical and Engineering News*, March 30, 24 (1987).
138. A.M. Zabolinsky, *Ber. Bunsenges. Phys. Chem.*, **84**, 303 (1980).
139. M. Orban, and I.R. Epstein, *J. Am. Chem. Soc.*, **111**, 2891 (1989).
140. L. Li, R.E. Perrier, D.R. Eaton and M.J. McGlinchey, *Canad. J. Chem.*, **67**, 1868 (1989).
141. A. Mackor, Th.A.J.W. Wajer and Th.J. DeBoer, *Tetrahedron Letters*, 2115 (1966).
142. S.F. Nelsen, R.T. Landis, L.H. Kiehle and T.H. Leung, *J. Am. Chem. Soc.*, **94**, 1610 (1972).
143. A. Calder and A.R. Forrester, *J. Chem. Soc., Chem. Commun.*, 682 (1967).
144. A. Calder and A.R. Forrester, *J. Chem. Soc.(C)*, 1459 (1969).
145. G. Chapelet-Letourneux, H. Lemaire and A. Rassat, *Bull. Soc. Chim. France*, 444 (1965).
146. A.R. Forrester and F.A. Neugebauer in "Magnetic Properties of Free Radicals", Landolt-Bornstein, Vol.9, Part C1, pp. 651-653.
147. A.K. Hoffmann, W.G. Hodgson, D.L. Maricle and W.H. Jura, *J. Am. Chem. Soc.*, **86**, 631 (1964).
148. T. Kawamura, S. Matsunami and T. Yonezawa, *Bull. Chem. Soc. Japan*, **40**, 1111 (1967).
149. S. Forshult, C. Lagercrants and K. Torssell, *Acta Chem. Scand.*, **23**, 522 (1969).

150. V.A. Golubev and G.N. Voronina. *Bull. Akad. Sci. USSR (Eng. Trans)*, **21**, 2024 (1972).
151. A.K. Hoffmann, A.M. Feldman, E. Geblum and W.G. Hodgson, *J. Am. Chem. Soc.*, **86**, 639 (1964).
152. B. Turcsányi, *Acta Chim. Acad. Scient. Hungar.*, **110**, 305 (1982). (Chem. Abs., 97 188877w)
153. D.P. Santry and A.J. Yarwood, personal communication.
154. G. Rabai, G. Bazsa and M.T. Beck, *International J. Chem. Kinetics*, **13**, 1277 (1981).
155. F. G. A. Stone., *Angew. Chem., Int. Ed. Engl.*, **23**, 89, (1984).
156. H. Vahrenkamp, *Adv. Organomet. Chem.*, **22**, 169, (1983).
157. Ch. Elschenbroich,; A. Salzer, *Organometallics — A Concise Introduction*; VCH Publishers, Weinheim, 1989, pp. 402-405.
158. D. Seyferth, *Adv. Organomet. Chem.*, **14**, 97, (1976).
159. (a) B. R. Penfold, and B. H. Robinson, *Acc. Chem. Res.*, **6**, 73, (1973).
(b) A. J. Downard, B. H. Robinson, and J. Simpson, *Organometallics*, **5**, 1122; 1132; 1140, (1986).
160. R. Hoffmann, *Angew. Chem., Int. Ed. Engl.*, **21**, 711 (1982).
161. H. Beurich, and H. Vahrenkamp, *Angew. Chem., Int. Ed. Engl.*, **20**, 98 (1981).
162. (a) M. Mlekuz, P. Bougeard, M. J. McGlinchey and G. Jaouen, *J.*

- Organomet. Chem.*, **253**, 117 (1983).
- (b) S. Jensen, B. H. Robinson, and J. Simpson, *J. Chem. Soc., Chem. Commun.*, 1081 (1983).
- 163 (a) H. -T. Schacht, and H. Vahrenkamp, *Chem. Ber.*, **122**, 2239 (1989).
(b) H. Bantel, A. K. Powell and H. Vahrenkamp, *Chem. Ber.*, **123**, 1607 (1990), and references therein.
164. F. G. A. Stone, *Pure and Applied Chem.*, **58**, 529 (1986).
165. M. J. McGlinchey, M. Mlekuz, P. Bougeard, B. G. Sayer, A. Marinetti, J. -Y. Saillard, and G. Jaouen, *Can. J. Chem.*, **61**, 1319 (1983).
166. M. Mlekuz, P. Bougeard, B. G. Sayer, S. Peng, M. J. McGlinchey, A. Marinetti, J. -Y. Saillard, J. Ben Naceur, B. Mentzen, and G. Jaouen, *Organometallics*, **4**, 1123 (1985).
167. (a) F. A. Cotton, *Inorg. Chem.*, **5**, 1083 (1966).
(b) J. Evans, *Adv. Organomet. Chem.*, **16**, 319 (1977).
(c) E. Band, and E. L. Muetterties, *Chem. Rev.*, **78**, 639 (1978).
168. M. D. Brice, B. R. Penfold, W. T. Robinson, and S. R. Taylor, *Inorg. Chem.*, **9**, 362 (1970).
169. T. W. Matheson, and B. R. Penfold, *Acta Cryst.*, **B33**, 1980 (1977).
170. R. C. Sievert, D. S. Strickland, J. R. Shapley, G. R. Steinmetz, G. L. Geoffroy, *Organometallics*, **1**, 214 (1982).
171. J. R. Shapley, D. S. Strickland, G. M. St. George, M. R. Churchill, C.

- Bueno, *Organometallics*, **2**, 185 (1983).
172. H. Beurich, and H. Vahrenkamp, *Angew. Chem., Int. Ed. Engl.*, **17**, 863 (1978).
173. M. J. Chetcuti, P. A. M. Chetcuti, J. C. Jeffery, M. R. Mills, P. Mitprachachon, S. J. Pickering, F. G. A. Stone, P. Woodward, *J. Chem. Soc., Dalton Trans.*, 699 (1982).
174. M. F. D'Agostino, and M. J. McGlinchey, *Polyhedron*, **7**, 807 (1988).
175. K. A. Sutin, J. W. Kolis, M. Mlekuz, P. Bougeard, B. G. Sayer, M. A. Quilliam, R. Faggiani, C. J. L. Lock, M. J. McGlinchey, and G. Jaouen, *Organometallics*, **6**, 439 (1987).
176. T. V. Ashworth, M. J. Chetcuti, J. A. K. Howard, F. G. A. Stone, S. J. Wisbey, and P. Woodward, *J. Chem. Soc., Dalton Trans.*, 763 (1981).
177. E. Delgado, J. Hein, J. C. Jeffery, A. L. Ratermann, F. G. A. Stone and L. J. Farrugia, *J. Chem. Soc., Dalton Trans.*, 1191 (1987).
178. B. E. Mann and B. F. Taylor, *¹³C NMR Data for Organometallic Compounds*; Academic Press, New York, 1981, pp. 171-179.
179. This diastereotopic character would also be detectable in the non-equivalence of the ring protons and carbons of the C₅H₄CH₃ ligand.
180. L. Busetto, J. C. Jeffery, R. M. Mills, F. G. A. Stone, M. J. Went, and P. Woodward, *J. Chem. Soc., Dalton Trans.*, 101 (1983).
181. The room temperature ¹³C NMR solid state spectrum of C₆H₅-CCo₂Mo(CO)₈-

(C₅H₅), **64**, shows signals corresponding to the phenyl and cyclopentadienyl ring carbons of the major isomer; the carbonyl signals were broadened because of chemical exchange.

182. F. A. Cotton, B. E. Hansen, *Inorg. Chem.*, **16**, 3369 (1977).
183. A. A. Aichison, and L. J. Farrugia, *Organometallics*, **5**, 1103 (1986).
184. L. J. Farrugia, *J. Organomet. Chem.*, **310**, 67 (1986).
185. (a) R. J. Lawson, and J. R. Shapley, *J. Am. Chem. Soc.*, **98**, 7433 (1976).
(b) R. J. Lawson, and J. R. Shapley, *Inorg. Chem.*, **17**, 772 (1978).
186. W. I. Jr. Bailey, M. H. Chisholm, F. A. Cotton, and L. A. Rankel, *J. Am. Chem. Soc.*, **100**, 5764 (1978).
187. G. A. Carriedo, J. A. K. Howard, D. B. Lewis, and F. G. A. Stone, *J. Chem. Soc., Dalton Trans.*, 905 (1985).
188. P. Bougeard, S. Peng, M. Mlekuz, and M. J. McGlinchey, *J. Organomet. Chem.*, **296**, 383 (1985), and references therein.
189. In all of these clusters local rotation of each Co(CO)₃ group is assumed to be fast on the NMR time scale; this process, which interconverts axial and equatorial carbonyl environments, can only be slowed when the capping carbonyl group is very bulky: M. F. D'Agostino, C. S. Frampton, and M. J. McGlinchey, *Organometallics*, submitted for publication.
190. M. Savignac, G. Jaouen, C. A. Rodger, R. E. Perrier, R. G. Sayer, and M. J. McGlinchey, *J. Org. Chem.*, **51**, 2328 (1986).

191. D. T. Clark, K. A. Sutin, and M. J. McGlinchey, *Organometallics*, **8**, 155 (1989).
192. D. T. Clark, K. A. Sutin, R. E. Perrier, and M. J. McGlinchey, *Polyhedron*, **7**, 2297 (1988).
193. M. F. D'Agostino, C. S. Frampton, and M. J. McGlinchey, *Organometallics*, **9**, 2972 (1990).
194. M. F. D'Agostino, C. S. Frampton, and M. J. McGlinchey, *J. Organomet. Chem.*, **394**, 145 (1990).
195. (a) R. C. Cambie, G. R. Clark, S. R. Gallagher, P. S. Rutledge, M. J. Stone, and P. D. Woodgate, *J. Organomet. Chem.*, **342**, 315 (1988), and references therein.
(b) B. Mailvaganam, R. E. Perrier, B. G. Sayer, B. E. McCarry, R. A. Bell and McGlinchey, *J. Organomet. Chem.*, **354**, 325 (1988).
196. CHEM-X, developed and distributed by Chemical Design Ltd., Oxford, U.K.
197. (a) R. E. Benfield and B. F. G. Johnson, *Trans. Met. Chem.* **6**, 131 (1981).
(b) B. F. G. Johnson, and A. Rodgers, in *The Chemistry of Metal Cluster Complexes*; D. F. Shriver, H. D. Kaesz, R. D. Adams, Eds.; VCH Publishers Inc.: New York, N. Y., 1990, pp. 303-327, and references therein.
(c) G. Hawkes, L. Y. Lian, E. W. Randall, k. D. Sales, *J. Chem. Soc., Dalton Trans.* 225 (1985).
198. M. F. D'Agostino, M. Mlekuz, J. W. Kolis, B. G. Sayer, C. A. Rodger, J-F.

- Halet, J-Y. Saillard, and M. J. McGlinchey, *Organometallics*, **5**, 2345 (1986).
199. R. A. Gates, M. F. D'Agostino, K. A. Sutin, M. J. McGlinchey, T. S. Janik, and M. R. Churchill, *Organometallics*, **9**, 20 (1990).
200. T. W. Matheson, and B. H. Robinson, *Acta Cryst.* **B33**, 1980 (1977).
201. T. W. Matheson, and B. H. Robinson, *J. Organometal. Chem.* **88**, 367 (1975).
- 202 (a) M. D. Brice, B. R. Penfold, W. T. Robinson, and S. R. Taylor, *Inorg. Chem.* **9**, 362 (1970).
- (b) T. W. Matheson, E. H. Robinson, W. S. Tham, *J. Chem. Soc. (A)* 1457 (1971).
203. (a) F. A. Cotton, *Inorg. Chem.* **5**, 1083 (1966).
- (b) E. Band, and E. L. Muetterties, *Chem. Rev.* **78**, 639 (1978).
204. (a) B. H. Meier, and R. R. Ernst, *J. Am. Chem. Soc.* **101**, 6441 (1979).
- (b) Y. Huang, S. Macura, and R. R. Ernst, *J. Am. Chem. Soc.* **103**, 5327 (1981).
205. (a) A. E. Derome, *Modern NMR Techniques for Chemistry Research*; Pergamon Press, Oxford, 1987, pp. 241.
- (b) For a superb example see: A. A. Ismail, F. Sauriol, J. Sedman, and I. S. Butler, *Inorg. Chem.* **28**, 1007 (1989).
206. E. W. Abel, T. P. J. Coston, K. G. Orrell, V. Sik, and D. Stephenson, *J. Magn. Reson.* **70**, 34 (1986).

207. (a) Correlated rotation of the triphenylphosphine ligand in $[(C_5H_5)Fe(CO)(PPh_3)COCH_3]$ has recently been invoked; in this molecule, rotation about the Fe—P bond can also be slowed on the NMR time-scale: S. G. Davies, A. E. Derome, and J. P. McNally, *J. Am. Chem. Soc.* **113**, 2854 (1991).
- (b) For a clear explication of dynamic gearing at the molecular level, see: H. Iwamura, and K. Mislow, *Acc. Chem. Res.* **21**, 175 (1988).
208. S. Aime, L. Milone, R. Rossetti, and P. L. Stanghellini, *Inorg. Chim. Acta*, **25**, 103 (1977).
209. K. L. Malisza, M. F. D'Agostino, K. A. Sutin, and M. J. McGlinchey, submitted for publication.
210. (a) K. A. Sutin, L. Li, C. S. Frampton, B. G. Sayer, and M. J. McGlinchey, *Organometallics* **10**, 2362 (1991).
- (b) F. A. Cotton and B. E. Hanson, *Inorg. Chem.*, **16**, 3369 (1977).
211. D. D. Perrin, W. L. F. Armarego, and D. R. Perrin, *Purification of Laboratory Chemicals*; Pergamon Press: New York, 1980.
212. CHEMX, developed and distributed by Chemical Design Ltd., Oxford, U.K.
213. L. I. Smith and F. L. Taylor, *J. Am. Chem. Soc.* **57**, 2370 (1935).
214. L. I. Smith and F. L. Taylor, *J. Am. Chem. Soc.* **57**, 2460 (1935).
215. G. Evans, B. F. G. Johnson, and J. Lewis. *J. Organomet. Chem.* **102**, 507 (1975).

216. A. J. Birch, P. E. Cross, J. Lewis, D. A. White and S. B. Wild.
J. Chem. Soc.(A) 332 (1968).
217. R. E. Perrier, *Ph.D. thesis*, Department of Chemistry, McMaster University,
Hamilton, Ontario.
218. M. Mlekuz, P. Bougeard, B. G. Sayer, R. Faggiani, C. J. L. Lock, M. J.
McGlinchey and G. Jaouen, *Organometallics*, **4**, 2046 (1985).
219. R. Blumhofer, and H. Vahrenkamp, *Chem. Ber.*, **119**, 683 (1986).
220. M. F. D'Agostino, M. Mlekuz, and M. J. McGlinchey, *J. Organomet. Chem.*,
345, 371 (1988).